Copyright

by

Mauricio Xavier Fiallos Torres

2019

The Thesis Committee for Mauricio Xavier Fiallos Torres
Certifies that this is the approved version of the following thesis:

Modeling Interwell Fracture Interference and Huff-N-Puff Pressure Containment in Eagle Ford using EDFM

APPROVED BY
SUPERVISING COMMITTEE:

Supervisor:

Kamy Sepehrnoori

Wei Yu

Modeling Interwell Fracture Interference and Huff-N-Puff Pressure Containment in Eagle Ford using EDFM

by

Mauricio Xavier Fiallos Torres

Thesis

Presented to the Faculty of the Graduate School of

The University of Texas at Austin

in Partial Fulfillment

of the Requirements

for the Degree of

Master of Science in Engineering

The University of Texas at Austin

May 2019

Dedication

To my parents, **Mario** and **María**, and my sister **Carla Adriana**.

Acknowledgements

First, I would like to express my profound gratitude to my academic supervisor Dr. Sepehrnoori for the continuous guidance and support during these two years of graduate school. I am truly grateful for his interest and willingness to guide me since the very first day of my graduate studies. I would also like to express sincere gratefulness to Dr. Wei Yu for his dedication, expertise advises, and insistent valuable guidance. I will always appreciate how he shared part of his extensive expertise in unconventional reservoirs, and reservoir modeling with me. Also, I would like to thank Erich Kerr and his company for supplying the field data that made this research possible. I gained great practice and understanding through their suggestions for my research work. Their invaluable support received weekly through my entire career will always be appreciated.

There are not enough words to express how convinced I am that this would not have been possible without the support of my family. I thank my father Mario and my mother María for covering part of my tuition, and also my sister Carla Adriana for their continuous encouragement to pursue my dreams. I would like to thank Carolina for her caring love and support. I am indebted to my parents, my sister and my girlfriend who never stopped encouraging during both the good and the not so good times.

I would also like to thank Reza, Sutthaporn, Fabio, Jorge, and Esmail for their collaboration and assertive comments for my work and my research.

Finally, a very special acknowledgment is extended to the Fulbright Commission of Ecuador, the Department of State of the United States, and the Cockrell School of Engineering for being the sponsoring entities which provided me the scholarships to fund and make this accomplishment possible.

Abstract

Modeling Interwell Fracture Interference and Huff-N-Puff Pressure Containment in Eagle Ford using EDFM

Mauricio Xavier Fiallos Torres, MSE

The University of Texas at Austin, 2019

Supervisor: Kamy Sepehrnoori

Shale field operators have vested a tremendous interest in optimal spacing of infill wells and further fracture optimization, which ideally should have as little interference with the existing wells as possible. Although proper modeling has been employed to show the existence of well interference, few models have forecasted the impact of multiple inter-well fractures on child wells production and also implemented Huff-n-Puff and injection containment methods. These prognoses of the reservoir simulations abet to optimize further hydraulic fracture designs and improve the efficiency of Enhanced Oil Recovery (EOR) in unconventional reservoirs.

This thesis presented a rigorous workflow for estimating the impacts of spatial variations in fracture conductivity and complexity on fracture geometries of inter-well interference when modeling EOR Huff-n-Puff. Furthermore, we applied a non-intrusive embedded discrete fracture modeling (EDFM) method in conjunction with a commercial reservoir simulator to investigate the impact of well interference through connecting fractures by multi-well history matching, to propose profitable opportunities for Huff-n-

Puff application. In this sense, the value of our workflow relies on a robust understanding of fracture properties, real production data validation, and the add-on feature of multi-pad wellbore image logging interpretation in the process.

First, according to updated production data from Eagle Ford, the model was constructed to perform four (parent) wells history matching including five inner (child) wells. Later, fracture diagnostic results from well image logging were employed to perform sensitivity analysis on properties of long interwell connecting fractures such as number, conductivity, geometry, and explore their impacts on history matching. However, the estimation of these inter-well connecting fractures which were employed for enhanced history matching varied significantly from unmeasured fracture sensitivities. Finally, optimal cluster spacing was recommended considering interwell interference. The obtained results lead our study to the implementation of Huff-n-Puff models that capture inter-well interference seen in the field and their affordable impact sensitivities focused on variable injection rates/locations and multi-point water injection to mimic pressure barriers.

The simulation results strengthen the understanding of modeling complex fracture geometries with robust history matching and support the need to incorporate containment strategies when EOR Huff-n-Puff is implemented. Moreover, the simulation outcomes show that well interference is present and reduces effectiveness of the fracture hits when connecting natural fractures. As a result of the inter-well long fractures, the bottom hole pressure behavior of the parent wells tends to equalize, and the pressure does not recover fast enough. Furthermore, the EDFM application is strongly supported by complex fracture propagation interpretation from image logs through the child wells in the reservoir. Through this study, multiple containment scenarios were proposed to contain the pressure in the area of interest, considering more than 2000 hydraulic fractures.

The model became a valuable stencil to inform the impacts on well location and spacing, the completion staging, initial huff-n-puff decisions, and subsequent containment strategies (e.g. to improve cycle timing and efficiency), so that it can be expanded to other areas of the field. The simulation results and understandings afforded have been applied to the field satisfactorily to support significant reductions in offset fracture interference by up to 50% and reduce completion costs up to 23% while improving new well capital efficiency. Consequently, these outcomes support pressure containment benefits that lead to increased pressure build, reduced gas communication, reduced offset shut-in volumes, and ultimately, improvements in net utilization and capital efficiency.

Table of Contents

List of Tables

List of Figures

CHAPTER 1

INTRODUCTION

This thesis is a study of the application of innovative workflow to model Well Interference and Huff-n-Puff pressure containment. Special emphasis is dedicated to well interference whose impact has not been assessed during the application of Enhanced Oil Recovery (EOR) methods in unconventional reservoirs as a fundamental factor to characterize the multi well pressure response. This first chapter introduces the motivation and significance of the study, as well as a general overview of the method. The delimitations of the study are described at the end of this chapter.

1.1 MOTIVATION OF THE STUDY

Fracture hits are a common occurrence in infill drilling so that they also become the top concern in the shale development business, especially in North America, where shale producers are drilling new wells closer and closer together, and closer to older wells. For instance, the U.S. crude oil production averaged an estimated 12.1 million barrels per day as of February 2019, from which 7.46 million barrels per day were produced directly form shale oil resources. This was equal to about 61% of total United States oil production. (U.S. EIA, 2019a). Regarding natural gas, the U.S. Energy Information Administration (EIA) exposes that the dry shale gas production was 65.76 billion standard cubic feet per day as of February 2019, which represents 71% of total U.S. natural dry gas production (U.S. EIA, 2019a). This development of unconventional reservoirs has incited an exponential fever for drilling infill wells all in an effort to drain as much of the available reservoir area as possible. Because of this, characterizing unconventional reservoirs with interwell fractures often becomes a critical challenge to field development plans for

operators when related to complex inter-well interaction of hydraulic fractures with pre-existing natural fractures and heterogeneity in the reservoir. This reality is consistent with the conclusions of earlier work in which it has been unveiled that the decrease of well spacing increases the effect of well interference (Ajani and Kelkar, 2012; Kurtoglu and Salman, 2015). Therefore, these developments of shale reservoir areas and the reduction of the well spacing between infill drilling and primary producers have been demonstrated to promote the manifestation of interwell interference.

Additionally, these field development plans in unconventional reservoirs might contemplate implementing enhanced oil recovery (EOR) methods in order to increase extremely low primary ultimate recoveries (5-10% of original oil in place). One of the EOR methods that has received more attention for its greater potential in shale reservoirs is Huff-n-Puff. Through this enhanced oil recovery technique, one well alternates among injection, soaking and production cycles. Different types of gases are often employed as the enhancing fluid instead of water in unconventional reservoirs because of its high injectivity into shale rocks and its ability to develop miscibility with the shale oil. For instance, Eagle Ford, one of the main unconventional reservoirs in the world, is starting the transition from a race of drilling new wells to finding low–cost EOR methods that compete with primary development economics. Certainly, implementing EOR Huff-n-Puff strategies for shale oil exploitation depends on lower capital expenses (CAPEX), improvements in Funding and Development (F&D) costs, and favorable rate of returns. Positive economics are still achieved once fracture hit effects occur, and although there are many proven methods to reduce impacts, there is no consensus on complete prevention for infill development. As a consequence, EOR Huff-n-Puff can become a strong candidate for improving these low recovery factors in unconventional reservoirs.

In recent years, many researchers from both academia and industry have proposed different ways to identify these fractures interferences, to model them, and design field development plans according to their impact. However, fracture hits are believed to be the main culprit behind low oil recovery due to interwell interference. This interwell communication can be portrayed as "pressure sinks" that interfere with induced fracture effectiveness, and might affect unconventional EOR methods efficacy if they are overridden or not accounted for. For instance, numerous documented studies have demonstrated fracture interference occurrence and assessed this phenomenon in unconventional reservoirs (Ambrose et al., 2011; Manchanda et al., 2013; Portis et al., 2013; Sardinha et al., 2014; Sani et al., 2015; Awada et al., 2016; Morales et al., 2016; Klenner et al., 2018; Seth et al., 2018; Yu and Sepehrnoori, 2018). The current interest is focused on warding off negative impacts caused by fracture hits interwell propagation and affecting further productive wells. Most of the complex physical mechanisms of fracture hits and interwell communication have been described by current studies (Yu et al., 2016). Despite all the progress on characterizing interwell communication, there exist unresolved challenges, which need to be addressed in order to improve the understanding of fracture hits occurrence among wells and the need of enhanced reservoir resources management. In this sense, one of these unresolved challenges is related to EOR Huff-and-Puff and the existence/results of pressure leak off in different areas of the reservoir, which is the most significant in infill development areas where existing wells have experienced significant offset fracture interference from new wells.

1.2 Research Objectives

The aim of this thesis is to apply EOR Huff-n-Puff modeling in Eagle Ford reservoir, accounting for multiwell fracture interference and proper pressure containment strategies using non-intrusive embedded discrete fracture model (EDFM) methodology in combination with a commercial compositional simulator (CMG, 2018). The recommended workflow is applied to real field data from Eagle Ford reservoir to narrow down uncertainties associated with multi well induced fractures characterization and the optimal pressure containment strategies for efficient Huff-n-Puff designs.

1.3 Significance of the Study

Interwell interference by fracture hits in unconventional reservoirs has a tremendous impact on further field development plans, especially when implementing EOR methods. Reservoir simulation is a common tool to quantify the impact of multiwell fractures interference to forecast optimum recovery and to reduce uncertainty in EOR modeling. Even though there are numerous studies that address fracture interference, very few models have forecasted the impacts of these multiwell fracture interference in Huff-n-Puff modeling. Moreover, it is certainly important to remark that reservoir simulation for shale reservoirs requires proper characterization of hydraulic and natural fracture networks. An imprecise characterization would lead to the development of the wrong reservoir model and thus, misleading results would be obtained. Hence, uncertainty mitigation of fractures location and their properties is fundamental for decision making in reservoir developments, and this thesis is intended to reduce these uncertainties by the application of an innovative workflow.

In this study, the results of modeling interwell interference and Huff-n-Puff field implementation numerically, contemplating proper pressure containment strategies, are

presented using the non-intrusive EDFM methodology. Through non-neighboring connections (NNC), the EDFM can properly handle complex fracture geometries and pressure-dependent fracture/matrix permeabilities (Xu et al., 2017a, 2017b) non-intrusively. Local grid refinement (LGR) or unstructured gridding have been used to model fractures into a reservoir model but these methods are intrusive, not flexible, and anticipate high computational cost. First, a full field model was constructed considering interwell interference model that included four horizontal parent wells, five horizontal child wells, and more than twenty long interwell induced fractures and more than 2000 hydraulic fractures. This prior full model was verified and validated with proper history matching of field data parameters. The following stage of this work was to build a sector model from the validated full model in order to design and test Huff-n-Puff strategies by coupling EOR Huff-n-Puff with EDFM induced fractures communication. The latter model analyzed injection selection strategies, where scenarios with single and multiple injectors were considered through the area of the reservoir. As a consequence, this study exhibits a robust framework that couples field data with numerical simulation and the strength of EDFM to handle complex fracture geometries within lower computational costs.

From a professional standpoint, the implementation of the proposed workflow of these models into further field development, aids the operator to verify expected oil field recoveries. Also, our workflow included phase behavior analysis to switch from an initial black oil model to a compositional one due to the needs from implementing Huff-n-Puff designs even though the hydrocarbon in the reservoir corresponds to Eagle Ford black oil area. The decision of using produced gas streams as the injection fluid was supported by the availability of this resource in the field. Finally, EOR pressure communication was identified in the field by the operator via live BHP and surface gauges supporting the need for pressure containment analyses to understand and improve Huff-n-Puff efficacy.

Therefore, our model was able to characterize pressure leak off and its extent by conducting sensitivity analysis of different parameters. In this case, water injection was considered to generate barriers that provoked pressure containment in the reservoir. Water blocking is illustrated as an example in this study and has been field tested by the operator to prove effects on communication. Consequently, a robust and comprehensive model was built, for the field operators to be able to apply the workflow for further Huff-n-Puff and pressure containment analyses in other areas of the reservoir.

Similarly, a further analysis in the performance of the proposed Huff-n-Puff design through the first year of production will be helpful to validate the model and use the proposed workflow in further decision analysis of EOR implementation in the field. Moreover, it would be possible to evaluate, in detail, the cumulative oil recoveries from a reservoir engineering perspective and the rate of returns and capital efficiencies from a project finance perspective. In conclusion, the modeling assessment previously stated has never been used in the oil industry for the previously mentioned purposes, and this study produces insightful and handy findings for EOR Huff-n-Puff designs.

1.4 THESIS OUTLINE

This thesis consists of six chapters and it is organized as follows. Chapter 1 refers to introducing the scope of this work by stating the objectives, highlighting the relevance of the study, and defining the assumptions and limitations of this investigation.

Chapter 2 presents a literature review focused on previous studies about well interference modeling and huff-n-puff implementation in unconventional reservoirs. Furthermore, it provides a brief description of the Eagle Ford shale play. It also introduces wellbore image logging correlation as an innovative tool to rely on for estimating possible

fractures depth locations. At the end, a summary is presented with the most relevant concepts and descriptions employed for this thesis.

In Chapter 3, the general workflow for this study is introduced as a valuable guide in order to narrow down uncertainties when modeling Huff-n-Puff considering interwell fracture interference. First, the construction of the black oil full field model is presented. This models captures interwell interference by identifying long induced fractures. Additionally, history matching of the same full model is performed so that the considered parameters and the results are exhibited for all the wells of the model.

Chapter 4 describes the next stage of the general workflow, which corresponds to the compositional sector model construction and its validation through a consistent history match of the field data. This chapter also includes the description of the Huff-n-Puff sensitivities. These sensitivities are implemented in the sector model to define optimum parameters of injections such as number of injectors, rates of injection, injection pressure, and length of cycles. Finally, pressure containment strategies with water injection are proposed to improve efficiencies of the EOR Huff-n-Puff process in the reservoir.

In Chapter 5, this study presents an approach to evaluate the feasibility of implementing the modeled Huff-n-Puff and pressure containment design in this part of Eagle Ford reservoir in terms of Cash Flow, NPV and Capital efficiencies.

Finally, Chapter 6 summarizes the results of this study and provides recommendations for future work that potentially enhances the performance of the proposed Huff-n-Puff design considering pressure containment strategies and interwell interference.

1.5 LIMITATIONS

The boundaries and assumptions considered in this work are documented to avoid inaccurate generalizability.

- The petrophysical data obtained for the study is assumed to be representative of Eagle Ford field in the black oil window.
- All the employed wellbore image logs are already interpreted by a company service. Thus, this study relies on the well preprocessing of these logs.
- Hysteresis is not considered in this study when implementing different cycles of Huff-n-Puff.
- The PVT properties of our reservoir fluids are characterized based on information provided by the operator.

CHAPTER 2

LITERATURE REVIEW

Chapter 2 outlines comprehensive literature review of important related topics in the context of this research. These topics include definitions and concise descriptions of the Eagle Ford shale reservoir, fracture hits and well interference in unconventional reservoirs, and EOR Huff-n-Puff mechanisms and its opportunities from a field recovery performance point of view.

2.1 EAGLE FORD

A general background of the geological features and production history of the Eagle Ford reservoir is presented. Eagle Ford has become one of the major producers of shale oil and gas, transforming the economic and physical environment of southeast Texas. The following information has the purpose to introduce and summarize the general characteristics of the reservoir from which field data that is available. Also, this information serves as a foundation for the input of the simulation models used by the researcher to study and characterize the reservoir. Thus, a description of the Eagle Ford shale is presented in order to define the scope area of this study.

2.1.1 Reservoir Location

The Eagle Ford shale play is located in south central Texas, in the Gulf Coast Basin and comprises of Cretaceous sediments with an average thickness of 250 feet that spans 50 miles wide and 400 miles long, covering 30 counties (U.S. EIA, 2016a). This formation gently dips to the south east so that it can be found at vertical depths that range between 5,000 to 15,000 feet (Figure 2.2). Furthermore, this reservoir has four major boundaries according to the U.S. Energy International Agency: 1) the international border to the west, 2) a northern boundary above a minimum subsea depth of 3,650 feet to Frio County and

Maverick and Zavala counties, 3) a southern boundary that traces the Early cretaceous Sligo Reef margin, and 4) a north eastern boundary where the lower Eagle Ford thins and grades into more silica rich-units of the Pepper Shale of the East Basin (Cardneaux, 2012; Hentz et al., 2014). The Railroad Commission of Texas (TRRC) has updated a map with the current location of the wells in Eagle Ford (Figure 2.1).

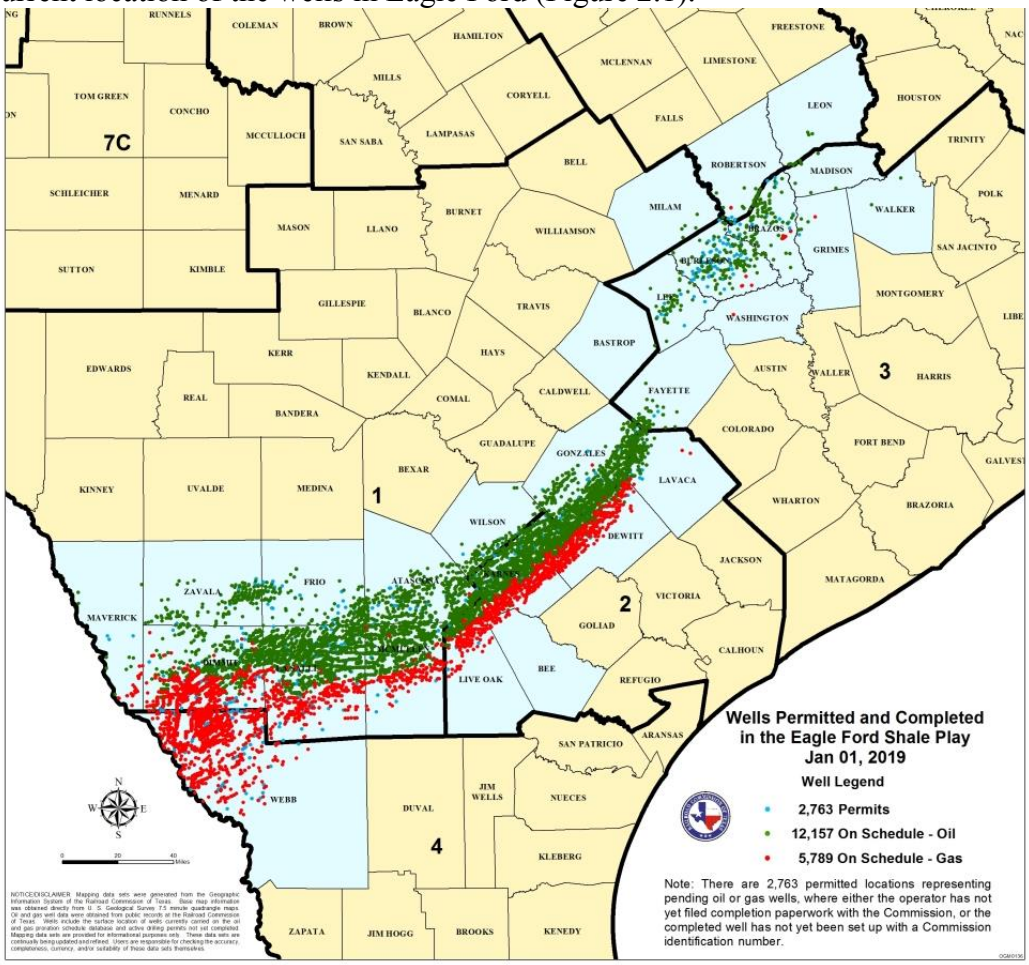

Figure 2.1: Map of wells permitted in the Eagle Ford shale and the counties of Texas through which it crosses (TRRC, 2019).

2.1.2 Summary of Eagle Ford Geology

The Eagle Ford shale is a hydrocarbon-bearing, Late Cretaceous formation that was deposited in a marine continental shelf environment. This formation consist of organic-rich calcareous-mudrock with mineralogy ranging from 40-90% carbonate minerals, 15-30% clay, and 15-20% silica (quartz) (U.S. EIA, 2014). The total organic carbon content (TOC) ranges from 2 to 12%, the thermal maturity (%Ro) is 0.45 to 1.4%, porosity is 8-12%, and pressure gradient is 0.5-0.8+ (psi/ft.) (ZaZa Energy, 2013). Furthermore, the Eagle Ford lies above the Buda Limestone and unconformably below the Austin Chalk (Parra et al., 2013). The shale is named for the town of Eagle Ford, Texas, approximately 6 miles west of Dallas, Texas, where it can be seen on the surface as clay soil. An outcrop of the Eagle Ford Shale can be seen in the Dallas-Fort Worth Metroplex.

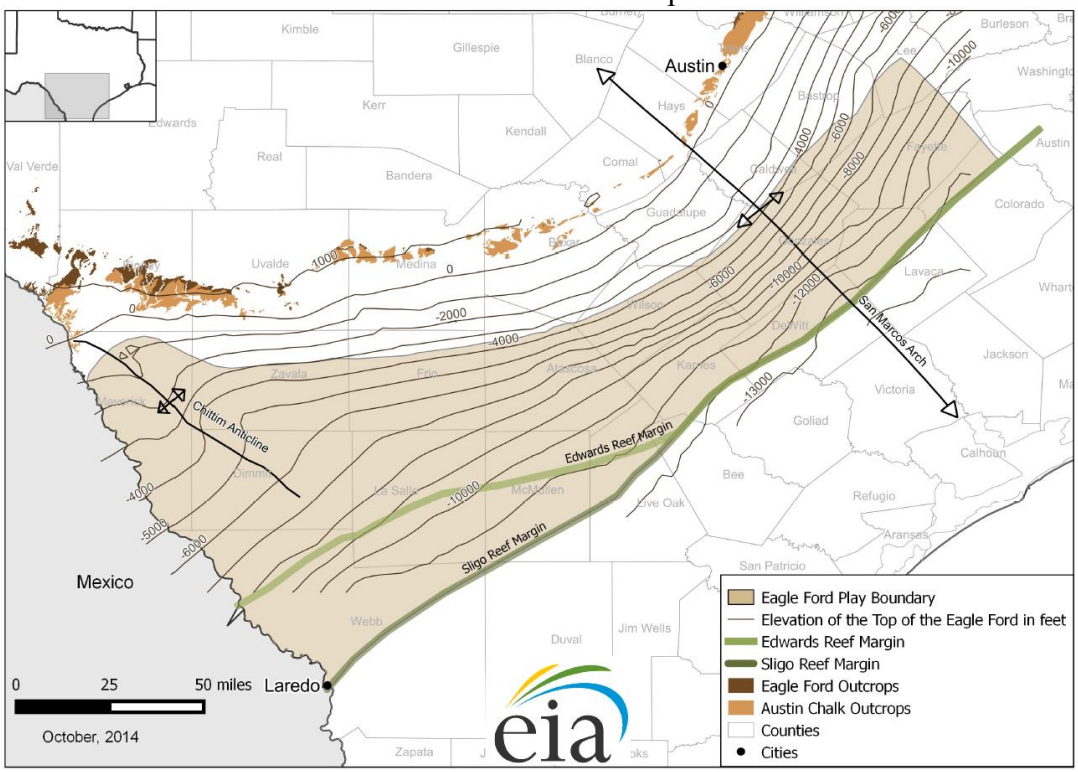

Figure 2.2: Map of the Eagle Ford Play boundaries, in the Western Gulf, Texas (EIA, 2019).

2.1.3 Eagle Ford Fluid Regions

Three main types of hydrocarbons are found in the Eagle Ford shale: oil, wet gas / condensate, and dry gas are identified and cumulated in different regions as seen in Figure 2.3. API gravity ranges from 28° to 62° (U.S. EIA, 2014). Additionally, there exist some minor areas that contain volatile oil. Thus, the distribution of initial GORs from this unconventional play generally depends on the depth of the reservoir. Deeper wells (up to 15,000 feet) to the southeast have higher initial GORs, or a relatively greater share of natural gas. On the other hand, the shallower wells to the northwest (below 600 feet) have lower initial GORs, or a relatively greater portion of oil. This study considers modeling just a window of the black oil area of Eagle ford reservoir, where field data was available.

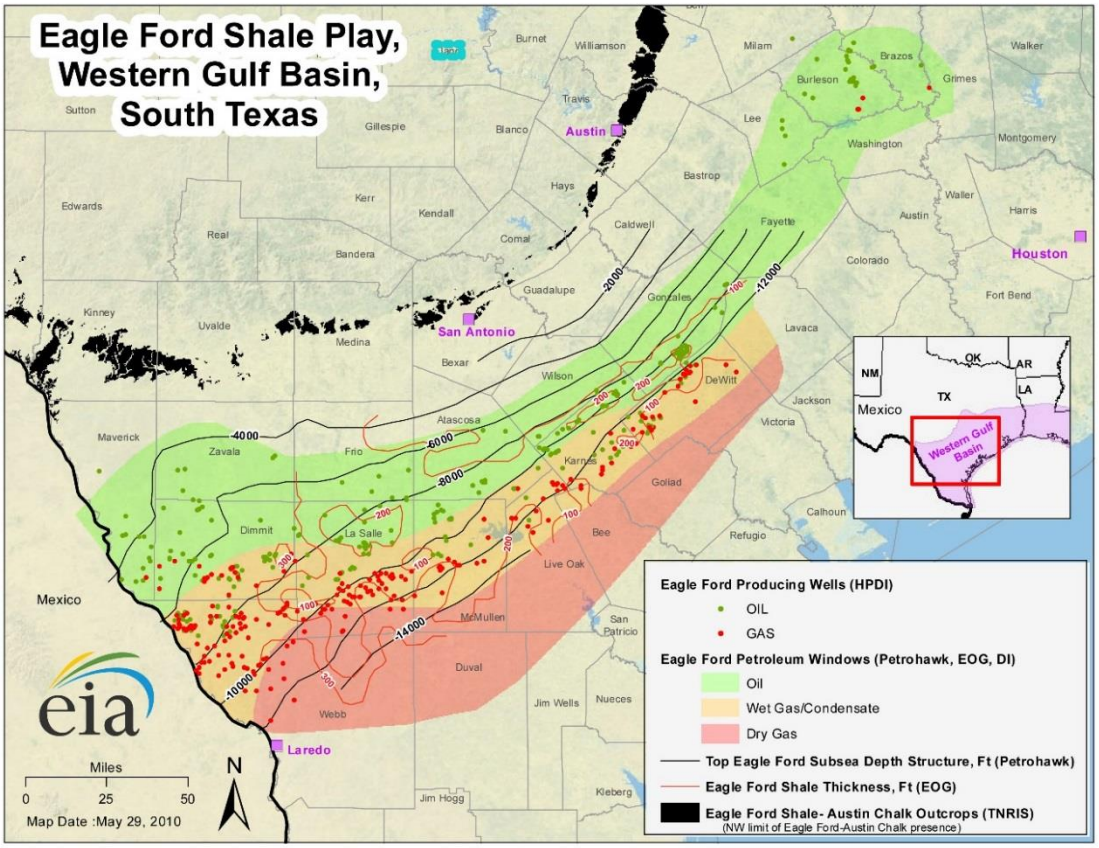

Figure 2.3: Eagle Ford map showing the different petroleum and agas windows (EIA, 2010).

2.1.4 Field Background

The Eagle ford shale contains about 6 billion barrels of technically recoverable oil and 32.1 trillion standard cubic feet of technically recoverable natural gas. (U.S. EIA, 2019a). Since development started in 2008, the Eagle Ford shale has become one of the most active drilling areas of the world. The well production varies widely across the reservoir. The average estimated ultimate recovery (EUR) for the Eagle Ford is 168,000 barrels per well (U.S. EIA, 2019b). Production has ramped up since 2017 as oil and gas prices are rising up. The average production for the year end 2018 was 843,606 BPD (TRRC, 2019). Due to confidentiality purposes, this thesis will name the oil field of study as Omega which considers a nine-well section of the black oil window of the Eagle Ford reservoir. In particular, this section of the Omega field, which started production in 2012, has a cumulative production at May of 2018 of 997 MBLS during its primary recovery.

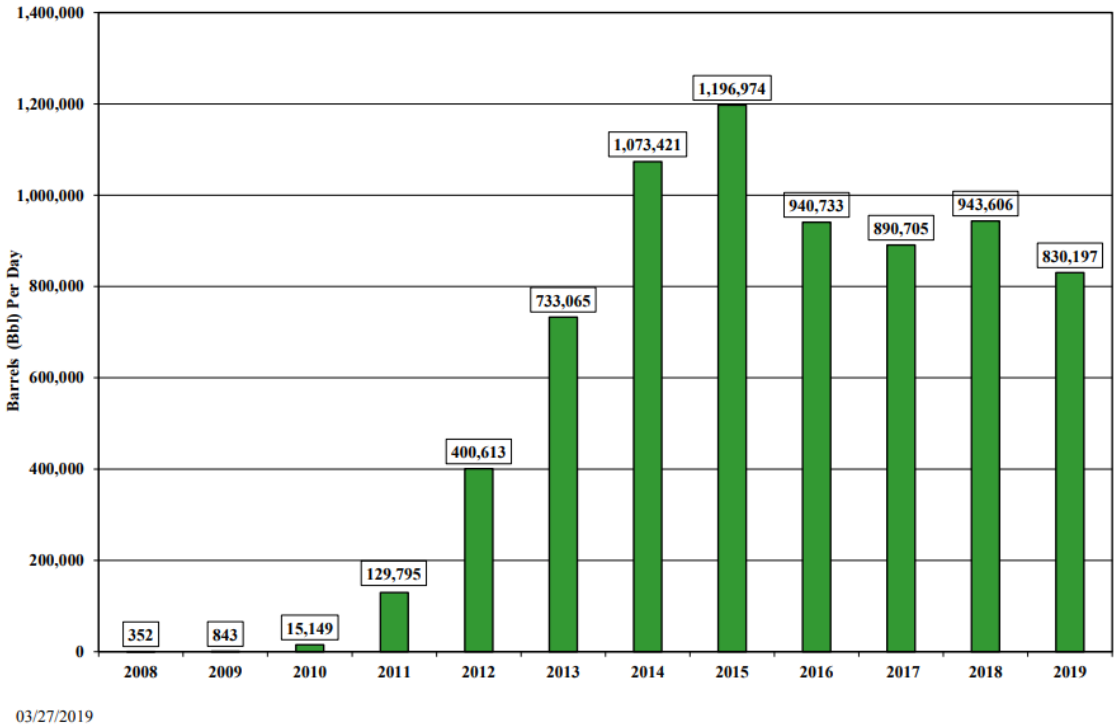

Figure 2.4: Eagle Ford oil production since 2008 through January 2019 (TRRC, 2019).

2.2 FRACTURE HITS

2.2.1 Fracture Hit Definition

A fracture hit is defined as an interwell communication occurrence where an offset well (parent well) is affected by a hydraulic fracturing treatment in a new well (child well). Martinez et al. (2012) addressed the concept of pressure sinks from previously stimulated and depleted parent wells area, which then generate a path of least resistance for a nearby and subsequent stimulation. These fracture hits might lead to mild, severe or complete production impairment of the primary well (Martinez et al., 2012). It is also known that complex fractures hits can have a detrimental effect on the production behavior of child wells because of different factors, such as the reduction of hydraulic fracture length/width and loss of fluid (Manchanda et al., 2013). In fact, it is known that these fracture hits can be strong enough to damage production tubing, casing, and even wellheads (Jacobs, 2017). The actual mechanisms that lead to these productivity deficiencies may encompass the removal of considerable portions of the proppant from the fractures in the near-wellbore region of the parent well and/or wellbore failures due to tension, lateral compression, axial compression, shear and/or bending as shown in Figure 2.5 (Morales et al., 2016).

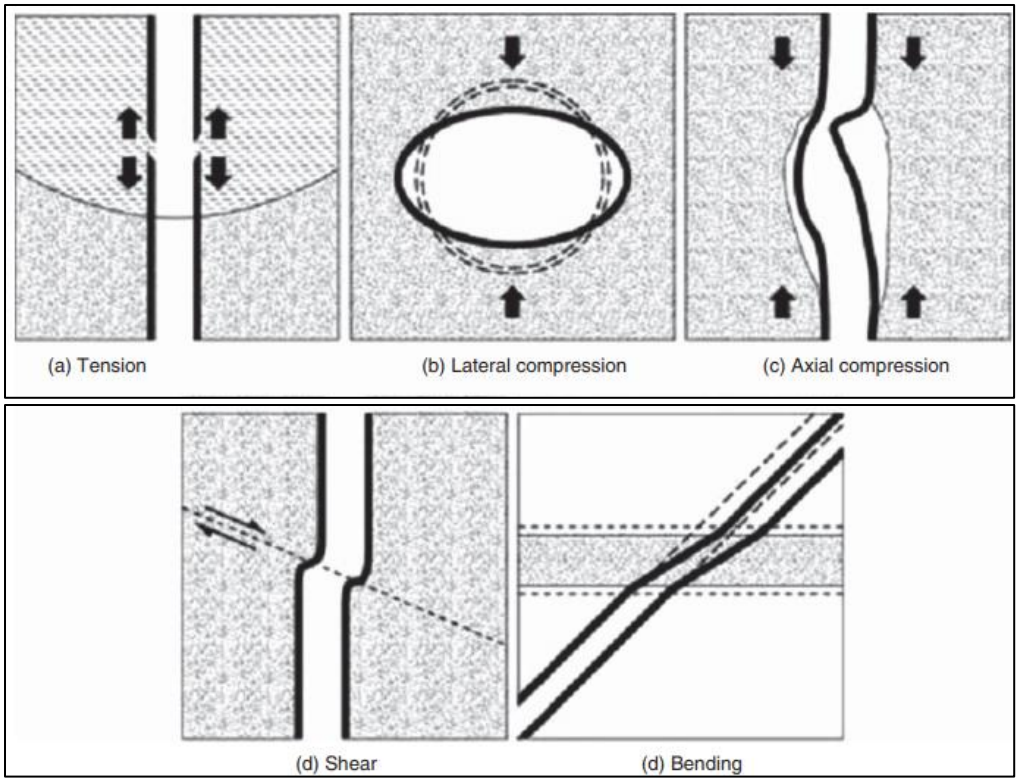

Figure 2.5: Possible fracture hits induced wellbore failure scenarios: (a) due to tension, (b) lateral compression, (c) axial compression, (d) shear, (e) fracture bending (Veeken, et al., 1994).

This study emphasizes that the general connotation of a fracture hit should always be negative, regardless of the degree of formation depletion, residual fluid saturation, wettability, or relative permeability.

2.2.2 Fracture Hits Characterization

Fracture hits need to be characterized in magnitude and duration in three types: as fracture shadowing hits, direct hits, and variable hits (Sardinha et al., 2014). The first group of hits is defined by pressure and/or stress, and has a gradual increase and declines almost immediately after the fracturing is complete (Figure 2.6.). The second type refers to direct hits, which are the result of the direct transfer of fluid between two fractures, showing a large pressure spike during the shut-in well after beginning the fracturing (Figure 2.7).

Lastly, the third group is variable hits, showing unstable fluctuations in pressure at the shut-in well (Figure 2.8). Furthermore, two main parameters should be considered when defining fracture hits, time and location. During the fracture treatment, fracture hits can be observed and monitored in offset wells. On the other hand, during production a fracture hit is identified when the pressure gradually decreases and drops to less than the closure pressure, closing any unpropped communication channels (Awada et al., 2016). The fracture hits characterization can provide an insight of the strength of the interaction among different wells. Regarding pressure-hit distances, studies demonstrated that they can reach up to 1500 m for an average pressure increase of around 420 psi (Sardinha et al., 2014).

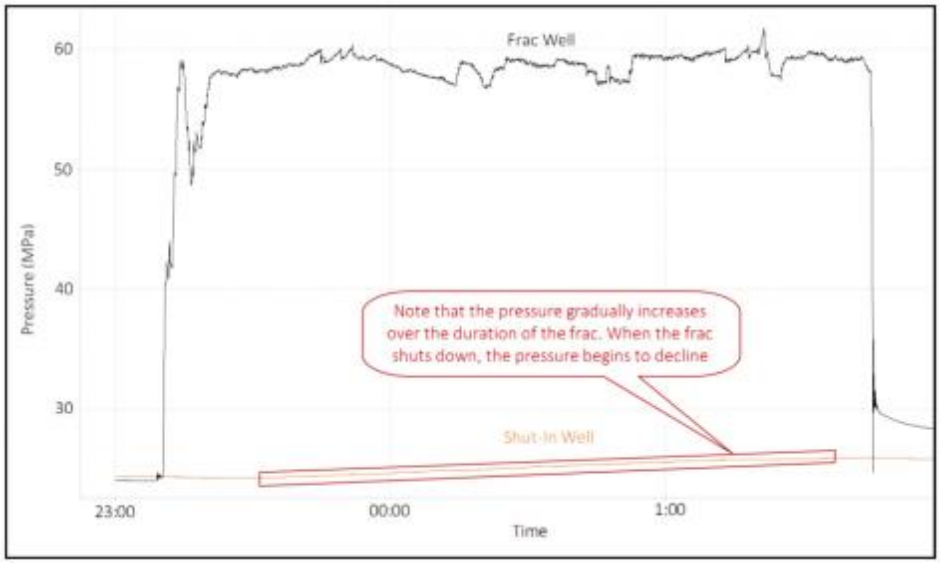

Figure 2.6: An example of fracture shadow (Sardinha et al., 2014).

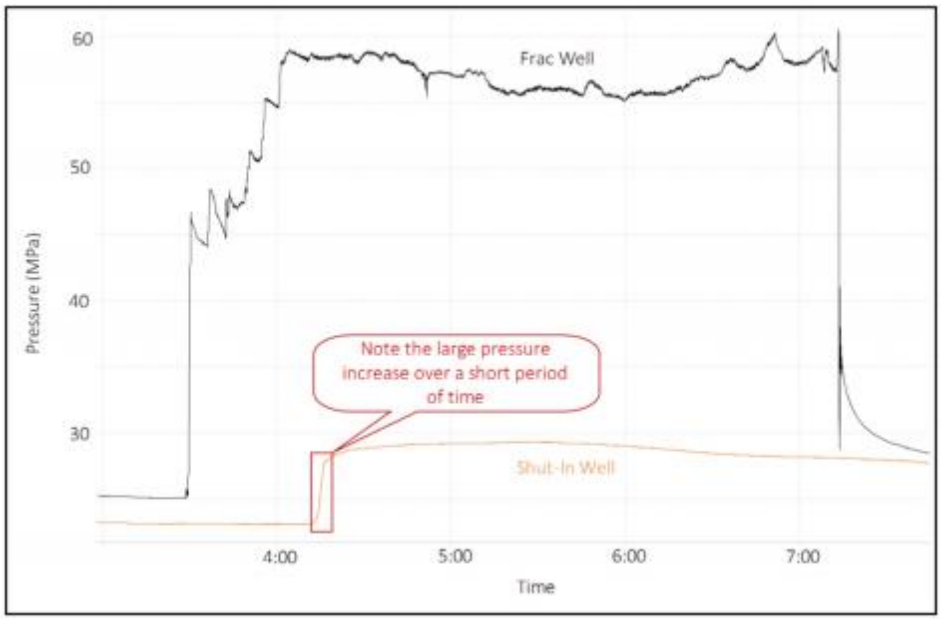

Figure 2.7: An example of direct hit (Sardinha et al., 2014).

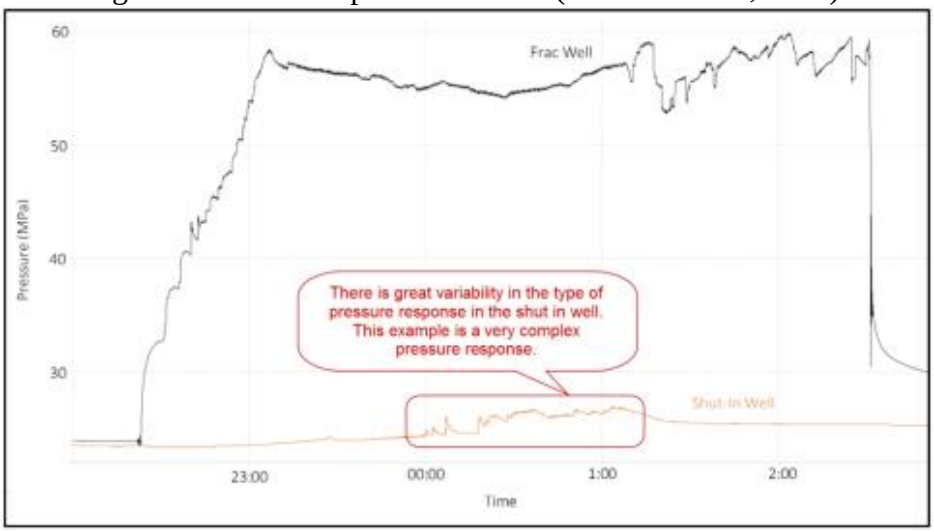

Figure 2.8: An example of variable hit (Sardinha et al., 2014).

Nonetheless, differentiating these kinds of pressure hits can become trivial when lower-magnitude direct hits occur. It is important to highlight that the degree of connectivity may not have a direct correlation to the type of hit, but more to the magnitude and frequency of the pressure interactions. Therefore, misinterpretation should be avoided when connectivity is related to the characterization of the fracture hits.

2.3 INTERWELL INTERFERENCE

Extensive studies have been conducted to demonstrate interwell communication. Awada et al. (2016) concluded that the fracture hits and fracture fluid production that suddenly appear at offset producing wells are indications of communication, but they do not necessarily imply that a strong connection will be preserved throughout the life of the wells. Sardinha et al. (2014) showed that the majority of pressure hits were found between adjacent or near-adjacent wells, so that each well delivered a high hit percentage to at least one other well in their neighboring pad, and often exhibited a strong connection with several wells even through different formations. Interwell connectivity can be evaluated with complex stimulated network using the "fracturing wave" technique, which quantifies a representative degree of pressure interactions during hydraulic stimulation in a prescriptive order, and progressing the fracturing process in pad wide sequence. As a consequence, general workflow (Figure 2.9) considers that interference mechanism needs to be defined first. Next, analytical simulations should be performed to reveal the expected behavior for interference through fractures and reservoir matrix. Next, buildup trends changes could be foreseen, so that finally, the data could be history matched with numerical models to confirm the interference mechanism (Awada et al., 2016).

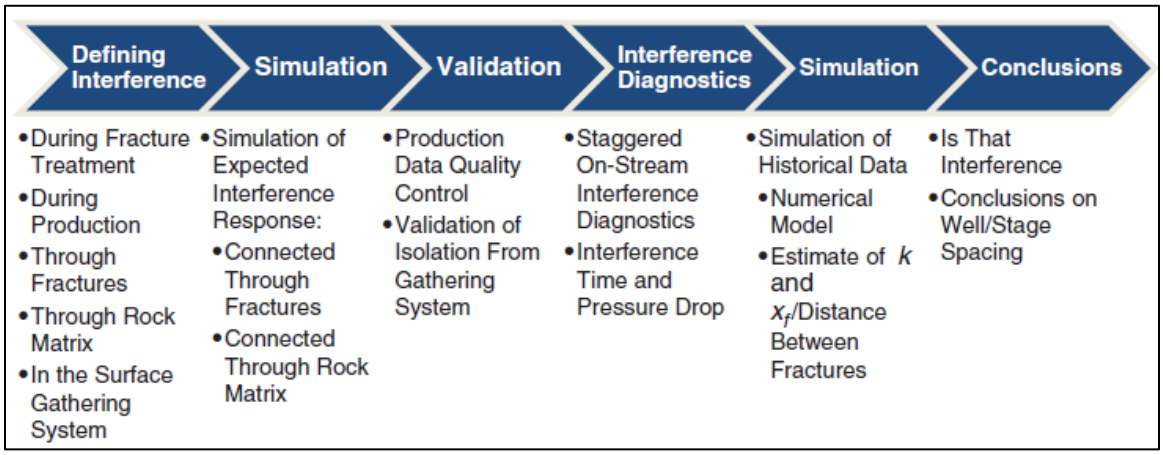

Figure 2.9: Workflow to identify interwell interference (Awada et al., 2016).

Further studies, at geomechanics and 3D wellbore simulation level, exhibited some satisfactory results of a fully-coupled 3-D finite volume geomechanical reservoir model which employs fracture modelling explicitly as open and compliant channels (Seth et al., 2018). In fact, mechanical stress interference is present between fractures, generating a perceptible impact. For instance the simulation results demonstrated that hydraulic fracture propagation towards the monitor well causes changes in stress on the monitor fracture. Closure and opening of the monitor fracture is clearly related to the increase/decrease in pressure in the monitor well fracture. Consequently, these pressure changes are due to elastic effect of mechanically squeezing the monitor fracture by the propagation of the hydraulic fracture, confirming interwell fracture interference occurrence (Figure 2.10).

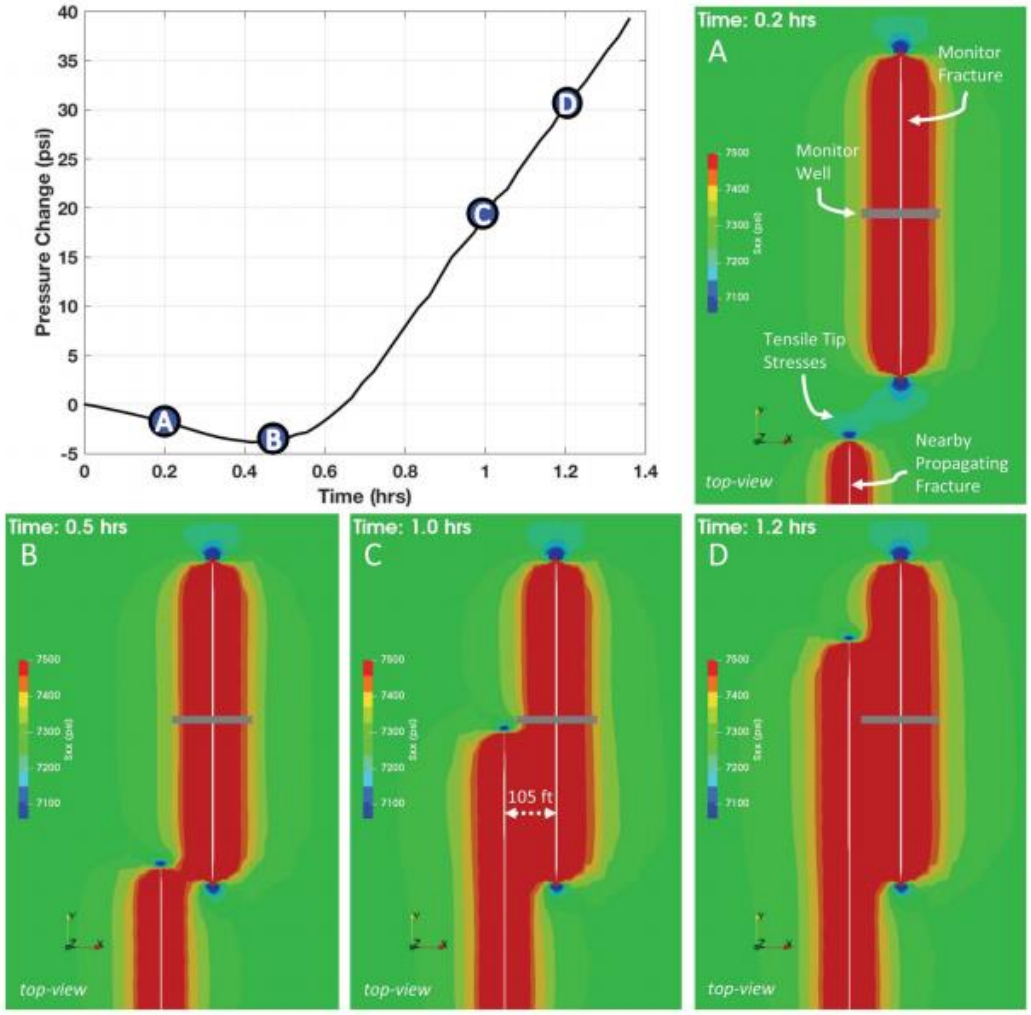

Figure 2.10: Example of pressure change observed in the monitor fracture due to stress changes that it experiences during fracture propagation from the treatment well (Seth et al., 2018).

Other studies found that during initial flowback, the pressure analysis is used to map the effective-interwell network development as it lessens over time (Sardinha et al., 2014). This has been corroborated with micro-seismic data (Figure 2.11), which shows a high degree of hydraulic fracture overlap and interaction between wells (Sardinha et al., 2014). This study only considered the interference diagnosis in order to use in further simulation models.

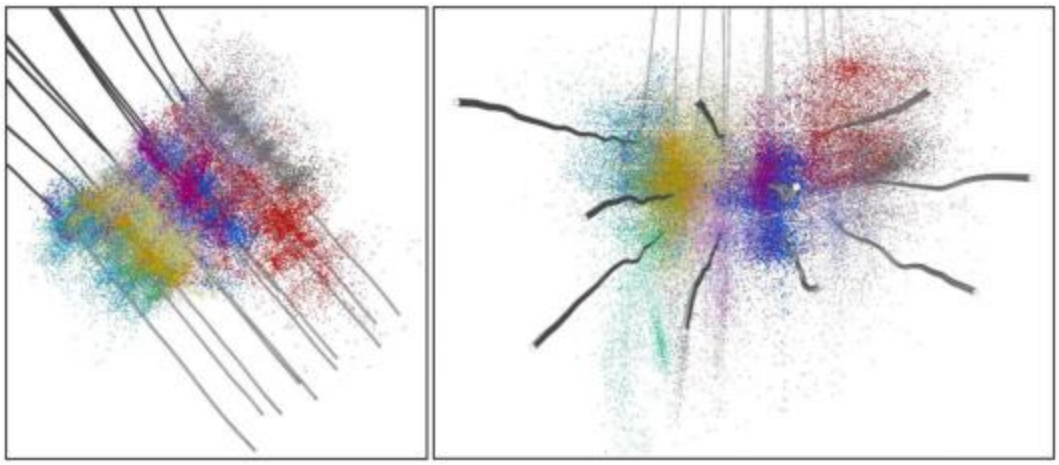

Figure 2.11: Microseismic events showing hydraulic fractures overlapping among wells (Sardinha et al., 2014).

Additionally to the progress on identifying and representing interwell interference by fracture hits, some new technologies have arrived to help to attain better description of interwell communication phenomena, and have been implemented with field data. Some studies focus on new models that reduce uncertainty and capture interwell interference and fracture hits propagation more accurately (Yu et al., 2016; Seth et al., 2018; Wu et al., 2018; Klenner et al., 2018, Fiallos et al., 2019). The purpose of the new approaches is to improve unconventional reservoir characterization and operational efficiency. Regarding pressure-hit distances, studies demonstrated that they can reach up to 4900 ft. for an average pressure increase of around 420 psi (Sardinha et al., 2014). For instance, interwell fracture communication can be assumed to occur after proper correlation of Well Bore Image (WBI) logs among different wells (Fiallos et al., 2019). As a consequence, interwell interference can be identified and analyzed with the integration of data diagnostics, production analysis, and pressure transient analysis.

2.4 EMBEDDED DISCRETE FRACTURE MODELING (EDFM)

EDFM provides efficient solutions to model complex fracture geometries in terms of reliability, flexibility, and simulation run time as exposed in different studies (Moinfar et al., 2012; Shakiba and Sepehrnoori, 2015; Zuloaga-Molero et al., 2016; Xu et al., 2017a, 2017b, 2018; Yu et al., 2018a, Fiallos et al., 2019a, 2019b). By using the EDFM method, each fracture plane in the reservoir is discretized into smaller fracture segments using the matrix grid block boundaries so that these fracture segments are embedded into extra virtual grid blocks that are added to the original matrix grid (Xu et al., 2017a, 2017b ; Yu et al., 2018a). This fracture construction constitutes the preprocessing in which the EDFM method assigns non-neighboring connections (NNCs) and/or effective wellbore indexes among the additional virtual grid blocks. Therefore, these NNCs are used to mimic the physical flow associated with these fracture segments and the matrix grids in different commercial reservoir simulators (Xu et al., 2017a) A simplified workflow is shown in Figure 2.12.

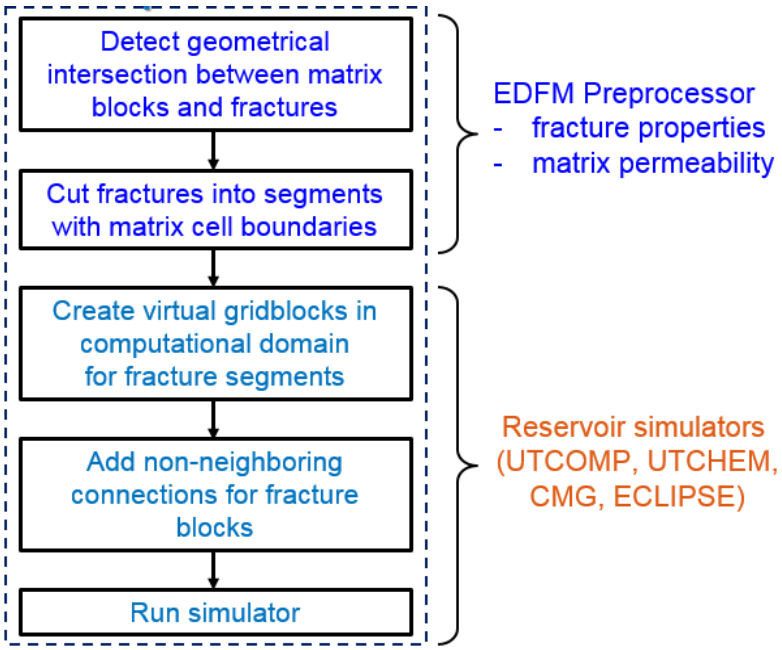

Figure 2.12: EDFM preprocessing workflow (Xu et al., 2017a)

The EDFM method is superior when comparing with traditional fractured numerical simulation methods such as Double Porosity/Double Permeability (DPDK), Local Grid Refinement (LGR), and Unstructured Grids models in terms of accuracy, flexibility, gridding, and computational efficiency (Xu, 2018). Accuracy accounts for the quality of the model regarding the degree to which the specification of the fracture design conforms to the expected performance. Flexibility is related to the quality of the model when replicating complex geometries and orientations of the fractures. Also, gridding stands for how the model is able to handle the structure of the grid cells geometries. Finally, computational efficiency is associated to the time and computational resources that are needed to use when running these different types of numerical simulation models. As observed in Figure 2.13, the EDFM method exhibits better performance after compelling different case studies where each comparison is executed (Xu et al, 2017, Yu et al, 2018). For example, unstructured grids are complex to generate due to the larger amount of refined grid cells around the fractures (more powerful parallel computing) than what EDFM uses.

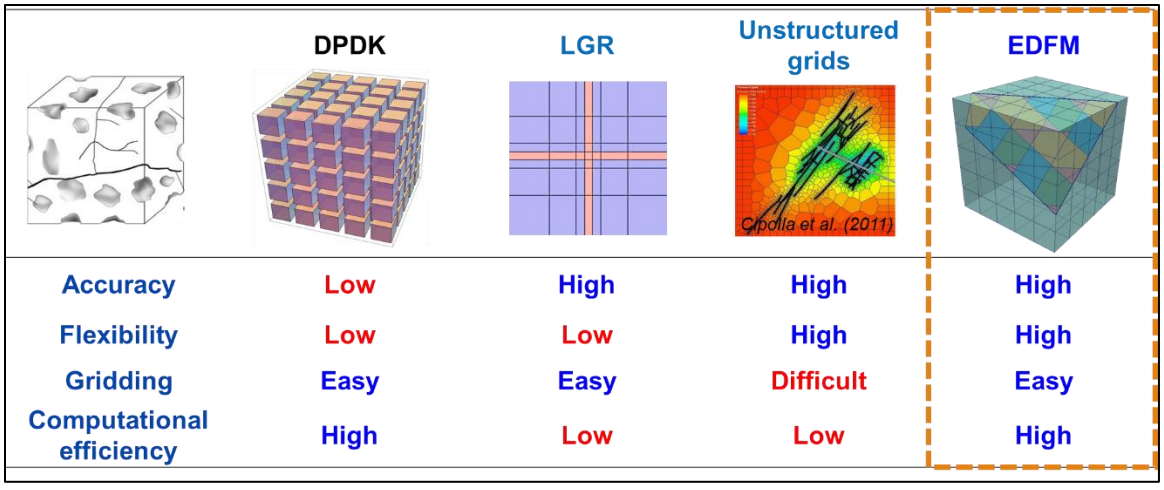

Figure 2.13: Comparison of the performance between EDFM and traditional fractured simulation methods in terms of accuracy, flexibility, gridding, and computational efficiency (Xu, 2018).

In particular, EDFM considers four types of connections among fractures, matrix and well (Xu et al., 2017a), as shown in Figure 2.14. For instance, its computations include the flow between matrix grid blocks and the corresponding fracture segments, the flow between fracture segments (same single fracture), the flow between intersecting fracture segments (crossing fractures), and the flow between the fractures and the wellbore. The following equation describes the transmissibility factor for the first three kinds of connections (Xu et al., 2017a):

$$T_{NNC} = \frac{k_{NNC} A_{NNC}}{d_{NNC}}, \tag{1}$$

where:

k_{NNC}: Permeability associated with the connection

A_{NNC}: Contact area between the NNC pair.

d_{NNC}: Distance between the NNC pair.

Likewise, the effective well index for the fracture-well connection is calculated by employing a modified Peaceman equation as follows:

$$WI = \frac{2\pi k_f w_f}{\ln\left(\frac{r_e}{r_w}\right)}, \tag{2}$$

$$r_e = 0.14\sqrt{L^2 + W^2}, \tag{3}$$

where:

k_f: Fracture permeability

w_f: Fracture aperture

r_w: Wellbore radius

L: Length of fracture segment

W: Height of the fracture segment

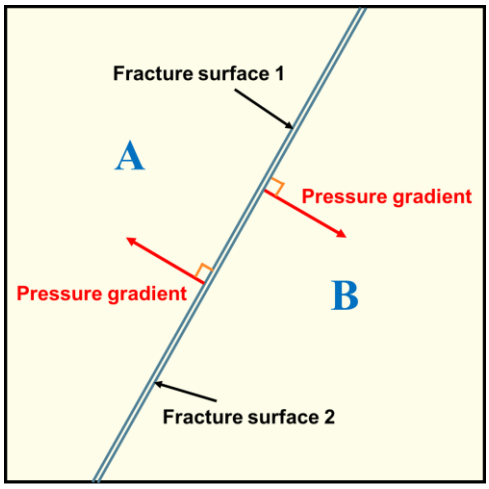

(a) Flow between matrix grid blocks and the corresponding fracture segments

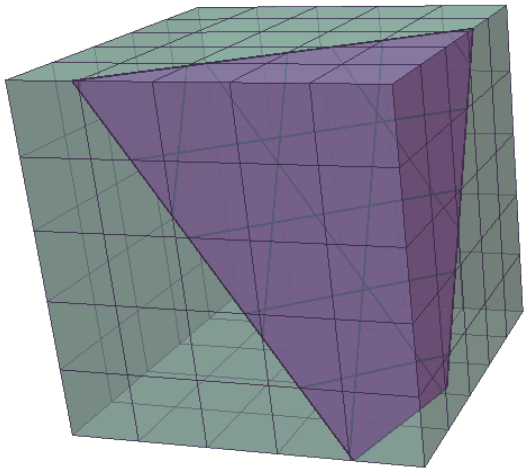

(b) Flow between fracture segments in the same single fracture

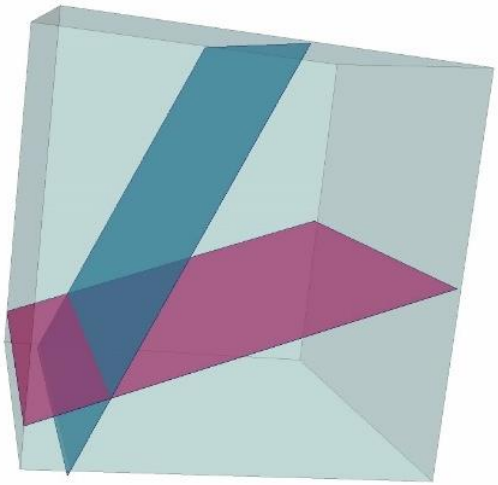

(c) Flow between intersecting fracture segments

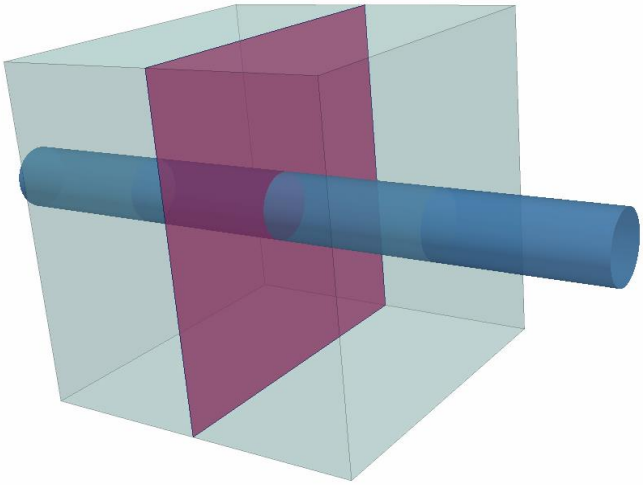

(d) Flow between the fractures and the well

Figure 2.14: Four types of connections among fractures, matrix and well by the EDFM method (Xu et al., 2017a).

These four types of connections can be illustrated in the example shown in Figure 2.15, where “Fracture 1” crosses through three grid blocks (1-3), and a smaller one “Fracture 2” stays within one cell block. Therefore, first, EDFM discretizes the fracture planes by the cell boundaries of the matrix and creates additional cells (number 1 to 3).

Then it adds extra grid block (number 4 to 7) the original grid mesh. On the computational domain, NNCs are generated between the cells that have contact in the spatial domain as shown by the different arrows, estimating transmissibility between them.

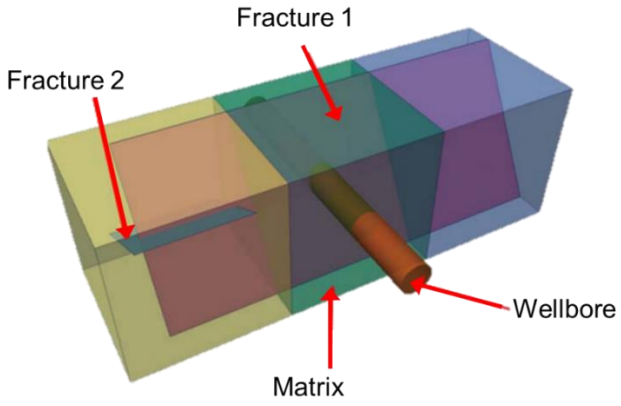

(a) Spatial domain

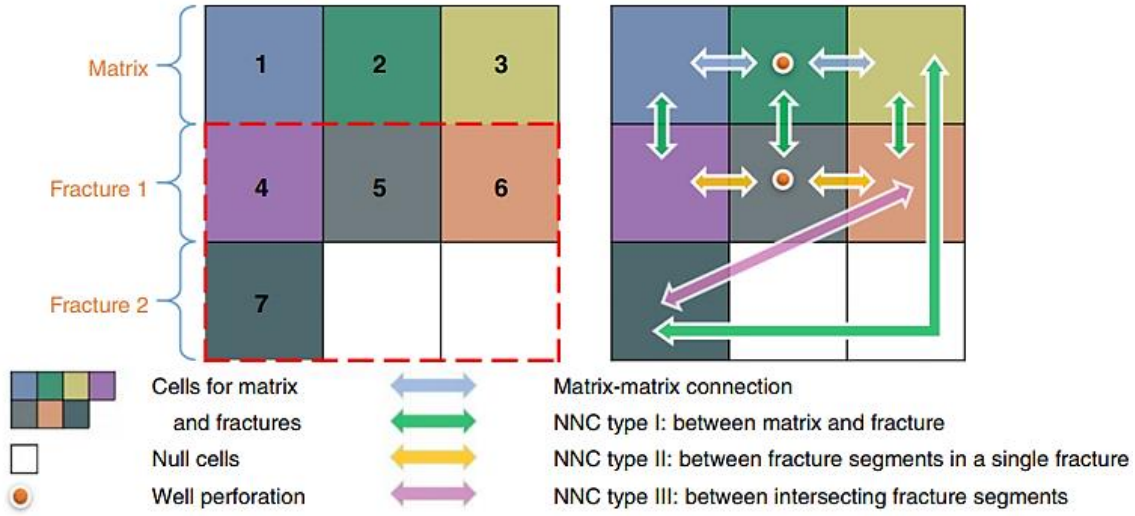

(a) Computational domain

Figure 2.15: Explanation of EDFM principle to process any complex fracture in 3D (Xu et al., 2017a)

Consequently, the EDFM method becomes a non-intrusive technology that can work for any reservoir simulator with non-neighbor connections and provides reliable efficient representation of fluid trough complex fractures modeling.

2.5 WELLBORE IMAGE LOGS

Ultrasonic image data processing can be a powerful tool to identify fractures in unconventional rocks around the wellbores in the reservoir. Borehole imaging has been one of the most rapidly advancing technologies in wireline well logging. Data acquired from an LWD acoustic imager tool can provide high resolution borehole images and borehole caliper while drilling in oil and water-based mud systems. Applications include: fracture detection, analysis of borehole stability, and identification of breakouts. Although the ultrasonic amplitude image does not have sufficient resolution away from the wellbore compared to the resistivity image for quantitative characterization, this kind of image log is still suitable enough for identifying larger scale features such as faults, drilling induced longitudinal fractures, bedding planes, and previously induced hydraulic fractures. In fact, individual large-scale open fractures can also be identified from ultrasonic image (Xian et al., 2018). Therefore, deterministic fractures are observed using WBI logs and fracture corridors that are directly imaged through ultrasonic image logs.

2.5.1 Static and Dynamic Image Quality Control

Standard quality control (QC) on ultrasonic wellbore image (WBI) logs interpretation needs to be performed. It is important to be cautious of the image quality over the intervals with severe hole collapse, or washout. An example of fracture detection for the Eagle Ford black oil area is shown in Figure 2.16, where ultrasonic WBI of well W5H denotes an evident fracture at a depth of 9093 ft., and where the Azimuth frequency (rose diagram) plots were used to identify the preferential direction of the dips of the open fractures in the borehole. When steep dips caused by fractures are isolated from lower angle bedding dips, the direction of maximum stress can be determined. Fractures usually

penetrate the formation in a plane parallel to the maximum stress. In this example, the direction is N30W.

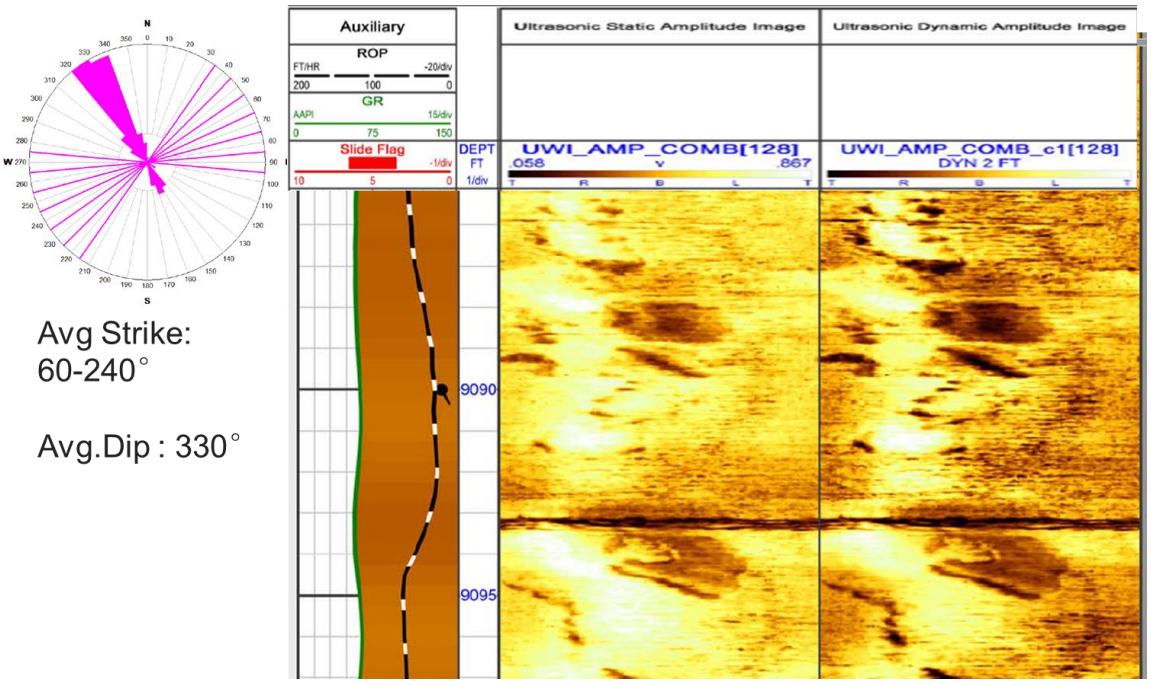

Figure 2.16: WBI logs QC where a fracture can be distinguished and general assumptions for Eagle Ford black oil fractures orientation: rose plot (top left purple), gamma ray (left track, shaded brown), ultrasonic static amplitude image (middle track), ultrasonic dynamic amplitude image (third track from left), standoff image (right track).

The quality of the model relies not only on the most accurate inputs, but also on the best interpretation. Further in this study, we will discuss how WBI interpretation was fundamental to estimate probable location of interwell fractures in the reservoir. These interwell fractures added great value to the reservoir modeling process since they create complex paths for fluid movement which impact reservoir characterization, and ultimately, production performance and total recovery.

2.6 HUFF-N-PUFF EOR

Huff-n-Puff Enhanced Oil Recovery is an advanced oil field development strategy that can be used to bolster unconventional fields where other EOR methods would be ineffective due to their very low permeabilities (Gunter and Longworth, 2013).

2.6.1 Fundamentals and Background of Huff-n-Puff

Huff-n-Puff has been defined as a cyclic process in which a well is injected with a recovery enhancement fluid (e.g. rich/lean gas) –"the huff– and, after an optional soak period, the very same well is put back on production –"the puff "– (Schulmberger, 2019). The process that drives the incremental recovery is based on the transport phenomena by which the gas interacts with the in-situ liquids and is likely a component of both advection (Darcy's law) and diffusion (Fick's Law). Over the last decade, numerous studies have been dedicated to Huff-n-Puff (Wan et al., 2013; Chen et al,.2014; Yu et al., 2014; Zu et al., 2015; Hoffman and Evans, 2016; Kanfar et al., 2017; Alharthy et al., 2018; Hoffman and Rutledge, 2019). In fact, in Eagle Ford, Huff-n-Puff pilots have also exhibited tremendous success over the last decade, but challenges remain as flow rates drop quickly and recovery factors are low (Hoffman and Evans, 2019). Likewise, experimental work has verified significant increments in recoveries from different simulation studies. High recoveries have been achieved in core flooding experiments using cores from different shale formations and different injected fluids (Kovscek et al., 2008; Song and Yang, 2013; Gamadi et al., 2014; Sorensen et al., 2015; Yu et al., 2016; Li and Sheng, 2017). However, most of these studies considered hydraulic fractures with ideal properties, which in reality, are not possessed by the hydraulic fractures due to different stimulation designs or implementation problems. The scope of this thesis does not cover any experimental core analysis.

In fractured reservoirs, such as the Eagle Ford, the gas may flow from the injectors to the offset producer wells directly via fractures without sweeping through the matrix (channeling), which can leave behind billons of reserves. Furthermore, cyclic gas injection is used to mitigate the adverse impact of fractures in this situation, as the process involves injecting gas and producing oil through the same well at different time intervals (Jin et al., 2016). In particular, the benefits of this EOR method include physical recovery mechanisms such as reducing oil viscosity, swelling the oil volume, and vaporizing and extracting hydrocarbons from oil (Jin et al., 2017). Also, many other variables contribute to the EOR efficiency related to the primary completions and reservoir fluid dynamics, which are not part of the scope of this study.

2.6.2 Huff-n-Puff Mechanisms

Multiple factors and mechanisms are behind Huff-n-Puff for increasing oil recovery. For instance, the injected gas will dissolve into the oil triggering it to expand and expel the oil back into the fractures. This mechanism is known as oil swelling. Additionally, other mechanisms such as oil viscosity reduction, increase in reservoir pressure, inmiscible and /or miscible flow according to minimum miscibility pressure (MMP), surface tension reduction, and vaporization and extraction of oil components by the injected gas may occur (Fragoso et al., 2018), but they are expected to have less impact for the liquid rich portions of unconventional reservoirs. Nonetheless, the main process for the injected gas entering the matrix and causing additional oil recovery has not been well identified by academia or industry.

2.6.3 Injected Gas Penetration into the Matrix

Two processes are assumed to be the main culprit to describe the transport phenomena by which the injected gas can enter into the matrix: diffusion and advection. In

contrast to conventional reservoirs, where diffusion/advection ratio is so small that can be neglected, unconventional reservoirs may be influenced by diffusion in the same proportion as by advection.

2.6.3.1 Diffusion – Fick's Law

The diffusion behavior can be simplified and described by Fick's second law in one dimension (Hoffman and Evans, 2019):

$$\frac{\partial C}{\partial t} = D\frac{\partial^2 C}{\partial x^2}, \tag{4}$$

where:

C: Concentration of the solute (injected gas) (fraction)

D: Diffusion coefficient (m^2/sec)

While C is a function of the distance from the fracture and t is time, the diffusion coefficient, D is a function of the solute, the in-situ fluid, and in this case, the porous media. Experimental results have exhibited that diffusion of injected gas into unconventional oil reservoirs is possible, but difficult to estimate (Vega et al., 2010; Hawthorne et al., 2013; Tovar et al., 2014). Furthermore, gas-into-liquid diffusion is much slower than gas-into-gas diffusion. Although this thesis acknowledges the diffusion physical phenomenon, it is not incorporated since the employed numerical simulation relies only on advection phenomenon.

2.6.3.2 Advection – Darcy's Law

During gas injection, the fractures are filled by the gas that flows into matrix due to a pressure drawdown. The linear, transient Darcy flow equation describes this process. In order to estimate amount of gas entering the reservoir matrix for a unit fracture area analytically, Hoffman and Evans (2019) presented the following equation derived from Lee (1982)

$$q = 0.345 \frac{\left(P_{inj} - P_r\right)}{\beta} \left(\frac{k\phi c_t}{\mu t}\right)^{\frac{1}{2}} \quad (5)$$

where:

P_{inj} : Injection pressure (psi)

P_r: Reservoir pressure (psi)

q: Flow rate (STB/day)

β: Formation volume factor (rb/STB)

k: Permeability (md)

ϕ: Porosity (fraction)

c_t: Total compressibility (1/psi)

μ: Viscosity (cp)

t: Time (hours)

2.6.4 Limitations of Huff-n-Puff

While Huff-n-Puff was conceived long time ago, it is not widely employed because of certain limitations. One the challenges of Huff-n-Puff EOR implementation is the acquisition of sufficient injection gas. In this sense, there are many experiments related to defining optimal recoveries with different injection gases such as CO_2, rich gas, lean gas (>95% C1), or nitrogen. All of these depend on the injecting gas availability and feasibility. Likewise, another challenge is the interruption of production that shale oil wells need to confront. Operators may set lower-producing wells to become EOR Huff-n-Puff pilots, expecting greater production performance and less impact when shutting-in these kinds of wells; however, other considerations include well landing zones, total rock surface areas (influenced from completion design), offset development strategies, fluid, and cycling options to name a few. Finally, another challenge is defining the in situ fluid composition

in order to establish the minimum miscibility pressure. After five years of production, the uncertainties about residual fluid composition will have certainly increased.

2.6.5 Pressure Leak off Extension Characterization

Characterizing the pressure leakage in the reservoir due to fracture reactivation is a current challenge for unconventional reservoirs with natural induced fractures. This phenomenon happens when injected gas moves so fast throughout fractures that it becomes too difficult to interact with stranded oil in the matrix. This occurrence is supported by the assumption of fracture reactivation in the Eagle Ford shale. This means that pre-existing fractures reactivate once fluids are injected with high pressure into the unconventional reservoir. The mechanism behind this fracture reactivation might be fracture shear-dilation or shear-slip. As stated by Taron et al. (2014), permeability is allowed to evolve under several constitutive models tailored to porous media and fractures considering dilation among other physical phenomena in a ubiquitously fractured medium. In fact, the application of shear dilation concept leads to stimulated reservoir volume that is dependent on the changes in pressure through time (Mittal et al., 2015). Hence, for unconventional fractured reservoirs, natural fractures reactivation might lead these natural fractures to acquire high conductivity features. Therefore, the injected gas will experience less exposure time with the formation and the banked oil, before it is produced back (Alfarge et al., 2018) or before it migrates to further zones of the reservoir. Consequently, in cases of high communication, the injected gas only penetrates in limited areas around the high conductivity fractures in the shale reservoir and bypasses most of the oil trapped in the matrix.

2.7 SUMMARY OF CONCEPTS

In summary, overall, one of the objectives of this thesis is to model multiple well interference in the Omega field and validate it with history matching. The research methods to prove the previous hypothesis and the results are presented in Chapters 3 and 4, respectively. Because Omega field, as mentioned above, is located in the black oil window of the Eagle Ford reservoir, an introduction to the location and geological framework of this important shale play is offered to the reader. Likewise, relevant concepts regarding interwell fracture interference and EOR Huff-n-Puff are described in detail in this chapter.

Chapter 2 familiarizes the reader with a theoretical background that is the support of the thesis and the research objectives that are investigated. The writer brought out the most relevant points related to the thesis, portraying the relevance of the Eagle Ford unconventional reservoir and emphasizing in the configuration of the full field model to an area within the black oil fluid region of this reservoir.

Then, a review explained the main reasons for the presence of fracture interference in unconventional reservoirs, which may cause detrimental performance to parent wells for subsequent infill drilling that occur within current industry field development plans in shale plays. This interwell fracture interference is blamed for impairing recovery efficiencies for both infill child wells production and EOR projects. Interwell fracture interference can be modeled, as mentioned, according to discrete fractures observed from well image logs. The concepts of WBI were introduced to base the fundaments and improve induced fracture identification on assumptions and discrete categorization of fractures explained in upcoming Chapter 3.

To preprocess complex fracture designs in the reservoir, reservoir engineers have numerical characterization tools such as the EDFM method, for prior assessment of modeling projects. The specific workflows and advantages of this non-intrusive technology

for modeling fractures were discussed and contrasted with traditional methods of different fracture generators. Therefore, an added value to this academic work is related to the application the emerging EDFM method in commercial simulators for multiwell numerical models of unconventional reservoir, as proposed in this thesis.

Finally, this thesis reviews basic concepts of Huff-n-Puff as a brief description that will be used to frame and design EOR field application in different forecasting sets. These Huff-n-Puff designs and forecasts scenarios will be explained in detail in further chapters. Furthermore, the concepts of advection and diffusion are also explained and their physical importance to mimic the flow from fractures to the matrix of the reservoir with the aim to relate them with the expected numerical solutions provided by the commercial simulators. Likewise, the physical mechanisms, such as oil swelling and viscosity reduction among others, by which EOR Huff-n-Puff can be beneficial to improve oil recoveries are presented as hypothesis. They will support the computational numerical solutions that describe the efficiency of this EOR method in the reservoir dynamics. Also, the limitations associated to this enhanced oil recovery are exposed so that the reader can constrain and frame its application to proper conditions. Finally, pressure leak off through communicating fractures is briefly described by remarking the impact of high fracture conductivities which lead to the injected gas to bypass most of the oil trapped in the matrix.

CHAPTER 3

METHODS

Chapter 3 presents the methods and processes used to study the impacts of multiwell facture interference when implementing EOR Huff-n-Puff modeling and pressure containment strategies to the black oil region of Eagle Ford. A novel robust simulation workflow is recommended in this chapter, which aids to narrow down uncertainties about the location and the properties of fractures, as well as the Huff-n-Puff optimum strategies. During this research, special emphasis is given to the analysis of geological wellbore image logs correlation for the identification of complex interwell fractures, whose modeling includes EDFM preprocessing, numerical simulation, and sensitivity analysis. Furthermore, history matching is performed to validate the simulation model with the field data. Finally, EOR pressure containment is studied to estimate the impact of implementing this EOR Huff-n-Puff in Eagle Ford from a field recovery performance point of view. The research methods have been reproduced in different iterations in order to be adapted according to the needs of the thesis.

3.1 General Workflow and Context

Since the uncertainties of interwell fractures characterization were dominant in the model, a general workflow is proposed to validate the simulation results with the field data. Thus, this study followed the workflow described in Figure 3.1. The process starts with preprocessing and generation of the fractures through the EDFM method. This fracture generation was based on correlating ultrasonic Well Bore Image logs interpretation to allocate fractures in each available wellbore and propagate them through the model. Later, this preprocessing was coupled with the numerical commercial simulator in order to

perform a dynamic characterization of this part of the reservoir for both a full field model and a sector model. Next, a history matching process comes to place based on different sensitivities of fracture properties such as fracture heights, fracture half lengths and fracture conductivities. Once history matching is achieved, the sector model is robust enough to start forecasting scenarios of EOR Huff-n-Puff injection. Finally, pressure containment strategies were required to be evaluated in order to improve Huff-n-Puff efficiencies and recoveries. The process became iterative when it needed to be readjusted. Therefore, long interwell fractures geometries and properties were recalibrated, as well as the whole process, in order to find validated solutions to the Huff-n-Puff and pressure containment.

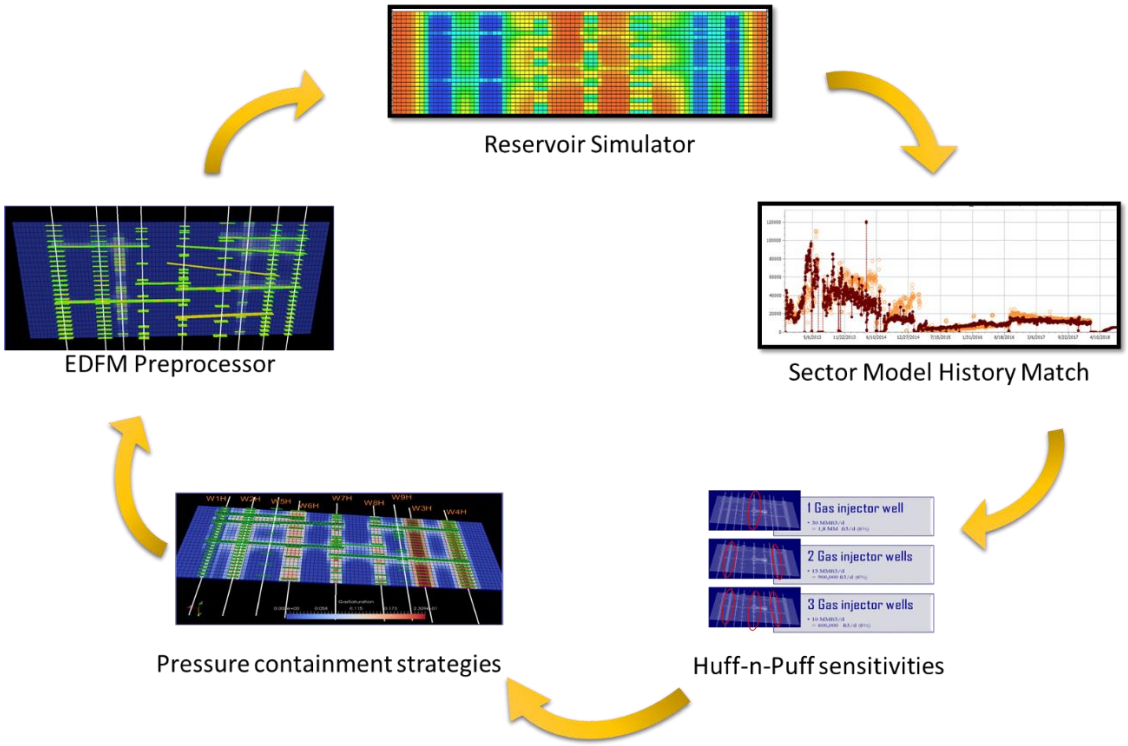

Figure 3.1: General workflow used to characterize the sector model for Huff-n-Puff pressure containment strategies.

The analysis of the multiple well fracture interference involves not only a quantitative perspective but also a qualitative scrutiny of the results. This work could be

categorized as a correlational research because it allows testing of expected relationships between and among fracture properties and/or reservoir variables, and the making of numerical forecasts regarding BHP and oil recoveries. The implications of the multiple well fractures interference aids to hypothesize about their effects on flow performance observed in the field. Alternatively, a secondary research type used in this written work is the descriptive approach because it uses inferential figures to analyze the data and provide a relatively complete picture of what is occurring at a given time. Moreover, the descriptive research is exposed as case studies for each numerical simulation that fits a fair good history match.

3.2 DATA ANALYSIS

The research was possible because of the availability of data from the Omega Field. Data from nine wells were available from the operator that included daily observed production rates (oil, water and gas), pressure data (THP and BHP), well stimulation designs, and petrophysical interpretation (WBI logs). Likewise, reservoir fluid PVT information was accessible as well as relative permeability curves for gas, oil and water, which will be discussed further in this chapter.

Two conceptualizations to represent the fracture systems are shown in Figure 3.2, in which (a) displays a more realistic fracture geometry description with fractures branching, splitting and creating complexity due to variations in rock structure, while (b) is a simpler representation with a series of parallel fractures. As long as the surface of the two systems is the same, their behavior will be similar but simplified in the model. The reason for this assumption is that at very short early times of the well, the system will present a transient flow regime, but once the pressure hits the non-flow boundary, the systems will move to a pseudo-steady state (PSS) flow regime. For both systems, (a) and

(b), PSS will be obtained. However, the only difference is that (a) will exhibit a transition flow regime (between transient and PSS), which is a function of the different sizes and shapes of the matrix blocks (Hoffman, 2019).

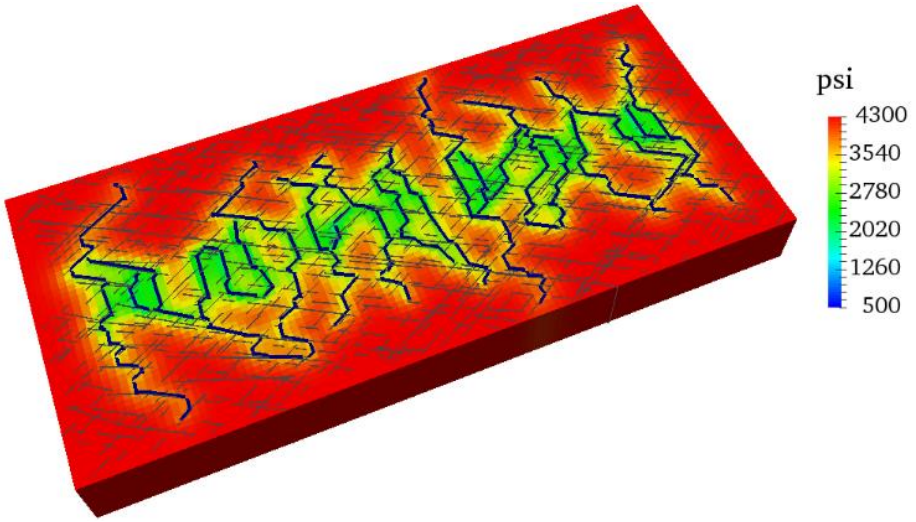

(a)

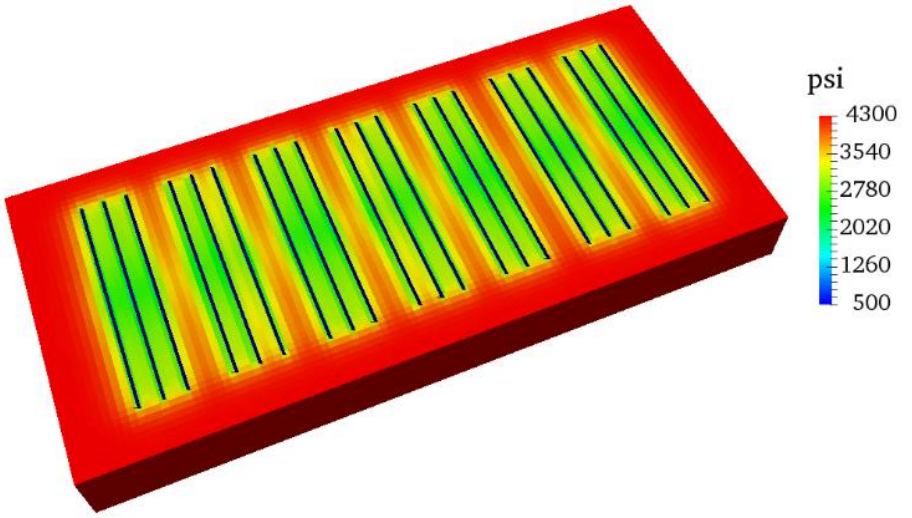

(b)

Figure 3.2: Simplification of complex fracture geometries into planar fractures when the surface of both systems are the same. (a) Realistic geometry description with fractures branching, and/or splitting. (b) Simpler representation with a series of parallel fractures. (Yu et al., 2018)

3.3 Fracture Identification by Wellbore Image Logs

Available ultrasonic image data processing is applied to identify fractures for the first time in unconventional shales around the wellbores of multiple child wells in the Eagle Ford reservoir. The operator provided the whole interpretation of the image logs corresponding to the child wells. For instance, the provided petrophysical WBI interpretation included gamma ray logs, ROP, LWD Ultrasonic Static and Dynamic image logs, interactive dip angle, and stereonet plots (see Figure 3.3).

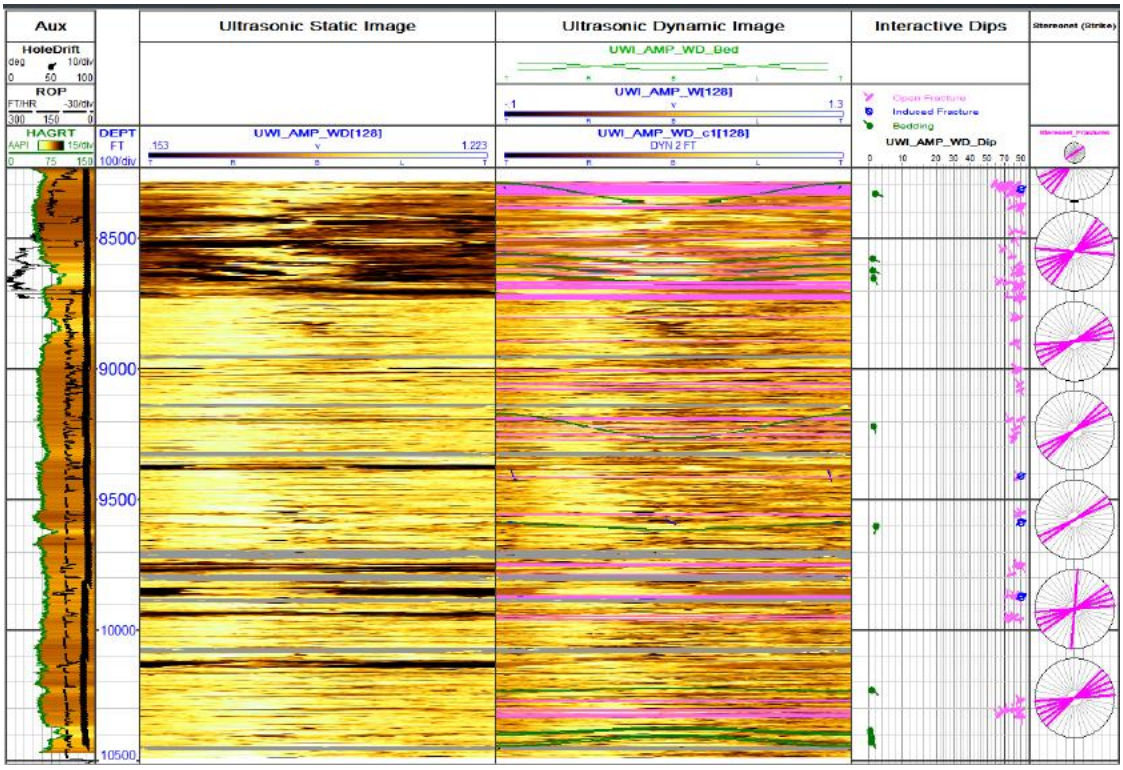

Figure 3.3: An actual example of LWD Ultrasonic WBI logs used to identify fractures location around the wellbore.

For this process, we examine the allocation of fractures in the reservoir based on correlating the depth of fractures seen in available ultrasonic WBI among different wells. For example, wellbores W7H, W8H, and W9H exhibit a clear fracture at similar depths (8,455 ft., 8,457 ft., and 8,458 ft.) as show in Figure 3.4.

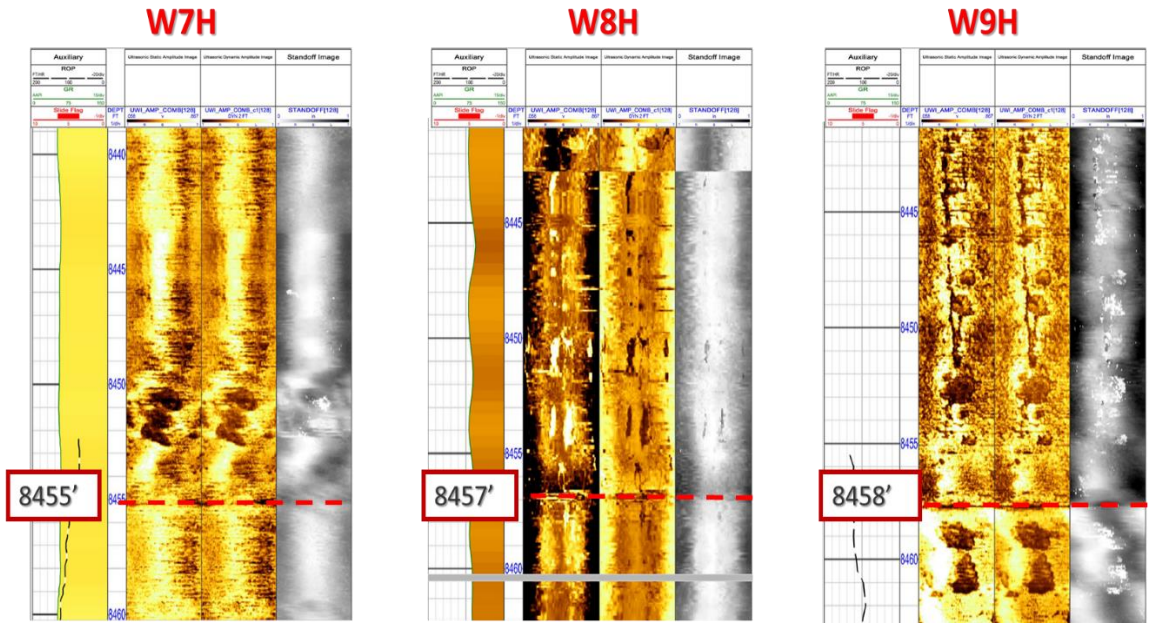

Figure 3.4: Fracture depth correlated among W7H, W8H, and W9H at 8,455 ft., 8,457 ft., and 8,458 ft. respectively.

As a consequence, the correlations are propagated all through the whole reservoir model after exhaustive quality control (QC) of the available wellbore images logs (see Figure 3.5). The identified fractures are categorized as evident or very weak. As such, the fractures whose interpretation is very clear will be considered as part of the future fracturing design plan for the child wells as seen in Figure 3.6. In this correlational figure, a color discretization is performed based on the fracturing design plan on the left and the fracture identification from WBI on the right. Thus, for every well on the left side, color green is given to planned perforations, while red belongs to the skipped perforation within the operations planning. Likewise, on the right side, green color denotes very distinct fracture marker on WBI, while red shows not clear fracture or very weak, due to reasons such as stick-slip in the tool (from the tool stabilizers, for instance), increased rates of penetration (reducing resolution due to less sampling points per area), unpropped fractures (reduced aperture size), or filled natural fractures. Moreover, for this particular case, the

planar fracture propagations are also supported by previous studies in Omega field with history matched 3D GOHFER geo-mechanical models and post-frac distributed temperature sensor (DTS) warm-back studies, and as well with previous unconventional shale mine back studies where planar fracture behavior was observed (Ambrose, 2011).

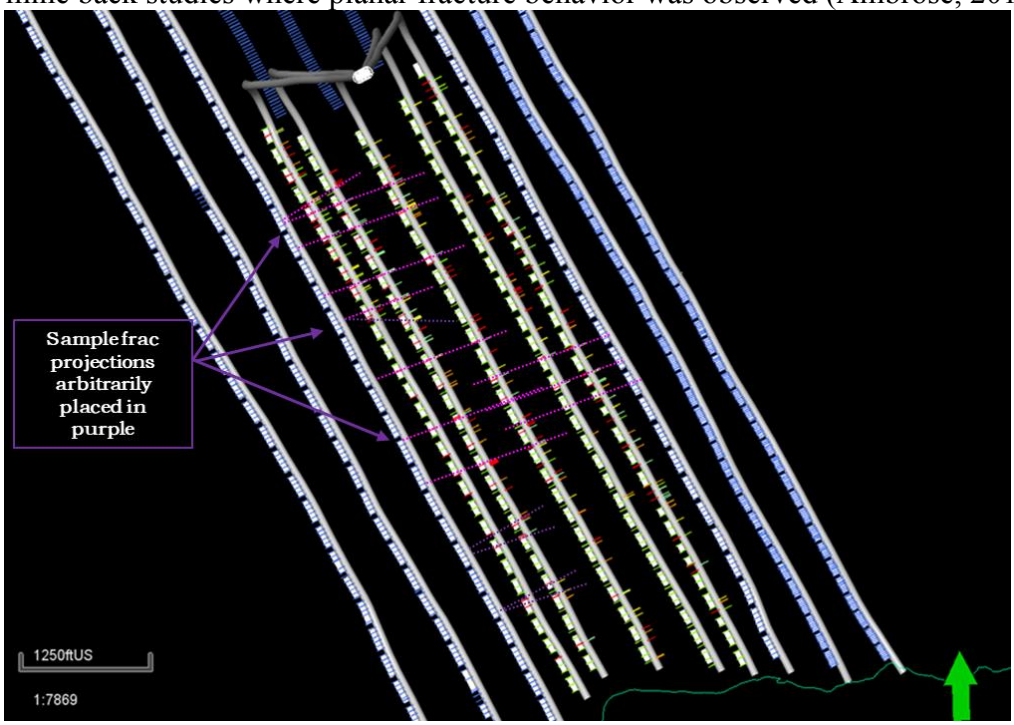

(a)

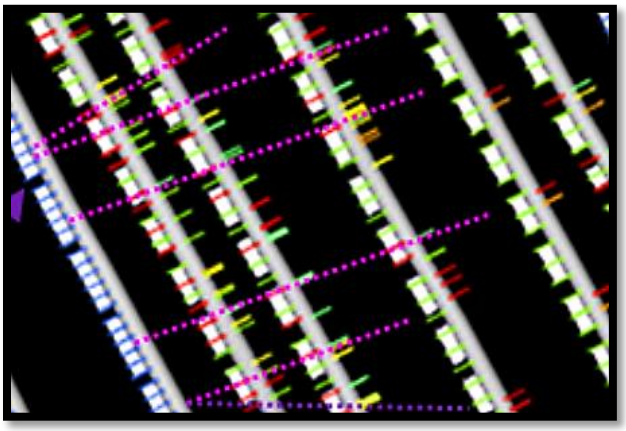

(b)

Figure 3.5: (a) Initial fracture depth correlations through the reservoir model. Purple line denotes possible induced interwell fracture. (b) Zoomed section showing the fracture categorization and the correlation.

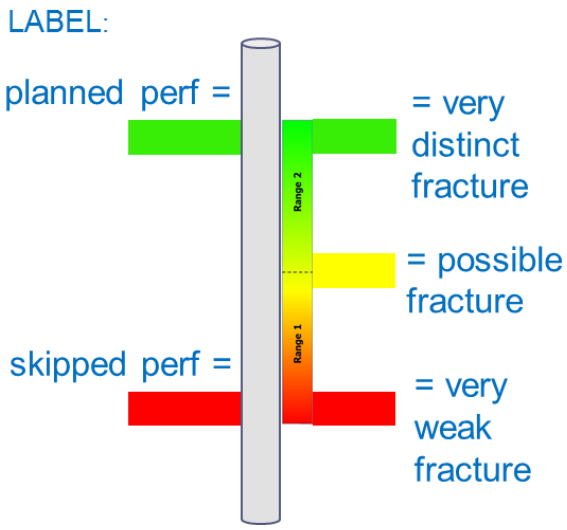

Figure 3.6: Fracture categorization after QC of WBI logs. Left side: green = planned perforation, red = skipped perforation. Right side: green = very distinct fracture marker on log, red = very weak distinction

Because every naturally fractured reservoir is unique, the combination of this systematic approach, optimal fracture models can be achieved. Through this approach, fracture characterization can be improved across all scales of operation, enhancing competency and performance in many areas including well planning, drilling and production optimization.

3.4 Multiple Well Fracture Interference in Eagle Ford

Initially, a black oil model was constructed for representing the interwell interference identified in an actual area of the Eagle Ford shale reservoir with updated available five-year production and pressure data. The location of the simulated reservoir corresponds to the images shown in Figure 3.7**,** in which the yellow box specifies the boundaries of the model projected on the surface of the field.

(a)

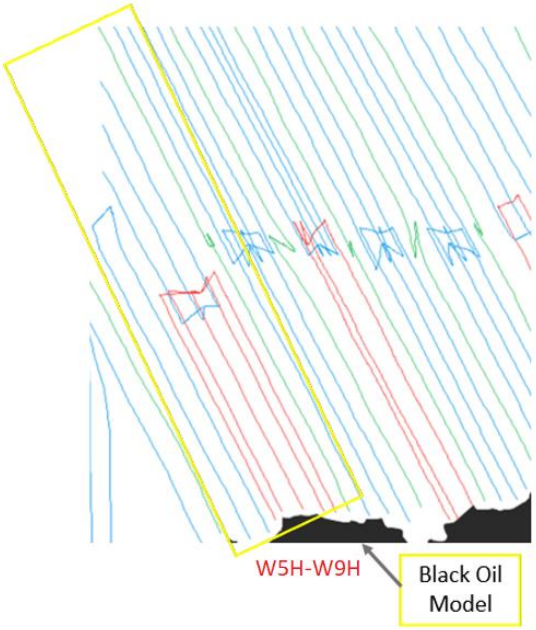

(b)

Figure 3.7: Well location in the Eagle Ford shale. (a) Actual black oil study area, the model was limited as the yellow boundaries are displayed; (b) Four parent wells (blue) and five child wells (maroon) distribution in the study area (yellow box).

3.4.1 Workflow to model multiple well fracture interference

A particular roadmap is considered for simulating numerically multiple well fracture interference. It starts by modeling only parent wells and, later, including child inner wells to the model (see Figure 3.8). First, a sector model is employed to history match prorated production data of the parent wells. The objective of this initial step is to perform broad sensitivity analysis of cluster spacing, hydraulic fracture conductivities, and hydraulic fracture lengths and fracture heights. By doing this, initial boundaries are set up for upgrading to the full model. Then, inner child wells are included, and once again, history matching is achieved in a reduced number of trials where sensitivities were tuned. Subsequently, fracture diagnostic results from the well image logging, which were discussed earlier in this thesis, will be incorporated into the model to perform a final sensitivity analysis of long interwell connecting fractures properties such as fracture number, conductivity, geometry, and explore their impacts on updated history matching. Finally, the optimal cluster spacing assessment can be performed, taking into account that clusters should avoid proximity to where induced long fractures were observed in the wellbore, so that interwell interference can be diminished and used to optimize future completion designs.

3.4.2 Black Oil Field Static Model Construction

The main characteristics of the constructed black oil model are discussed in detail as the following. The grid contains 411,075 cells. The width and length dimensions of the model are 4,050 ft × 1,450 ft. Moreover, the thickness of the model is 130 ft and it varies among 7 layers from top to bottom as well as their matrix permeability and porosity (based on pilot well and coring data) as listed in Table 3.1

Furthermore, the model includes four horizontal parent wells (W1H, W2H, W3H, and W4H) which are located on the lateral edges of the model, and five horizontal inner child wells (W5H, W6H, W7H, W8H, and W9H). Well spacing ranges from 300 to 550 ft (see Figure 3.8). Moreover, each well has a different fracture design configuration with multiple planar hydraulic fractures based on real data provided by the operator. For instance, cluster spacing varies from 20 ft to 70 ft, depending on the well. Fracture clusters are modeled and incorporated from the EDFM method preprocessing into the black oil model as hydraulic fractures without the use of local grid refinement, DPDK, method. Additionally, the dimensions of each grid block size are 50 ft × 20 ft in terms of x and y coordinates. Also, each fracture is assumed to penetrate all the vertical layers.

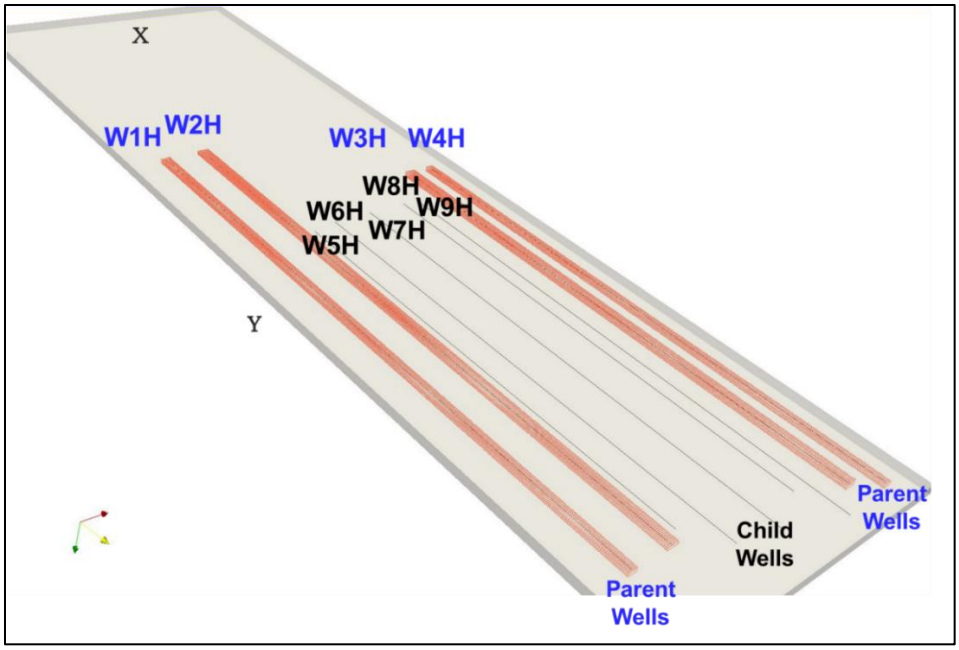

Figure 3.8: Initial reservoir model including 4 parent wells and 5 child wells.

LAYER	1	2	3	4	5	6	7
Thickness (ft)	12	27	19	20	21	18	13
Permeability (nD)	200	750	450	300	750	650	350
Porosity (ratio)	0.045	0.07	0.08	0.1	0.1	0.085	0.04

Table 3.1: Thickness, permeability, and porosity by each layer of the black oil model.

In addition, wells W5H and W9H were drilled and completed at shallower depths (7,955 ft.) than the rest of the wells (8,018 ft.). Therefore, the first mentioned wells corresponded to layer 2 in our model as seen in Figure 3.9, while the rest were located in layer 5. Finally, a summary of the reservoir parameters employed to characterize the black oil full field model are shown in Table 3.2.

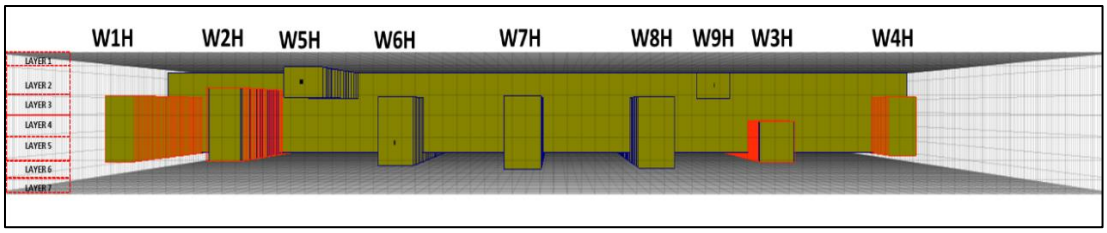

Figure 3.9: Z Plane view of the 9 wells in the model, which shows that well W5H and W9H were landed in shallower depths (layer 2) than the rest of the wells.

Parameter	Value	Unit
Dimensions (x × y × z)	40,50 × 14,500 × 130	ft.
Number of cells	411,075	-
Number of Grid Blocks (x × y × z)	81 × 725 × 7	-
Initial reservoir pressure	4725	psi
Reservoir temperature	215	°F
Initial water saturation	20%	-
Reservoir depth (Top)	7,930	ft.
Number of Wells	9	-
Well spacing	250-550	ft.
Cluster spacing	20 – 70	ft.
Total compressibility	2×10^{-6}	psi^{-1}

Table 3.2: Reservoir properties used for the black oil full field model.

3.4.3 Black Oil Field Dynamic Modeling

The dynamic behavior of a reservoir corresponds to the interaction of the reservoir fluids with respect to changes of pressure, temperature and volume, among the different fluids and the reservoir rock. As such, different physical properties of the fluids in the rock are associated to relative permeabilities, capillary pressure and phase behavior.

The relative permeability is defined as the relation between the effective permeability, at a defined wetting fluid saturation, and the absolute permeability, when two or more fluids are flowing in the same porous media. In the case of lack of reliable lab data, it is acceptable to use permeability functions from nearby fields or previous studies in the area. Curves for the shale matrix were provided by the operator from previous compositional simulation models of the Omega field and are shown in Figure 3.10.

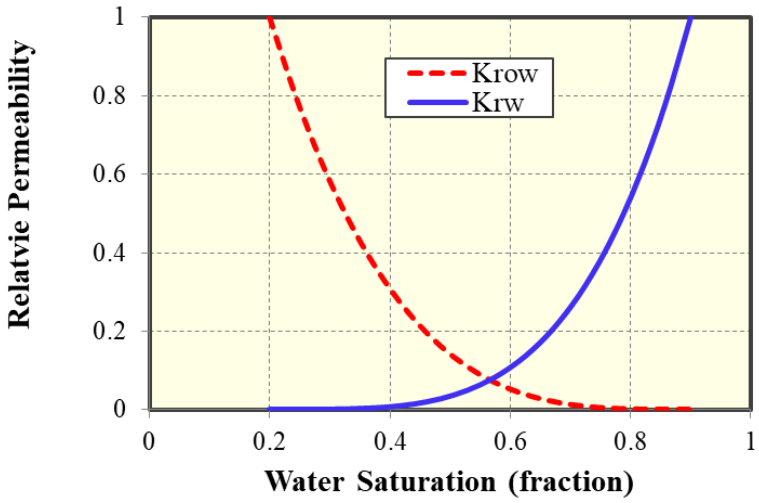

(a)

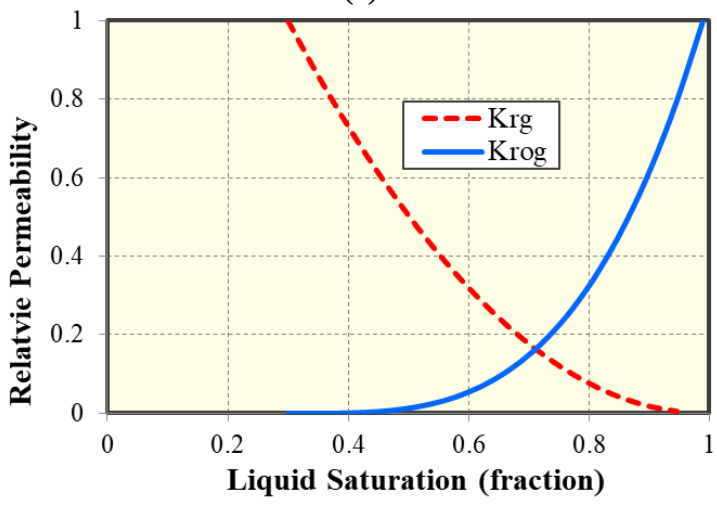

(b)

Figure 3.10: Relative permeability curves used in this study for modeling the matrix of Eagle Ford reservoir. (a) Water-oil relative permeability curve; (b) Liquid-gas relative permeability curve.

Furthermore, for the particular case of the fractures, another set of relative permeability curves is used. This kind of relative permeability tries to avoid any restriction of flow in the fractures. Therefore, straight relative permeability lines will be used as a standard for fractures in the model (see Figure 3.11).

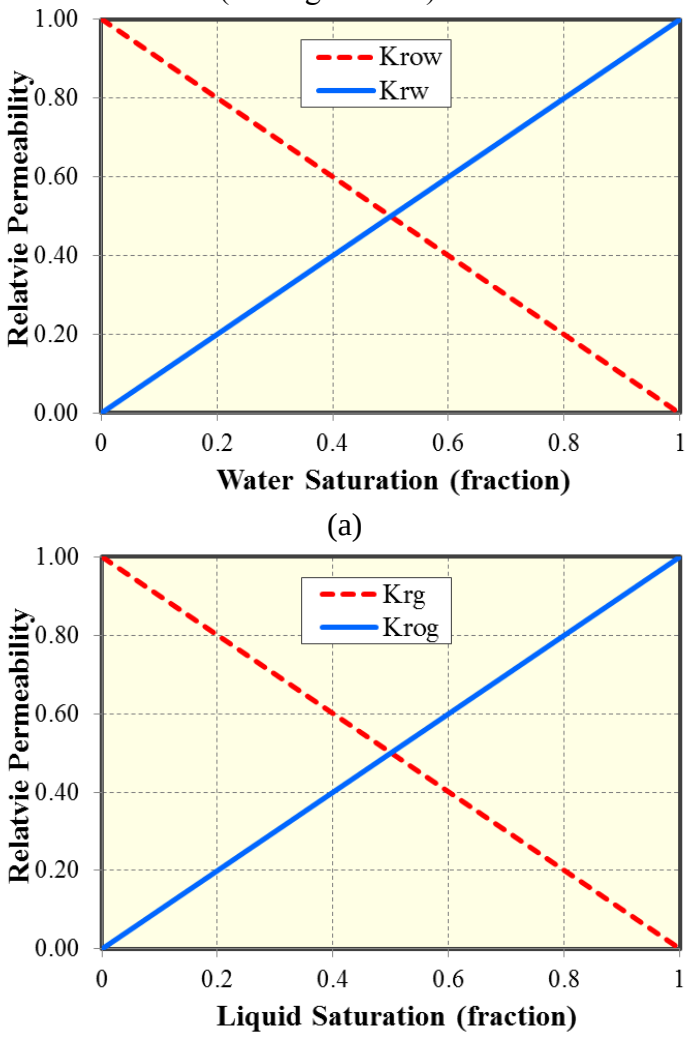

Figure 3.11: Relative permeability curves used in this study for modeling fractures flow in Eagle Ford reservoir. (a) Water-oil relative permeability curve; (b) Liquid-gas relative permeability curve.

Additionally, in unconventional reservoirs, the capillary pressure value is very small, which is often ignored in phase-equilibria calculation. For this thesis the effect of capillary pressure is disregarded and out of the scope of the objectives.

Based on fluid properties and phase behavior calculation, the black oil fluid properties such as viscosities, solution gas oil ratio, and formation volume factor can be determined. These and other fluid properties should be examined within a wide range of pressure and temperature. Hence, an initial fluid characterization will be performed, using a black oil numerical simulator (CMG, IMEX). Later in this study, the model will be switched to a compositional numerical one (CMG, GEM) after the reservoir model is validated with proper history match, and once Huff-n-Puff is modeled. The fluid characterization data of our case is provided by the operator from a flash calculation and separator tests, and its main properties are validated and summarized in Table 3.3. All the fluid properties correspond to values under reservoir condition at all times.

Reservoir Fluid Analysis	
Well Depth Parameter (ft)	8082-14325 MD
Reservoir Temperature (°F)	215
Static Reservoir Pressure (psig)	4726
Bubble Point Pressure @ Saturation (psig)	2120
Oil Compressibility @ Saturation (vol/vol/psi)	1.58E-05
Average Undersaturated Compressibility (vol/vol/psi)	1.07E-05
Reservoir Fluid Flash to Ambient Conditions	
Formation Volume Factor @ P_{BP} (rb/stb)	1.3962
Oil Density @ Bubble Point (g/cc)	0.6809
Oil Density @ Standard Conditions/ Stock Tank (g/cc)*	0.8217
Gas Specific Gravity @ Standard Conditions	0.948
Stock Tank Oil Gravity (°API) @ 60°F	40.54
Separator Tests	
Formation Volume Factor @ P_{BP} (rb/stb)	1.3442
Solution GOR, R_{sfb} (scf/stb)**	538
Gas Specific Gravity @ Standard Conditions	0.83745
Oil Specific Gravity	0.8133
Stock Tank Oil Gravity (°API) @ 60°F	42.49
* 14.65 psia, 60 °F	
**R_{sfb} is sum of separator and stock tank gas from separator test in scf/stb at 60°F	

Table 3.3: Summary of the PVT properties of Eagle Ford used in the black oil model.

3.4.3 Sensitivity Analysis and History Matching

The purpose of sensitivity analysis is to determine how sensitive an objective function is to different parameters qualitatively and quantitatively (Alfarge et al., 2018). In this study, sensitivity analysis starts founded on prior unconventional engineering data about reservoir and fracture properties, assuming initial values within a reasonable extent with uniform distribution (Yu et al., 2018b). Therefore, sensitivity analysis is part of an iterative process shown previously in the general workflow (Figure 2.9) in order to achieve a reliable history match and define the optimal cluster spacing.

The next stage in the workflow of our study was to achieve a robust history match of the reported production and pressure response of the model. History matching depends on two types of parameters: (1) the unknown or uncertain and (2) the response parameters. For our study, fracture half-length, fracture height, and fracture conductivity were grouped into the category of uncertain parameters. On the other hand, response parameters category included flowing BHP, oil flow rate, gas flow rate, and water flow rate. For the purposes of this study, water flow rate was discarded due to uncertainty in the reported values from the field operator, since it had been back allocated previously. In that sense, the simulation constrain for the history matching process was set to be the oil flow rate of each well. Hence, bottom-hole pressure and gas flow rate acted as the variables to be matched by performing sensitivity analysis on fracture geometries and fracture conductivities (see Figure 3.12).

Finally, history match allows us to make more reliable forecasts about the reservoir area of study. A brief comparison is performed between primary recovery with and without considering inner child wells in order to evaluate the benefit of having these child wells with the cluster spacing recommended. Therefore, short primary recovery forecast is included in this stage of the general workflow.

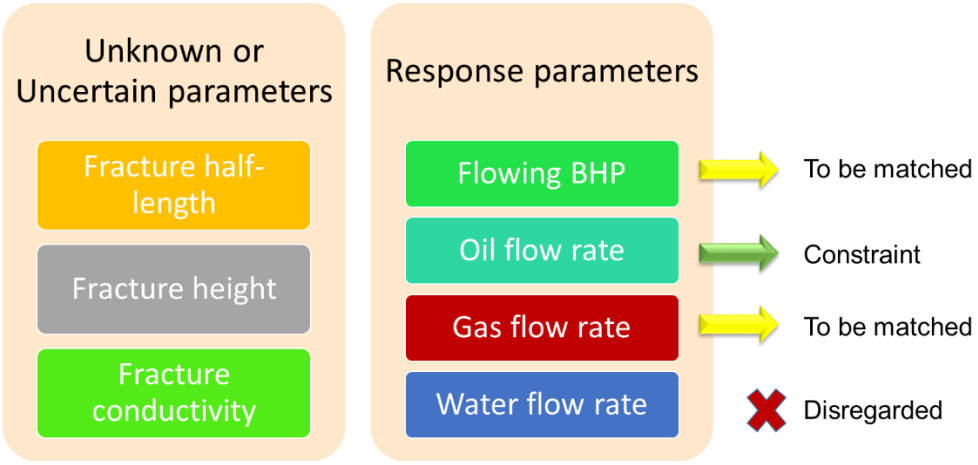

Figure 3.12: Parameters identification for sensitivity analysis and history matching processes.

3.5 Huff-n-Puff and Pressure Containment Strategies

Once the full field model has been validated by fulfilling all the previous steps in the proposed workflow, EOR Huff-n-Puff implementation has been assessed and included in the 8-year forecasts of the model. For this purpose, a compositional sector model has been constructed in order to improve computational efficiencies and obtain faster approximations. Consequently, this sector model adopts all the validated parameters of the full field model as an input for modeling Huff-n-Puff. Nonetheless, some minor tuning was needed for better pressure and gas history match when switching form a black oil simulation to a compositional one, which will be discussed below.

3.5.1 Compositional Sector Model Grid Construction

Sector modeling allows the user to simulate a part of the reservoir or a region of interest using the boundary conditions that were extracted from a full field model previously. The boundary conditions can be either flux or pressure related and obtained from a full field model run. Due to the fact that the reservoir of study is an unconventional (shale) play, these boundary conditions of flux or pressure do not have a big impact on total flow (Influx) or pressure depletion from all surrounding blocks into a flux sector. As a

consequence, a shale-oil sector model was built based on available field data information in order to reduce computational requirements for sensitivity results when compared to full field forecasts.

Given the proposed downscaling, the sector model grid contains 14,350 cells and encompasses the six percent of the full field model. Also, grid block size remains with the same dimensions as the full field model, which were 50 ft × 20 ft in terms of x and y direction. Hence, the sector model displayed the following width and length dimensions: 4,100 ft × 500 ft × 130 ft. However, the thickness of the model is still irregular and it fluctuates among seven layers from top to bottom as well as their matrix permeability and porosity values (based on pilot well and coring data) as listed in Table 3.1. Additionally, this sector model includes the same four horizontal parent wells (W1H, W2H, W3H, and W4H) which are located on the lateral edges of the model, and the same five horizontal inner child wells (W5H, W6H, W7H, W8H, and W9H) that were part of the initial full model. The different parameters of the sector model can be summarized in Table 3.4. Also, permeability and porosity models were kept from the full field model.

Parameter	Value	Unit
Dimensions (x × y × z)	4,050 × 500 × 130	ft.
Number of cells	14,350	-
Number of grid blocks (x × y × z)	81 × 25 × 7	-
Block size	50 × 20	ft.
Initial reservoir pressure	**4,725**	**psi**
Reservoir temperature	215	°F
Initial water saturation	20%	-
Reservoir depth (Top)	7,930	ft.
Number of wells	**9**	**-**
Well spacing	**250-550**	**ft.**
Cluster spacing	**20 – 70**	**ft.**
Total compressibility	2×10^{-6}	psi^{-1}

Table 3.4: Reservoir and grid properties used for the compositional sector model.

3.5.2 Compositional Sector Dynamic Model Considerations

Although our study is enclosed in the black oil Eagle Ford area of the reservoir, and in spite of the fact that compositional models are computationally expensive due to large number of components, for injection fluid characterization purposes, a compositional model is applied in the sector model to represent our Eagle Ford reservoir fluids. Also, Appendix A-1 and A-2 provides the Peng-Robinson equation-of-state parameters and the corresponding reservoir fluid composition. Furthermore, relative permeabilities are not subject of sensitivity analysis in this study, and are taken from the full field model.

3.5.3 EOR Huff-n-Puff and Pressure Containment Modeling

In this study, we use the numerical simulation of the history-matched sector model to appraise EOR Huff-n-Puff feasibility implementation in the Eagle Ford reservoir. Due to the fact that the low sweep efficiency could be a potential concern for EOR operations in unconventional reservoirs, simulating cyclic gas injection "Huff-n-Puff" is considered for the forecast cases of the sector model. For gas injection to be effective and affordable, the reservoir must allow the operator to pressure it up, preserve the injected gas contained in the reservoir for the adequate period of time to have an impact, and recover the gas for reuse or sale. However, the forecasts of EOR gas injection in this sector of the Eagle Ford reservoir demonstrate the need to consider pressure containment strategies, which will also be implemented in the model and discussed further in this thesis.

3.5.4 Huff-n-Puff design

The application of Huff-n-Puff is modeled in the nine-well sector model described previously in this thesis. Different scenarios are considered regarding the number of gas well injectors, the location of these gas well injectors, the periods and rates of injection, soaking and production (see Figure 3.13). For instance, different sensitivities include

evaluating the performance of one, two or three injector wells both at the same time or different cyclic times of gas injection. Likewise the locations of these gas injectors are subject of another sensitivity analysis. Moreover, the simulation forecasts were constrained by a maximum injection pressure of 3500 psi and gas injection rate of 1.8 MMSCF per day (i.e. equivalent to 30 MMSCF), considering that the sector model represents only six percent of the full field model. Hence, these values will be selected as a result of combining the technical reservoir needs and operator's available capacity of the surface facilities.

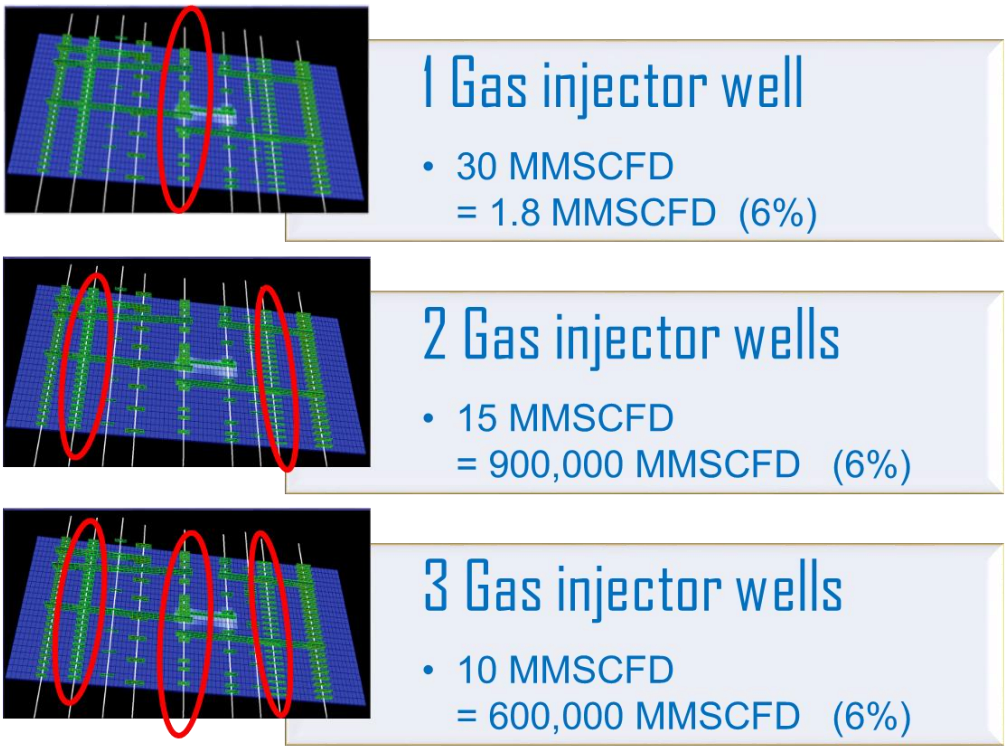

Figure 3.13: Gas injection sensitivities (injection rates, location, and number of injector wells).

The injecting fluid compositions and properties are essential to guide the reaction scheme design for simulating gas injection. For instance, in one model case, the injection gas was a recycled rich gas from the field whose molar composition is showed in Table 3.5

Comp.	Composition, Mole Frac.

C1+N2	0.76864
C2+C3+CO2	0.18946
C4-C6	0.04190
C7+	0.00000

Table 3.5: Molar composition of the injection gas used in the sector model for Huff-n-Puff.

As a common scheme for the Huff-n-Puff design, the injector well was set to be in the middle of the model (i.e. Well W7H) to evaluate its impacts on the rest of the wells in terms of pressure and gas saturation response (see Figure 3.14).

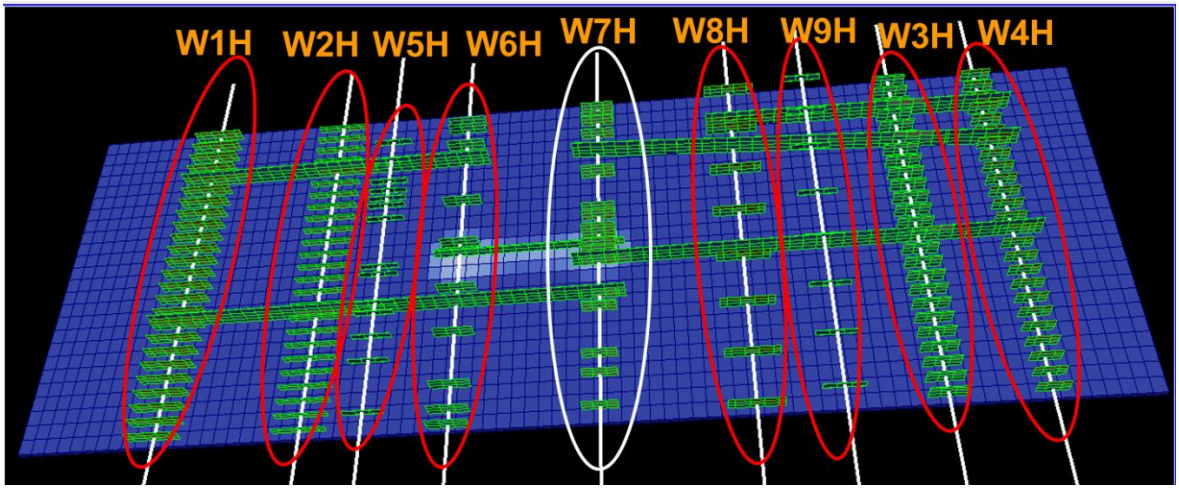

Figure 3.14: 3D view of the wells arrangement used in the sector model for Huff-n-Puff modeling in which the white ellipse identifies the gas injector, and the red ellipses identify the producer wells.

Also, sensitivities regarding the adequate length time of the injection and production cycles are performed. In this sense, different forecasts take place evaluating this cyclic times within ranges of 30-120 days for both injection and production. Despite soaking periods are initially considered in the runs, they are disregarded later since they do not contribute significantly to improve the recoveries while reducing production time. Likewise, the number of cyclic periods was tested in the sensitivities in order to find the Huff-n-Puff designs with higher cumulative oil recoveries.

Finally, the EOR Huff-n-Puff performance results need to be evaluated. This simulation outcome is validated by field data, which should mimic the field real behavior, in which the presence of the injected gas is found in further zones of the reservoir. Consequently, pressure leak occurrence seems inevitable in this part of the field so that it is necessary to characterize pressure leak off in this sector model to determine optimal strategies.

3.5.5 Pressure Leak-off Characterization

The sector model characterized the pressure leak-off through higher fracture intensity, and higher conductivities of the long induced interwell fractures. The interwell fractures can display longitudinal extension of up to 2,000 ft as reported by the operator. Pressure and gas profiles comparison, which will be presented in the next chapter, are used to identify this rapid communication among the seven wells located in the fifth layer of the model at different subsequent early times.

Initially, in order to generate better pressure build-up in the sector model, different scenarios of Huff-n-Puff, regarding the number and location of injector wells, demand other pressure containment attempts. Thus, in order to cover further zones of the model when injecting gas, three injectors (W2H, W7H, and W3H) are also proposed, as shown previously in Figure 3.13. Additionally, gas dynamic behavior is evaluated and traced through gas saturation changes in the grid of the sector model, as shown in Figure 3.15. Thus, these gas saturation changes through the blocks were identified and modeled when integrating the EDFM method and the compositional simulator.

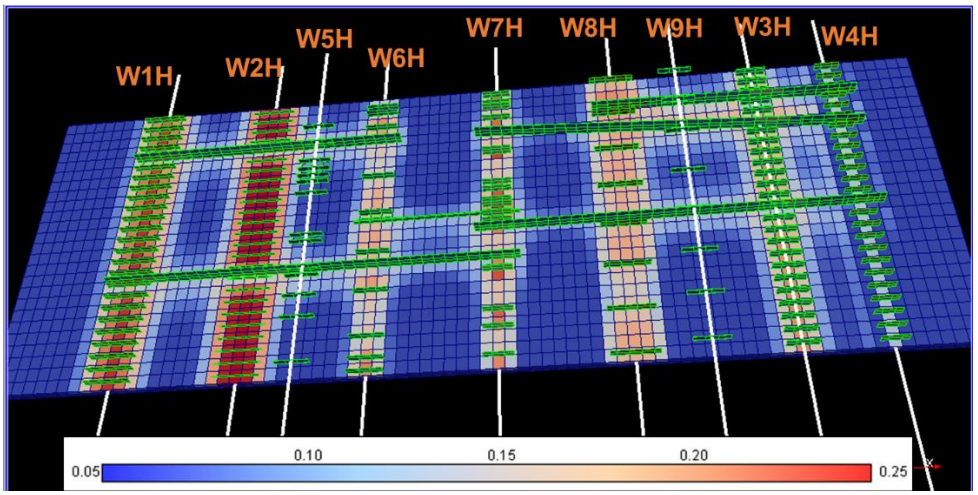

Figure 3.15: 3D view of initial gas saturation response through the interwell fractures modeled by EDFM after being injected by wells W2H, W7H, and W3H.

Later, in order to replicate the aforementioned fast dispersion of the injected gas through exceptionally far zones of the reservoir, three simulation experiments are proposed. The first one corresponded to increasing of interwell fractures intensity (see Figure 3.16). This assumption was supported by the need to increase interwell communication so that gas could flow faster through the fractures so that it can reach further zones of the reservoir effortlessly.

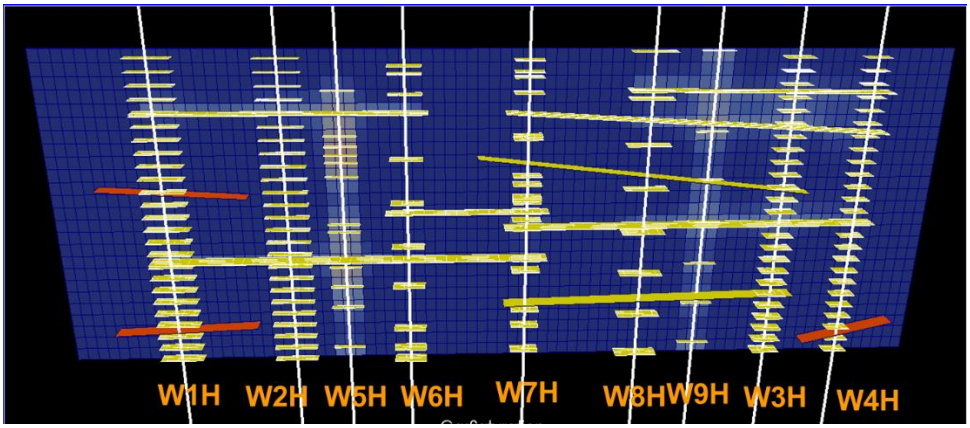

Figure 3.16: 3D View of additional fractures (interwell fractures intensity increased) modeled by EDFM.

The second experiment consists on implementing relative permeability curves for the fractures that are different than the standard (straight lines, see Figure 3.11). In this

particular case, downward concave permeability curves are employed based on the idea of the presence of layered heterogeneity in the shale formation (see Figure 3.17). The use of these concave downward relative curves for gas flow is also supported by the assumption of the presence of low interfacial tension (IFT). According to Peters and Gharbi (1993), relative permeability curves are affected by interfacial tension only at interfacial tensions lower than 0.1 dyne/cm. Also, Amaefule and Handy (1981) concluded that the relative permeabilities to gas and oil increase as the interfacial tension decreased. The residual fluid saturations decreased as the interfacial tension decreases as expected from the effect of capillary number on residual fluid saturations. These concepts are corroborated by Kalla et al. (2015), when correlating Corey exponents lower than 1.0 with IFT and stating that at the lowest IFT (i.e. 0.4), the relative permeability curves for gas were concave downward.

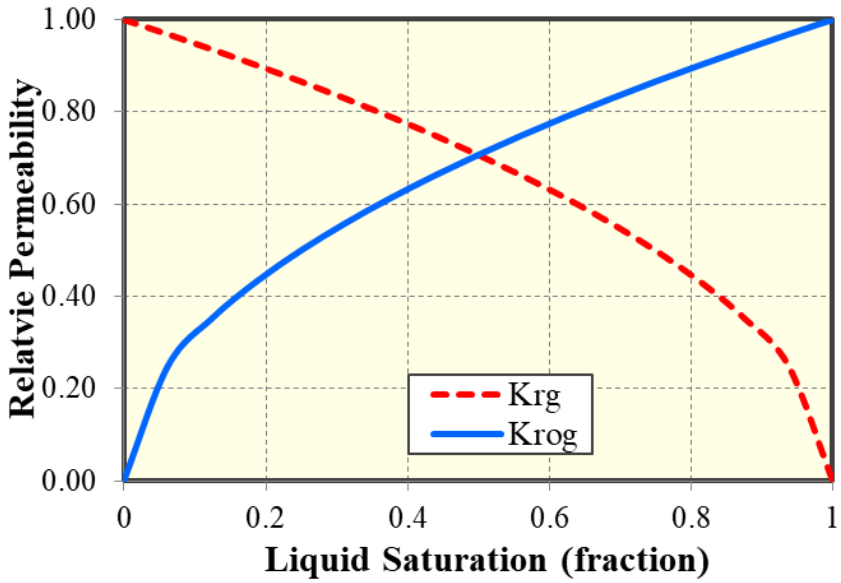

Figure 3.17: Relative Permeability curves for the fractures comparison used to characterize the flow of liquid and gas fluids. Concave shape is expected due to laminar heterogeneity and low IFT.

The third experiment is applying a new capability to model EOR well interference, developed in collaboration with the operator, in order to identify fluid saturations and

interwell communication pathways, by which wellbore cell communication is enhanced through the use of additional non-neighboring connections that assign a transmissibility factor among wellbore cells. This new capability is called EDWM, and is explained in detail as follows.

3.5.5.1 Embedded Discrete Wellbore Model (EDWM) development

This new approach strengthens the wellbore flow behavior reproducibility for unconventional reservoirs. Therefore, EDWM is developed to provide efficient and accurate solutions to the traceability of fluids through the wellbore (e.g. the injected gas in our study). Nevertheless, results like this with higher resolution and higher accuracy demand longer computational times to run, so it is important to understand when its implementation is required, since the EDFM method can approximate answers much faster. In this thesis, the sector model considers well W7H as the gas injector, and evaluates the changes in the gas saturation to mimic the gas flow (See Figure 3.18 and Figure 3.19).

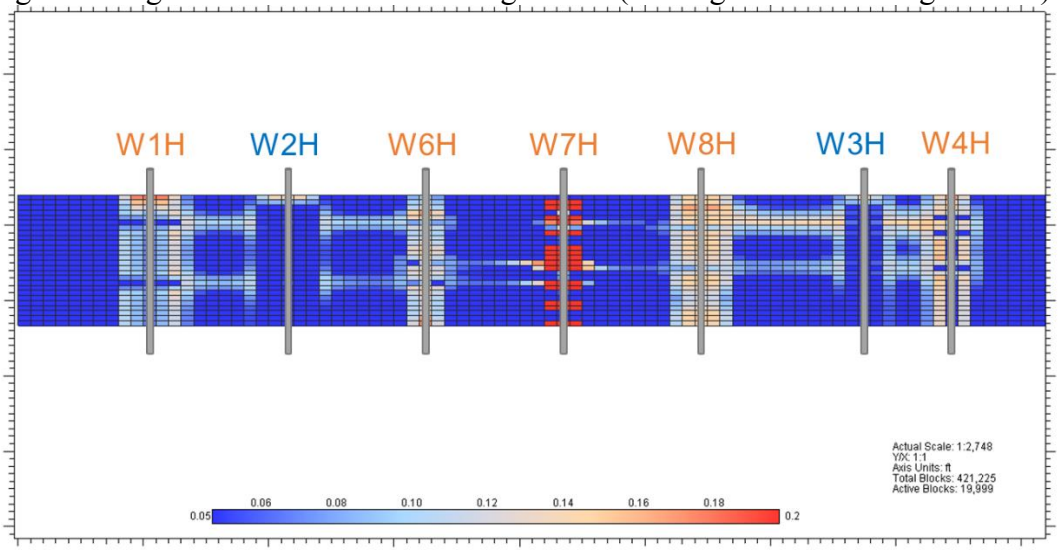

Figure 3.18: Gas saturation (2026-Sep-21) response in the sector model without EDWM, in which the injected gas from W7H does not flow too far.

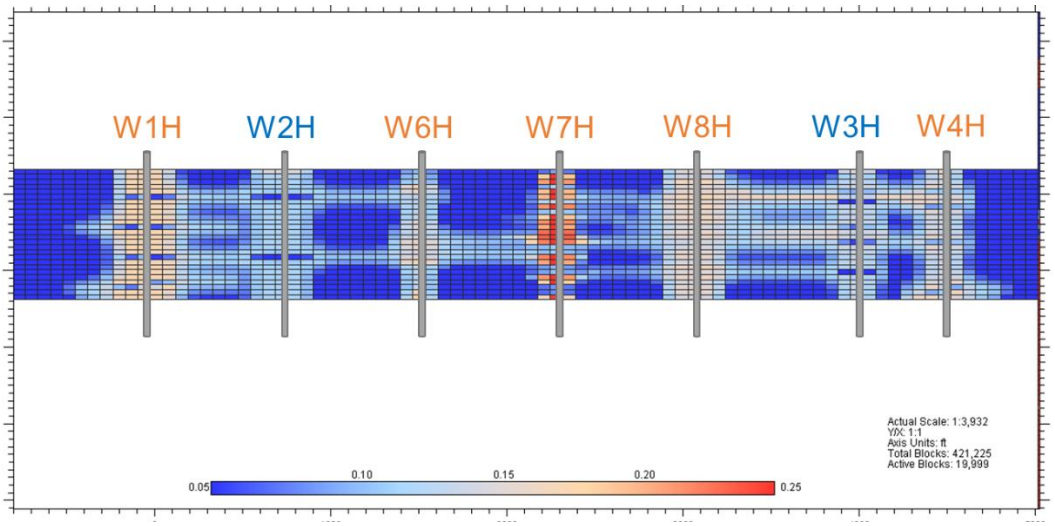

Figure 3.19: Gas saturation (2026-Sep-21) response in the sector model using EDWM, in which interwell communication mimics the field reports.

3.5.6 Pressure Containment Strategies

Different approaches are envisioned to mitigate and understand interwell communication impacts in the sector model during EOR Huff-n-Puff so that cumulative produced oil forecast can be maximized. Since there exist a lot of uncertainty whether these pressure containment field practices are really applicable to mitigate fracture hit effects in general or if they are very particular solutions, they need to be simulated and assessed.

For instance, the considered approach is loading up low-profit producing wellbores with water injection so that this setting could cause to create barriers for the interwell interference and protective pressure shields around the area of interest. Furthermore, it may reduce the propagation area where the injected gas might flow and confine it to a feasible area of containment. Initially for this study, wells W2H and W3H were employed as water injector wells due to their location and low production forecasts. As seen in Figure 3.20, transforming these producer wells into water injectors allows us form a barrier that interrupted the flow of the injected gas.

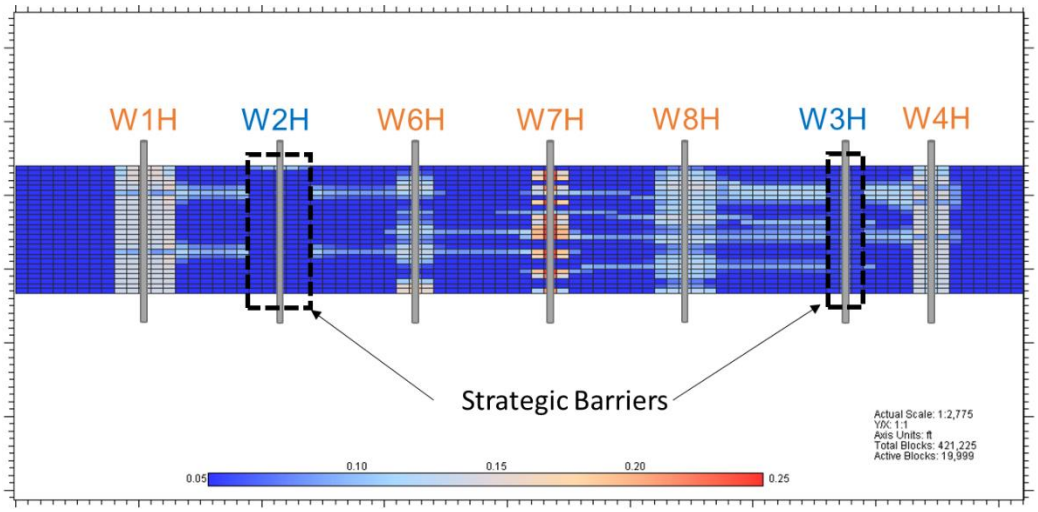

Figure 3.20: Gas Saturation (2020-Nov-11) layout for layer 5 considering wells W2H and W3H as water injectors acting as barriers to injected gas flow in the reservoir.

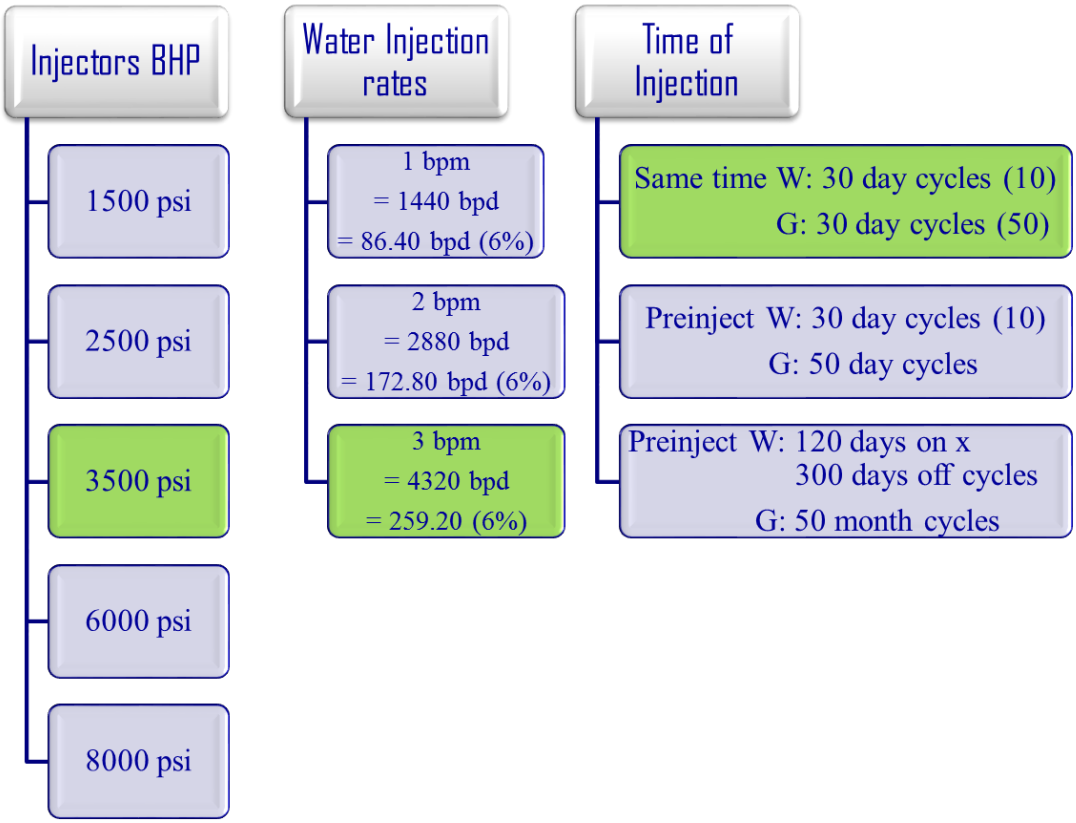

Figure 3.21: Summary of main sensitivities performed to define adequate water and gas injection pressures, rates and time of injection. The green boxes show the scenarios for water injection with greater cumulative oil recoveries.

In this stage of implementing water injection in the model, a series of sensitivities are simulated. These sensitivities include injection BHP, water injection rates, and time of injection when combining water injection with gas injection. The BHP variable of injection was constrained to 3,500 psi due to surface capabilities of the operator, which possess compressors that can provide up to that BHP efficiently. Also, from surface the facilities can inject up to 3 barrels per minute. Finally, regarding the lengths of the injection cycles, sensitivities varies from injecting 10 to 50 cycles for 30 to 120 days of water and gas either simultaneously or not. The most efficient scenarios of these sensitivities can be summarized in Figure 3.21, in which the green boxes identify the best probable results.

3.6 METHODOLOGY SUMMARY

To summarize, this chapter describes a novel methodology used in this research to model Huff-n-Puff considering multiple well fracture interference and evaluate the best scenarios for pressure containment based on actual field data from Eagle Ford. Moreover, EDFM method is introduced to preprocess and model fractures with complex features that can better describe the flow performance with respect to other traditional methods. It was specified how the full field model and a posterior sector model (with multiple wells and numerous fractures) were validated with the field data for further forecast analysis. The numerical computation of the BHP measures and the gas flow rate of each well was history matched through black oil and compositional simulators. Finally, different Huff-n-Puff designs were specified and used to forecast incremental oil recoveries in Omega field and execute optimal pressure containment strategies in the field in terms of cumulative oil efficiency. Chapter 4 yields the results of the research in a descriptive, qualitative, and graphical procedure.

CHAPTER 4

RESULTS

As stated in Chapter 1, this study has the purpose to model interwell interference in Eagle Ford, as well as to study the Huff-n-Puff implementation and its scope as an EOR method for unconventional reservoirs when considering pressure containment strategies joint application. This chapter is organized in terms of the two research questions posed in Section 1.2 and the results obtained will be presented in the same order as the procedures and guidelines of Chapter 3. As a consequence, the lessons learnt of the history matching and the comparative studies are captured.

4.1 Impact of Interwell Fracture Interference

Considering the proposed workflow in Chapter 3, the results expose that production rates are impacted by interwell interference. Therefore, history matching infill wells is definitely altered by pre-existing hydraulic fractures from existing wells, which is why modeling the existence/effect of these fractures is critical to understanding infill well behavior.

4.1.1 Sensitivity Analysis Results for Full Field Black Oil Model

Prior to achieving history matched results, sensitivity analysis is performed based on conventional engineering information about reservoir and fracture properties, assuming initial values within a reasonable range with uniform distribution (Yu et al., 2018b) as shown in Table 4.1. Therefore, sensitivity analysis results produced the fracture properties summarized in Table 4.1 in order to achieve a reliable history match and define the optimal cluster spacing.

Well	Number of Hydraulic Fractures	Fracture conductivity, md-ft	Fracture half-length, ft	Fracture height, ft
W1H	429	6	75	65
W2H	429	14	100	45
W5H	98	252	75	30
W6H	119	8.25	75	75
W7H	130	4.5	65	75
W8H	95	360	100	75
W9H	121	270	75	30
W3H	368	8	70	75
W4H	379	10	55	65

Table 4.1: Summary of fracture properties in parent wells after sensitivity analysis in the black oil full field model.

4.1.2 Interwell Fractures Modeling

Multiple well fracture interference is accounted for when validating the black oil model with the observed production data from Omega field in the Eagle Ford shale. As a result, 28 long interwell fractures are identified and located in the black oil model among different wells through the model with an approximate orientation of N60E. This orientation aligns with the concepts used to develop the area when drilling and completing the wells of this part of the field. The length of these fractures ranges from 750 ft up to 3,400 ft (see Figure 4.1) with a fracture conductivity of 0.5 md-ft, whose low value is the characteristic of natural fracture conductivities seen in other case studies. We can infer from this model that most long interwell fractures are observed to reach 2,000 ft, and this is directly in line with offset pressure/water communication, gross fracture lengths observed in the aforementioned geo-mechanical model studies, water tracer studies, and in micro-seismic events performed for these wells (Ambrose, 2011).

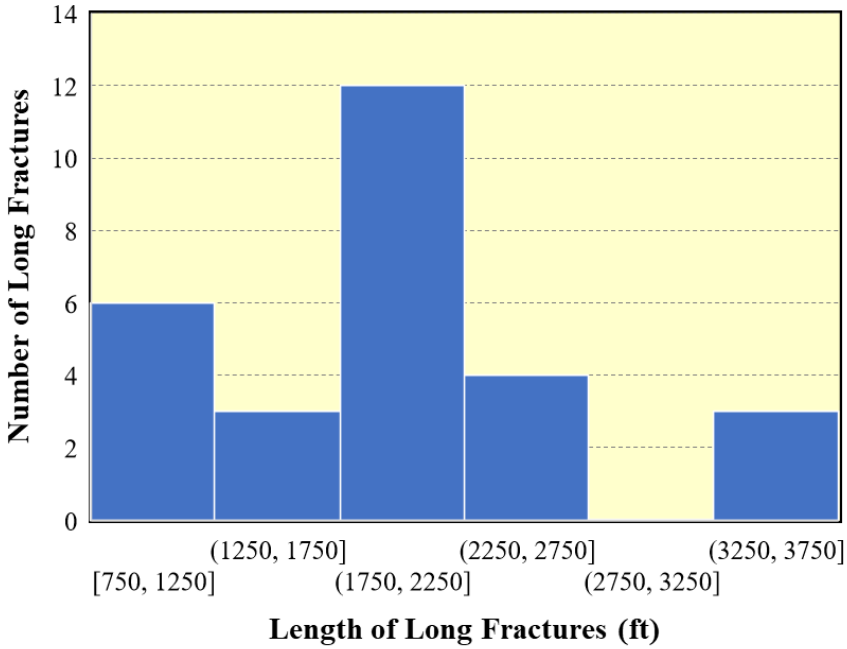

Figure 4.1: Histogram of the length of long interwell fractures employed in the model, as a result of correlating WBI logs.

Furthermore, the distances between one long fracture to another are variable and show no reliable trend (5 common cases out of 28). However, some cases show very close distances (less than 100 ft) as seen in the Figure 4.2, which is likely related to cluster spacing (high cluster interference on many of the wells supported by previous geo-mechanics studies and RTA/Analytical Model cluster efficiency studies) and rock heterogeneities along the wellbore that impact decline characteristics (Ambrose et al., 2011). This long fracture closeness when compared to the grid block size (50 ft × 20 ft) was well resolved by the EDFM which allows multiple fractures in one single grid block.

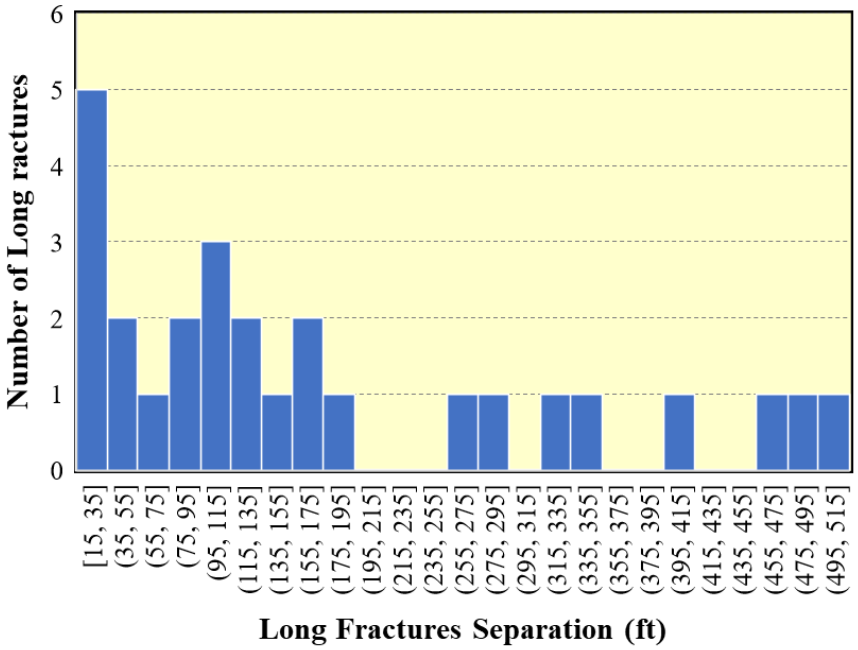

Figure 4.2: Histogram of the long interwell fractures separation among each other employed in the model after correlating WBI logs.

4.1.3 Black Oil Model History Matching

After sensitivity analysis and fracture depth correlations from WBI logs, final history matching results are achieved. The simulation constrain for the history matching is the oil flow rate of each well. Thus, BHP and gas flow rate are the parameters to be matched by varying fracture geometries and fracture conductivities parameters, as described previously in this document. The history matching solutions for our study offers the fracture arrangement shown in Figure 4.3. This full field black oil model contains more than 2000 hydraulic fractures spread in nine wells (i.e. 4 parent wells and 5 inner child wells) and in 7 layers with different nano-darcy permeabilities. Furthermore, the child inner wells fracture designs consider cluster spacing of 70 ft in these cases. This suggested cluster spacing is the result of sensitivities in the model in order to maximize recovery by mitigating well interference and locating the clusters at a distance far enough to reduce the interference from long induced interwell fractures but without losing oil.

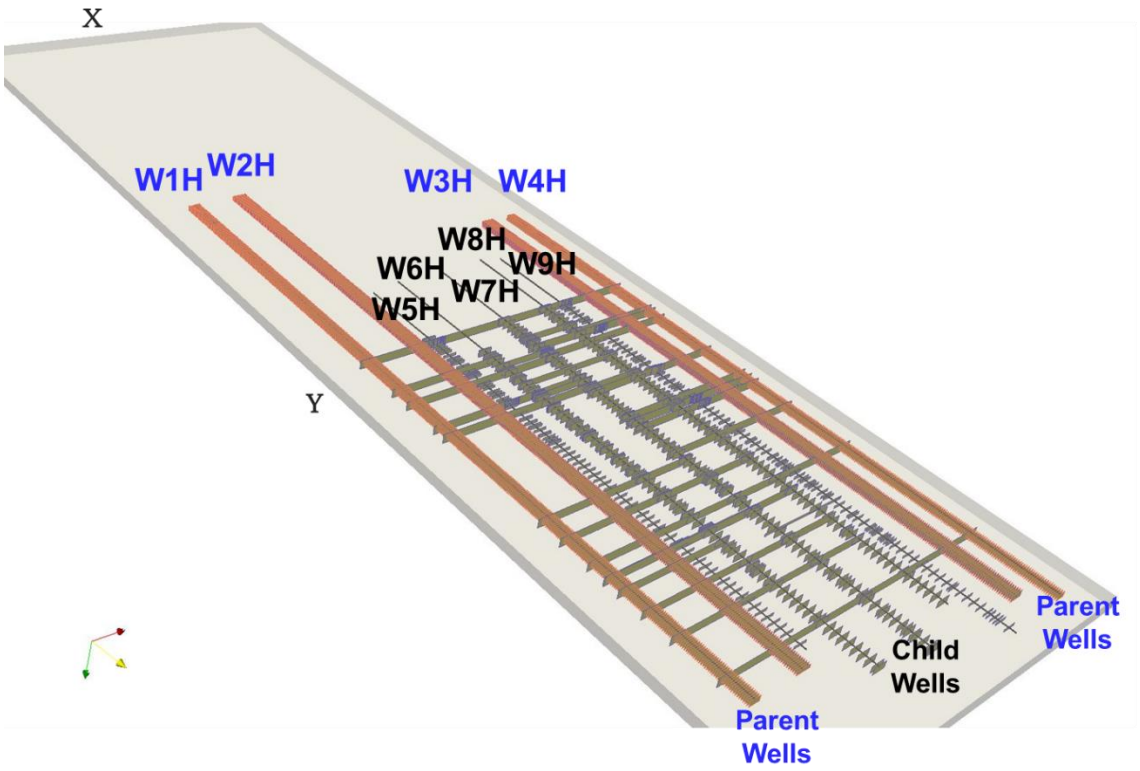

Figure 4.3: 3D view of the full black oil model considering 4 parent wells, 5 child wells and long interwell fractures.

The history matching results of four parent wells and five child for the full field black oil model wells are presented in Figure 4.4, Figure 4.5, Figure 4.6, Figure 4.7, and Figure 4.8. It is important to remark that there might be other solutions for history matching which will not be considered in this thesis. However, as shown, great agreements between simulation results and field data are obtained. The metrics to gauge quality of history matching consider analysis by visual curve fitting.

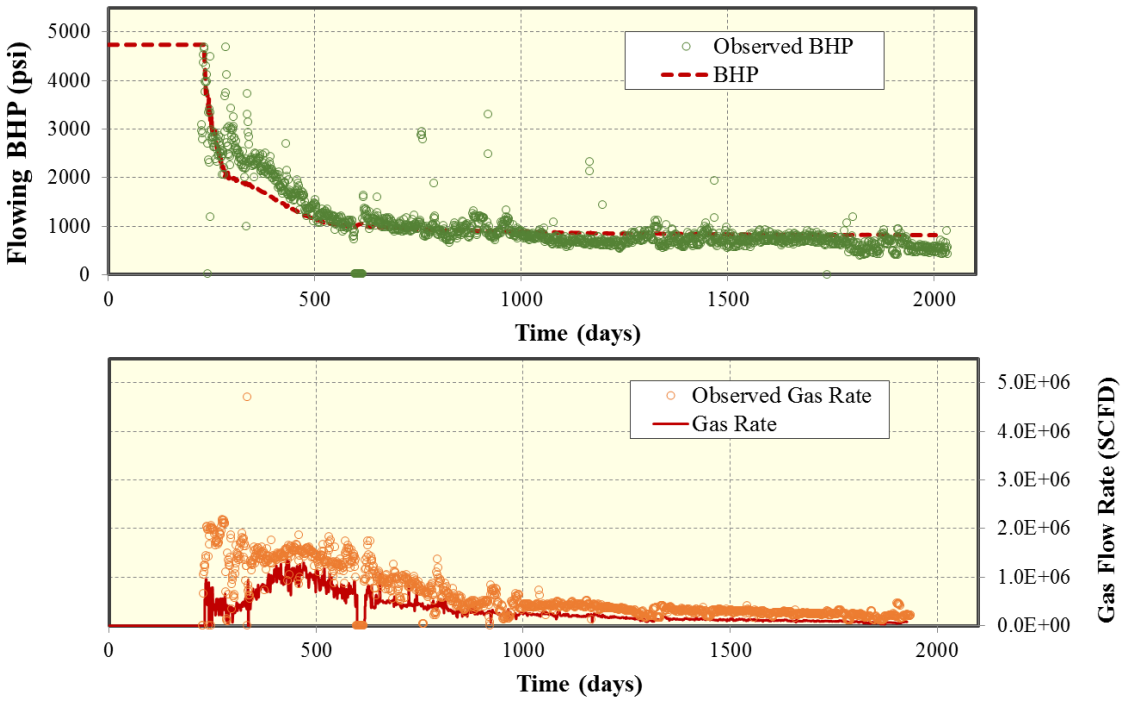

(a) BHP match and (b) Gas flow rate match of parent well: W1H

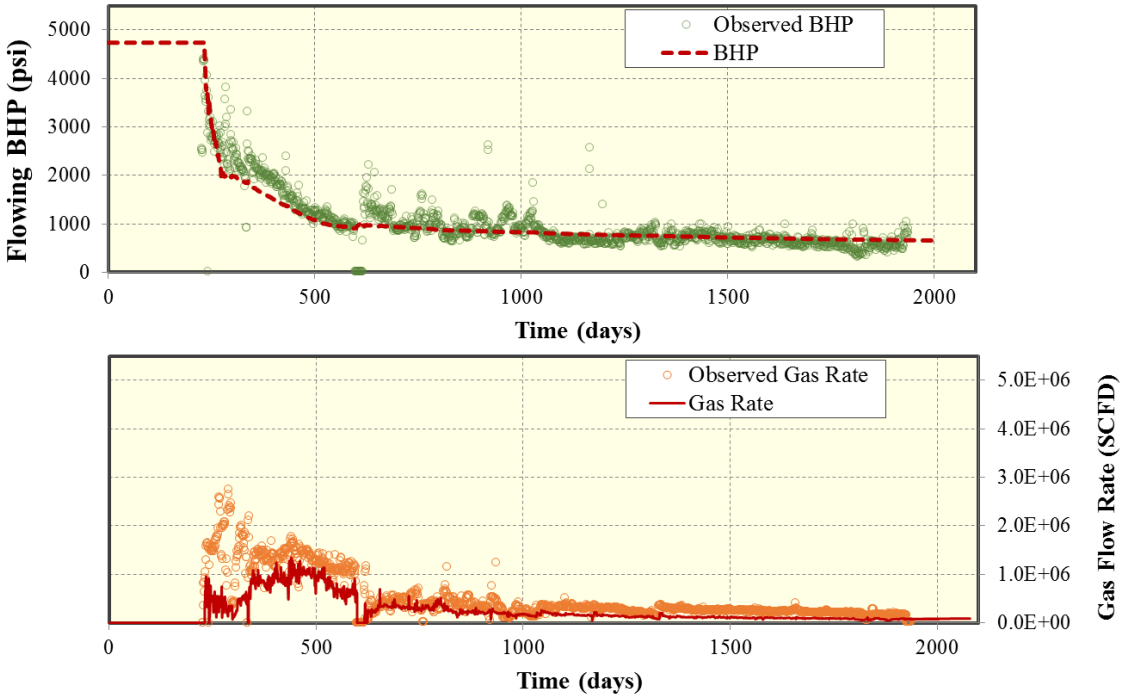

(c) BHP match and (d) Gas flow rate match of parent well: W2H

Figure 4.4: Black oil history matching results of parent wells W1H and W2H.

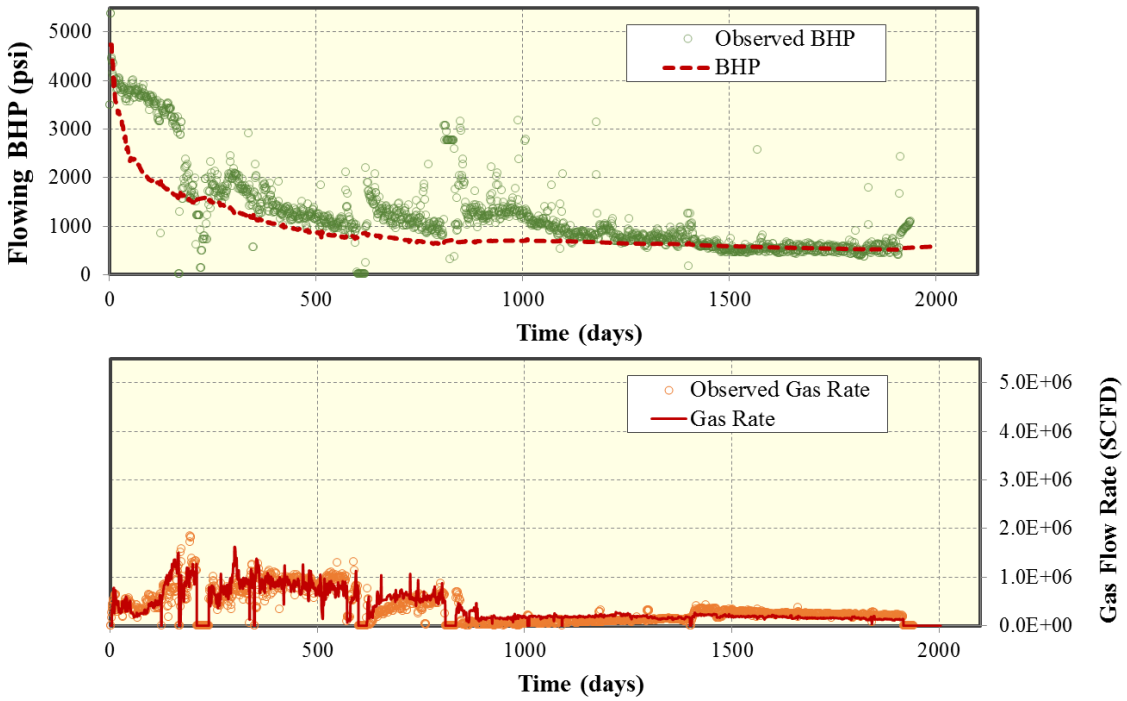

(e) BHP match and (f) Gas flow rate match of parent well: W3H

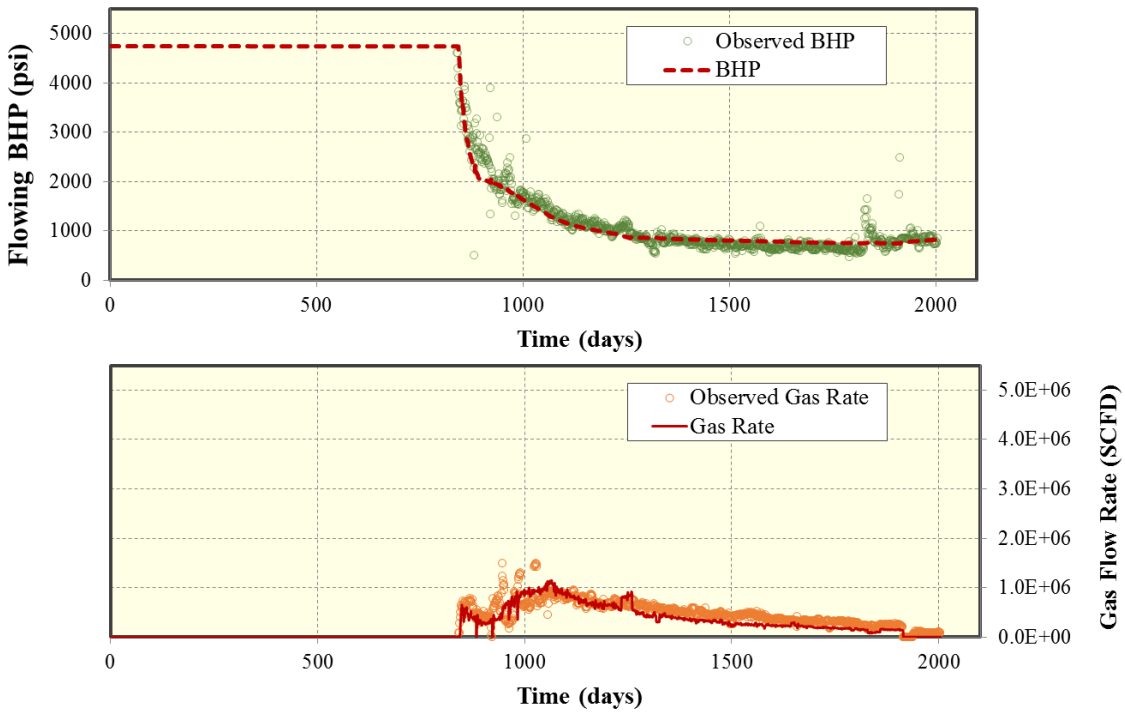

(g) BHP match and (h) Gas flow rate match of parent well: W4H

Figure 4.5: Black oil history matching results of parent wells W3H and W4H.

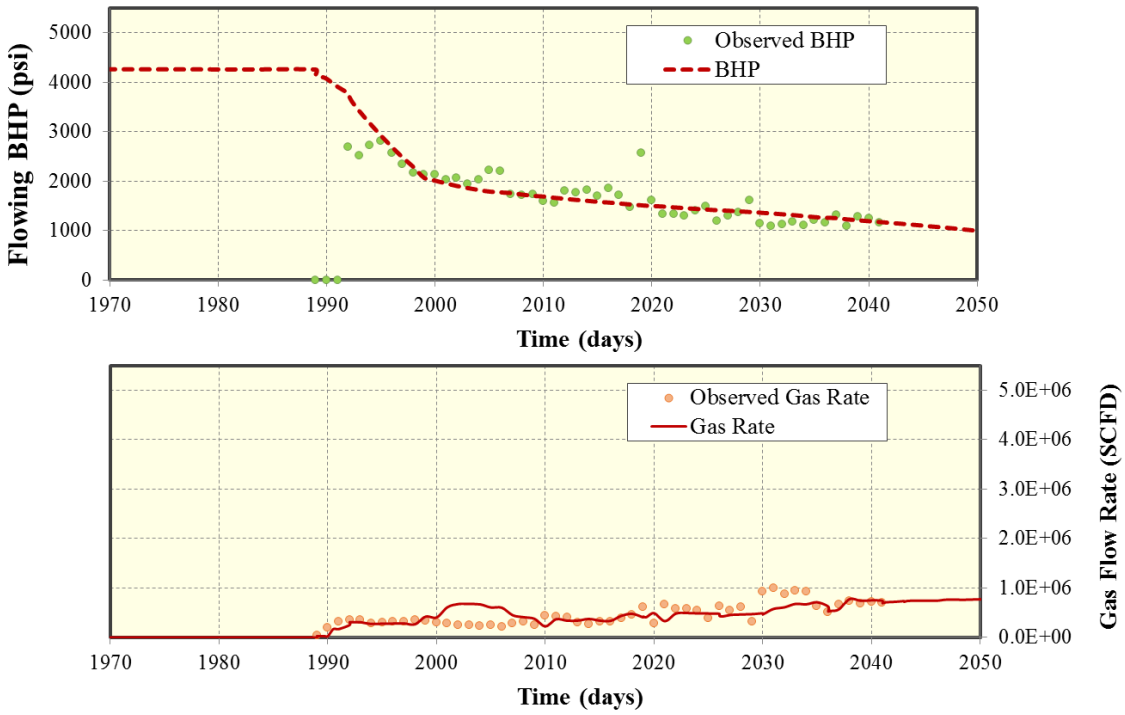

(a) BHP match and (b) Gas flow rate match of child well: W5H

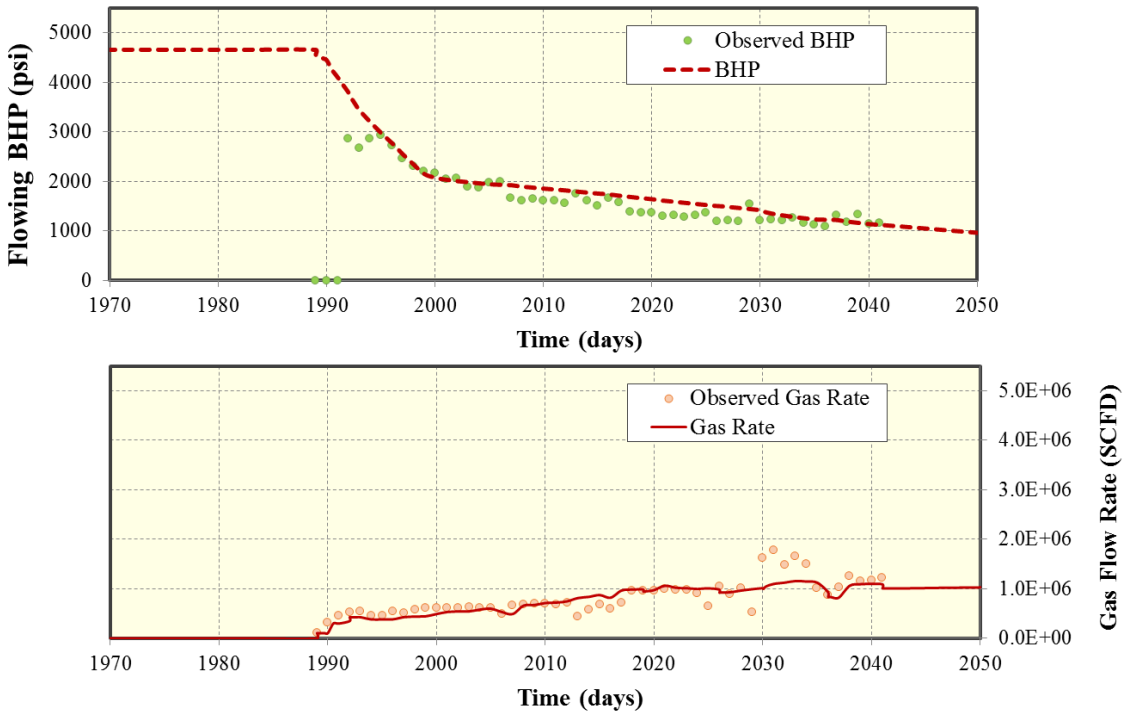

(c) BHP match and (d) Gas flow rate match of child well: W6H

Figure 4.6: Black Oil history matching results of child wells W5H and W6H.

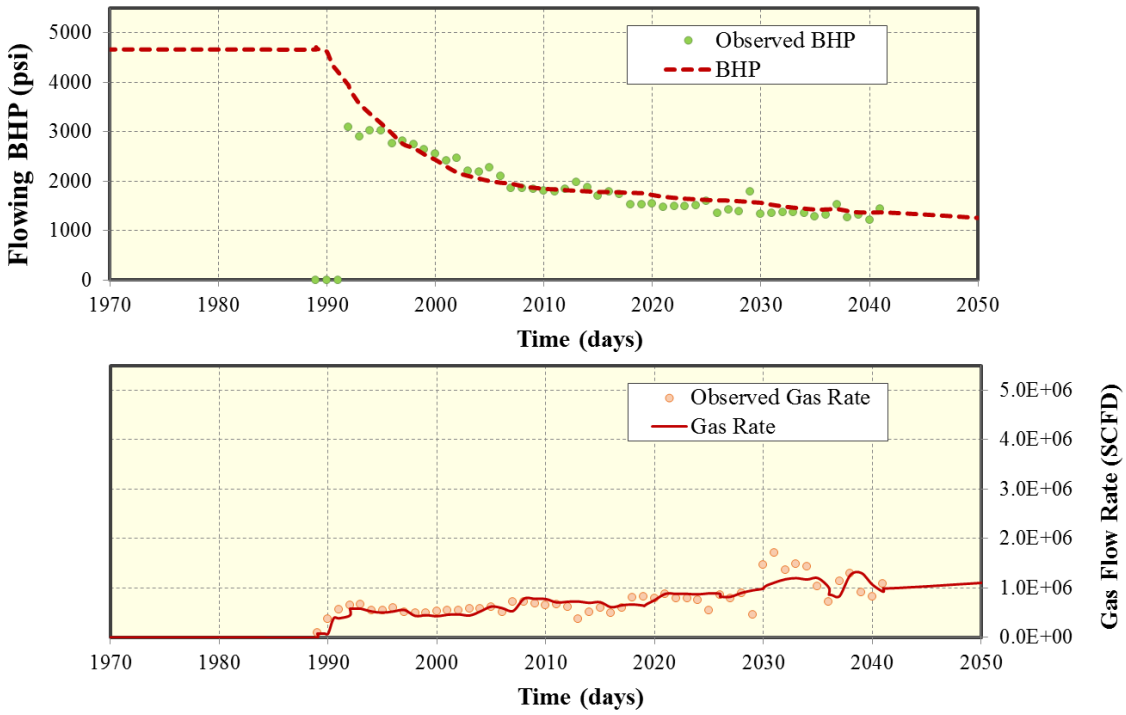

(e) BHP match and (f) Gas flow rate match of child well: W7H

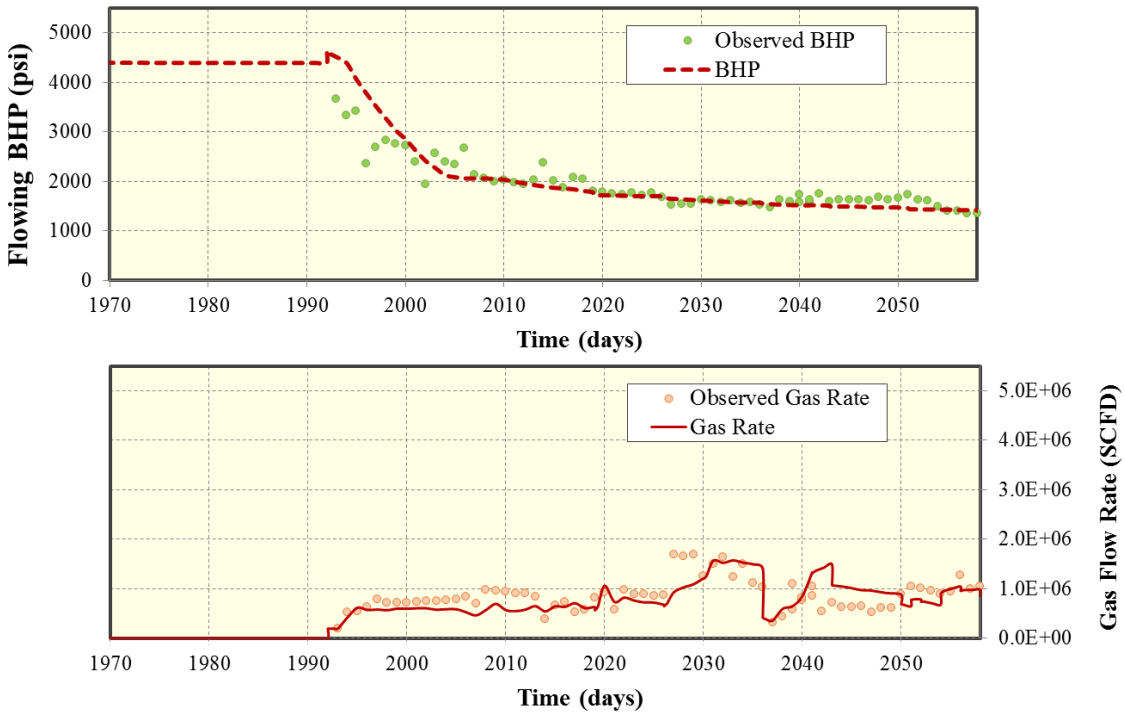

(g) BHP match and (h) Gas flow rate match of child well: W8H

Figure 4.7: Black Oil history matching results of child wells W7H and W8H.

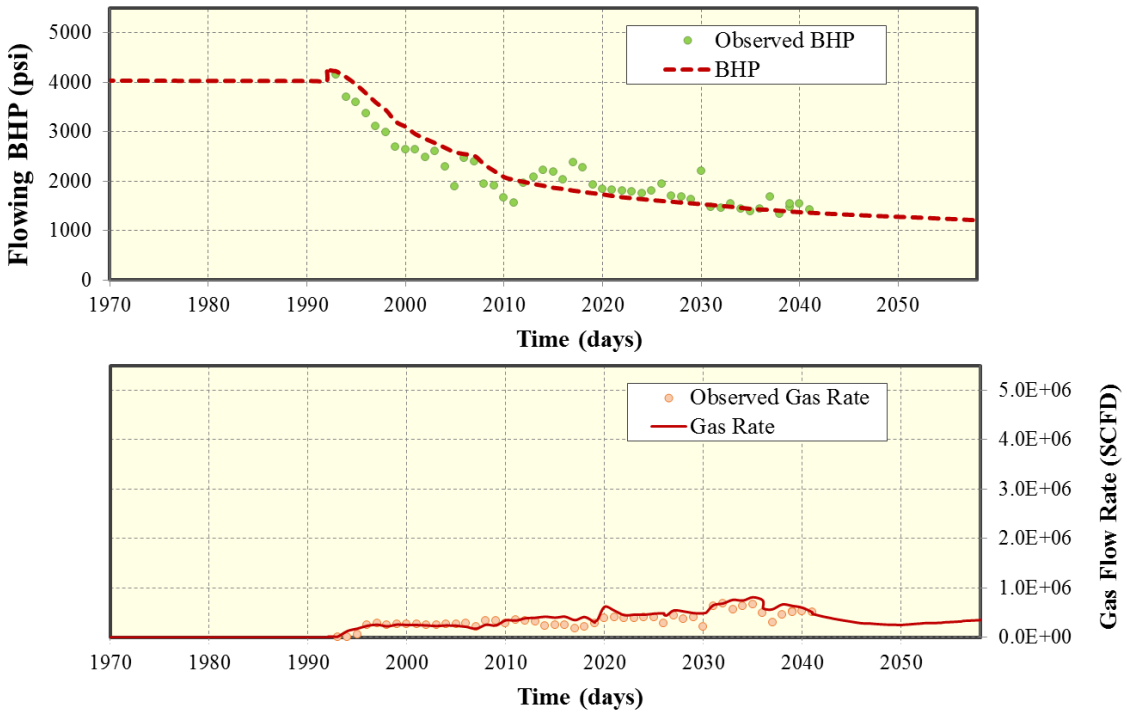

(i) BHP match and (j) Gas flow rate match of child well: W9H

Figure 4.8: Black Oil history matching results of child well W9H.

Similarly, pressure response is evaluated in the model to identify how long interwell communication is happening through time in the initial period of production of the child wells, as shown in Figure 4.9. All these long fractures start to reactivate and show interference in their reported production BHP. Hence, bottom-hole pressure tends to equalize throughout the reservoir once long fractures reach further wells. This approach gives an insight to future implementation of development plans which might include gas Huff-n-Puff strategies for enhanced oil recovery and detailed infill development strategies.

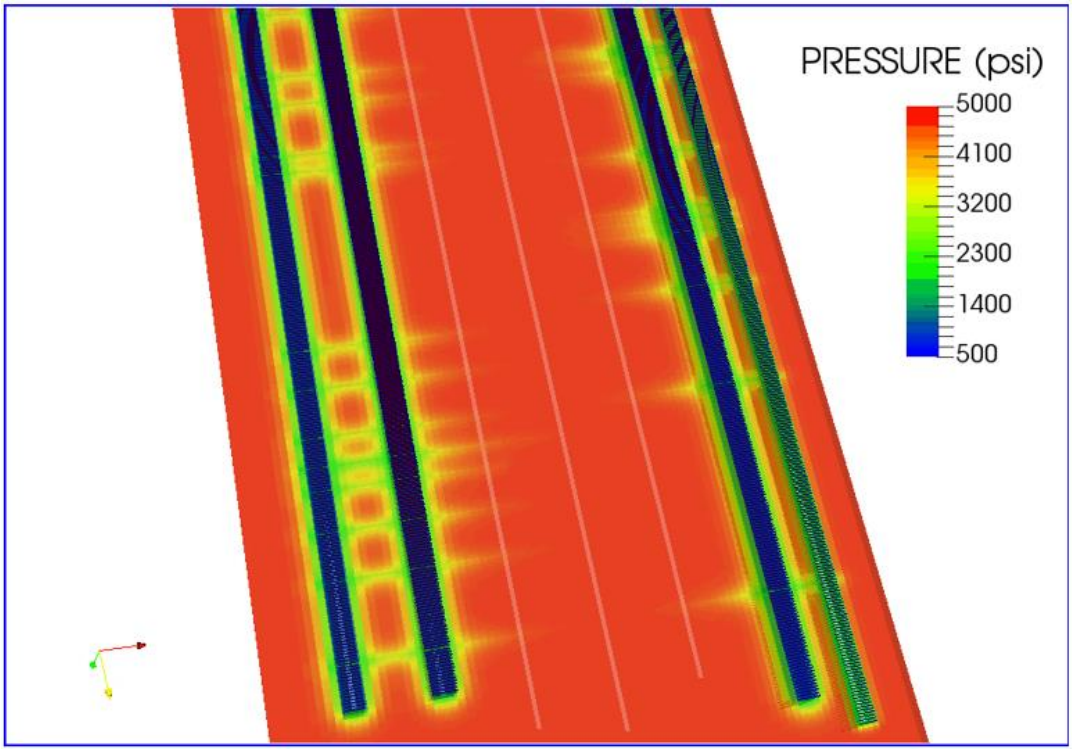
PRESSURE (psi)
5000
4100
3200
2300
1400
500

(a)

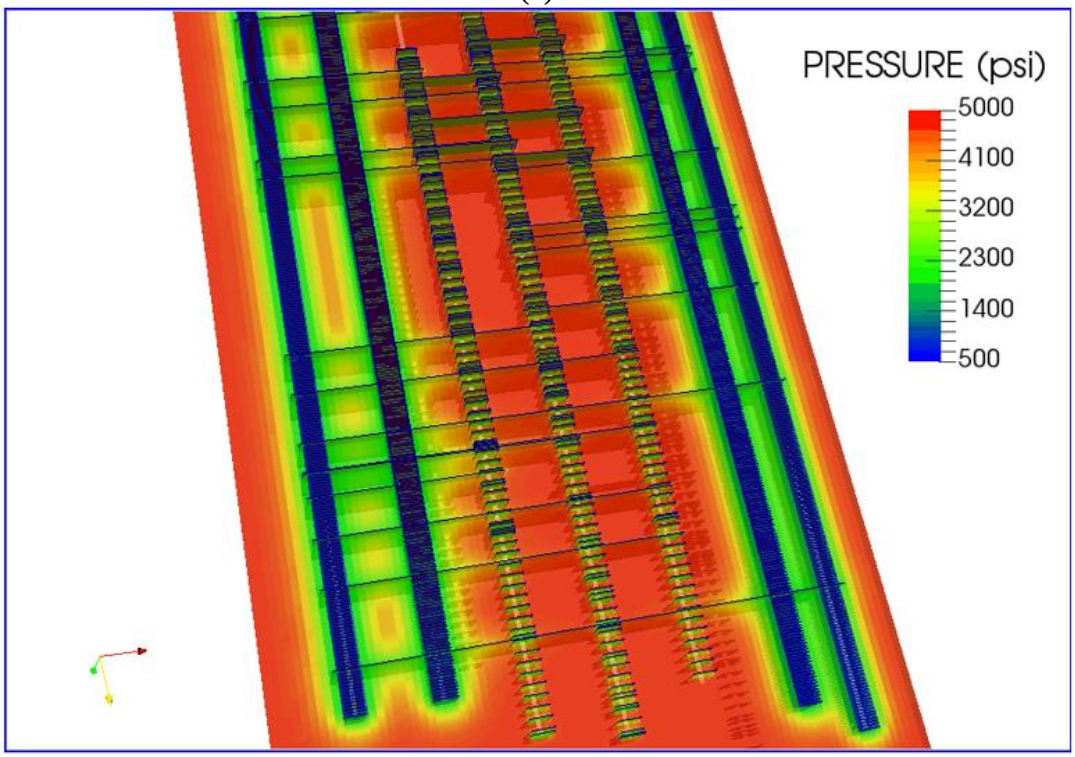
PRESSURE (psi)
5000
4100
3200
2300
1400
500

(b)

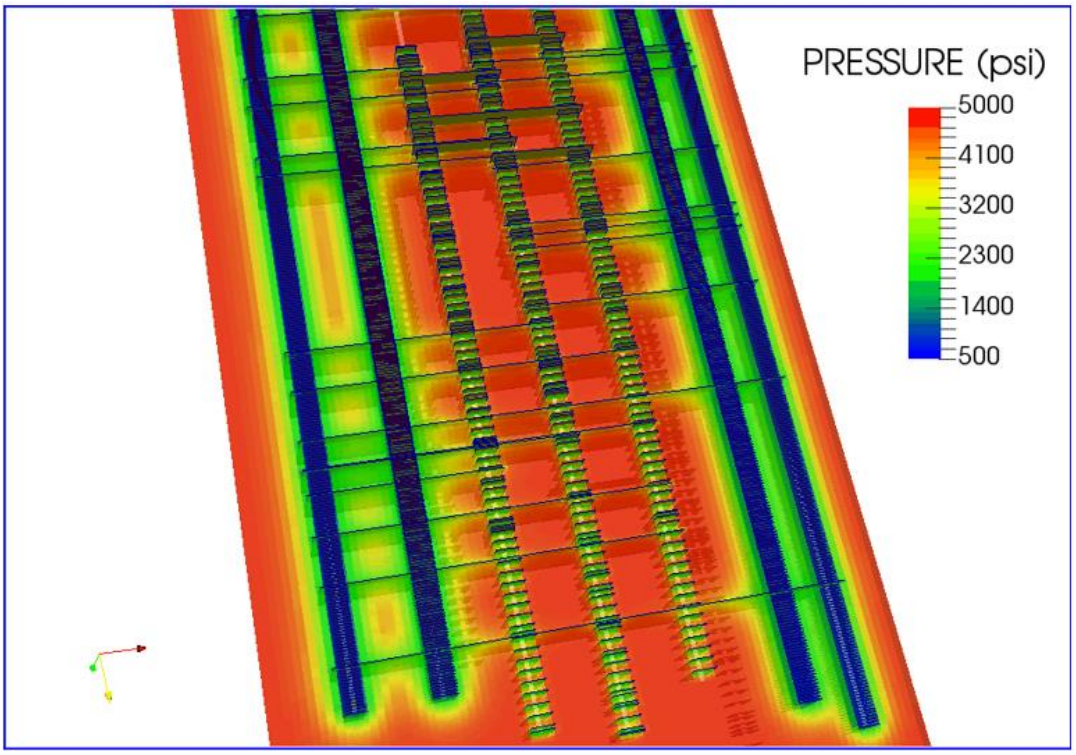

(c)

Figure 4.9: Pressure response through the interwell fractures in layer 5 of the black oil model, (a) before initiating child wells production, (b) after 12 days and (c) 42 days of CW production.

4.2 HUFF-N-PUFF RESULTS

EOR Huff-n-Puff performance results are presented in this section of the thesis. These outcomes include hydraulic fracture properties from initial sensitivity analysis as well as the interwell induced fracture layout and properties. Also, history matching results of the compositional sector model are displayed, proving its validation when compared to actual production data. Finally, more than 60 different forecasts have been performed regarding Huff-n-Puff implementation. In this thesis, a summary of these predictions will be exhibited with the best Huff-n-Puff designs that also considers pressure containment schemes.

4.2.1 Sensitivity Analysis Results for Sector model

Identical to applied in the black oil model previously, the sensitivity analysis allows the user to tune and specify optimal reservoir and fracture parameters that generate reliable history match solutions with respect to real production field data, and therefore, mimic the actual conditions of flow in the reservoir. A summary of fractures properties (e.g. parameters investigated) that were used in the sector model are shown in Table 4.2.

Well	Number of hydraulic fractures	Fracture conductivity, md-ft.	Fracture half-length, ft.	Fracture height, ft.
W1H	25	40	100	65
W2H	25	40	100	45
W5H	14	8	75	30
W6H	13	3	75	75
W7H	21	16	65	75
W8H	9	30	100	75
W9H	8	21	75	30
W3H	25	12	65	75
W4H	25	8	55	65

Table 4.2: Summary of fracture properties in parent and child wells after sensitivity analysis for the compositional sector model.

Also, as a result, eleven long interwell fractures are identified, modeled by EDFM, and located in the compositional sector model. Furthermore, these interwell long fractures are characterized with lengths ranging from 438 ft to 1,750 ft as seen in Figure 4.10 and Figure 4.11. Seven out of eleven fractures exhibit a length over 1,000 ft, which are directly correlated with the aforementioned full field black oil model. Beyond this distance, the resolution of the imaging tool may not be enough to capture apertures. Also, these long fractures share a common conductivity of 1.0 md-ft as a congruence on the assumption of their characterization as natural fractures in different academic studies. Moreover, this sector model captures the high frequency of the interwell fractures observed within very

close distances (less than 100 ft) with a greater resolution due to the EDFM features which allow multiple fractures in one single grid block (See Figure 4.12). This is related to high cluster interference on different wells supported by previous geo-mechanics and RT Analytical Model cluster efficiency studies (Ambrose et al., 2011).

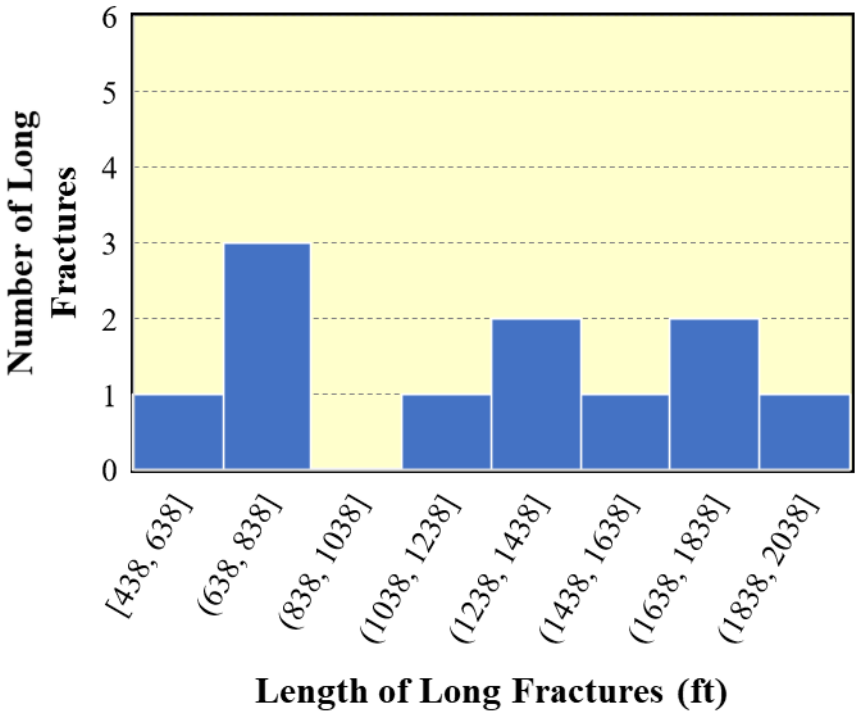

Figure 4.10: Histogram of the length of long interwell fractures employed in the sector model, as a result of correlating WBI logs.

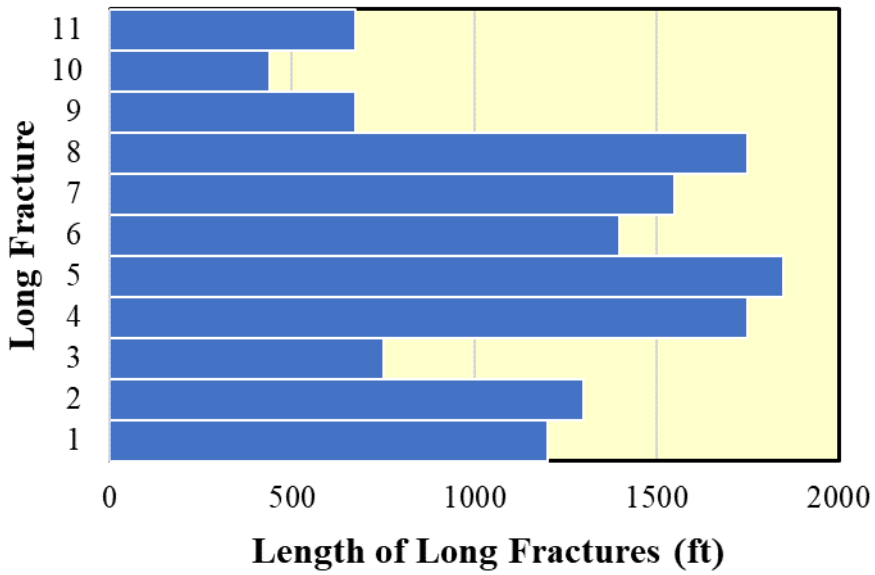

Figure 4.11:Fracture Length identification by long interwell fractures employed in the sector model.

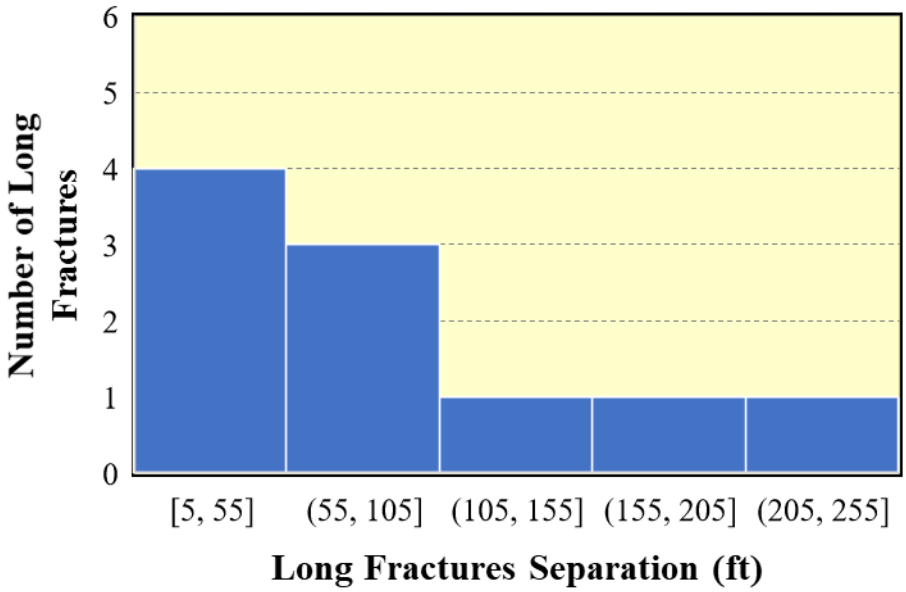

Figure 4.12: Histogram of the long interwell fractures separation among each other used in the sector model after correlating WBI logs.

Achieving a reliable history match allows us to define the optimal base case to start forecasting EOR Huff-n-Puff application in the model to anticipate expected fluid recoveries.

4.2.2 Compositional Sector Model History Matching

The history matching solutions define a layout of the fractures for the sector model as shown in Figure 4.13. Also, the results, which are consistent, denote the capability of the EDFM and are exposed in Figure 4.14 to Figure 4.22. It should be noted that as in all the history matching studies, the fracture parameters obtained from this study can be non-unique. However, for the purposes of this study, the presented scenario is satisfactory to continue to the next stage which is EOR huff-n-puff modeling.

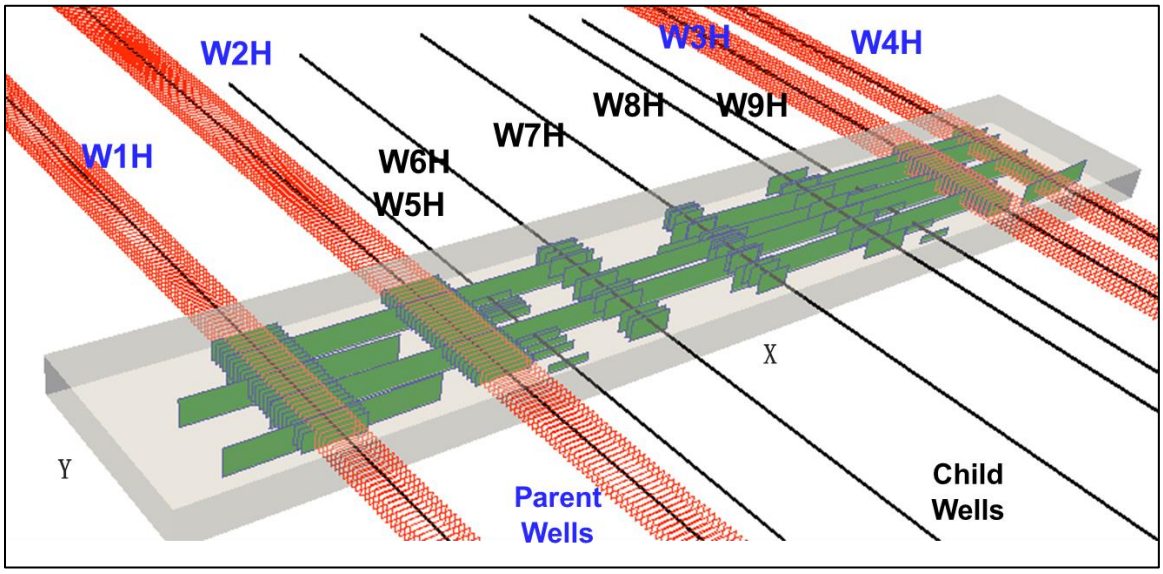

Figure 4.13: Sector model (4,100 × 500 × 130 ft) view extraction from the full field model.

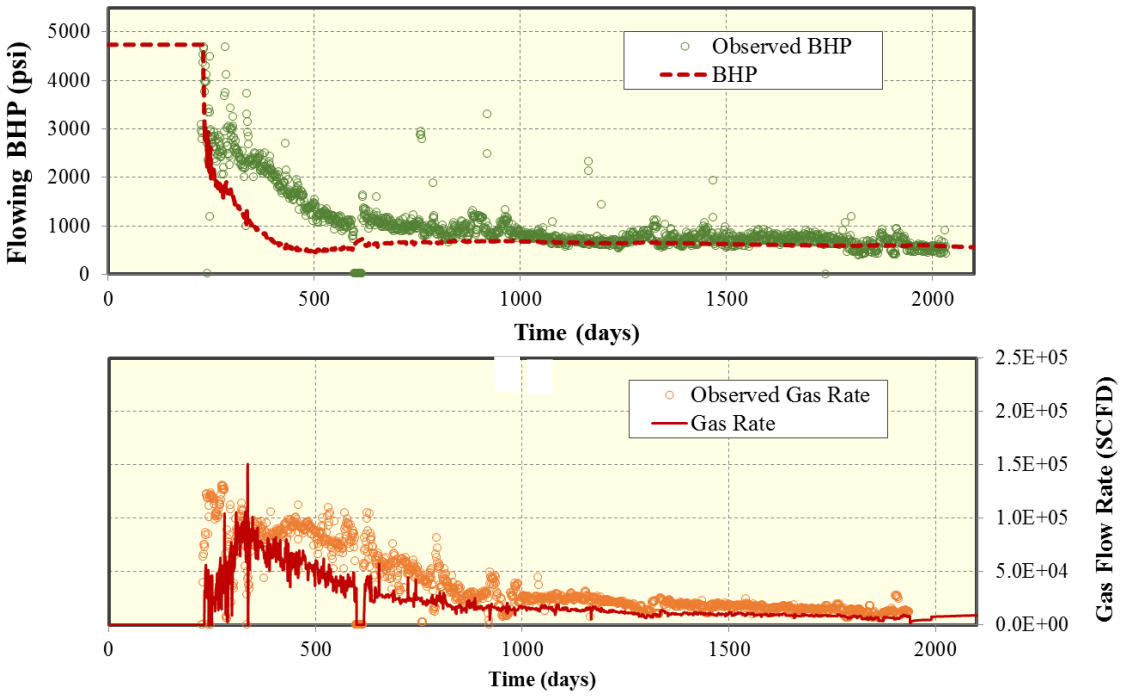

Figure 4.14: (a) BHP match and (b) Gas flow rate match of parent well of W1H in the sector model.

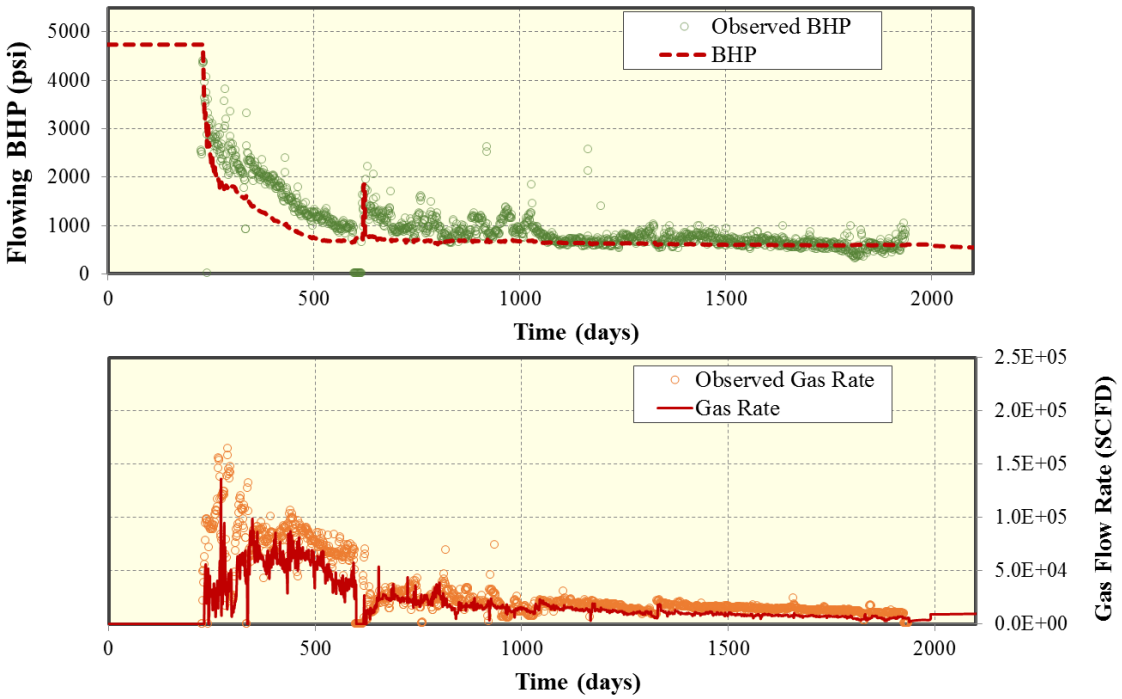

Figure 4.15: (a) BHP match and (b) Gas flow rate match of parent well of W2H in the sector model.

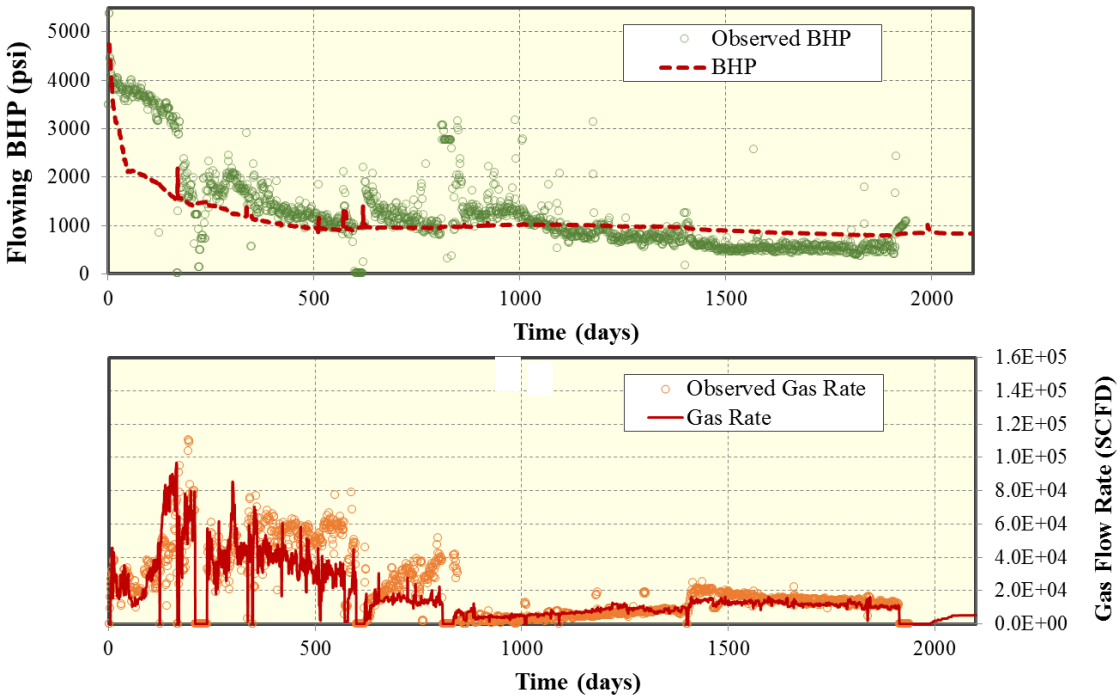

Figure 4.16: (a) BHP match and (b) Gas flow rate match of parent well of W3H in the sector model.

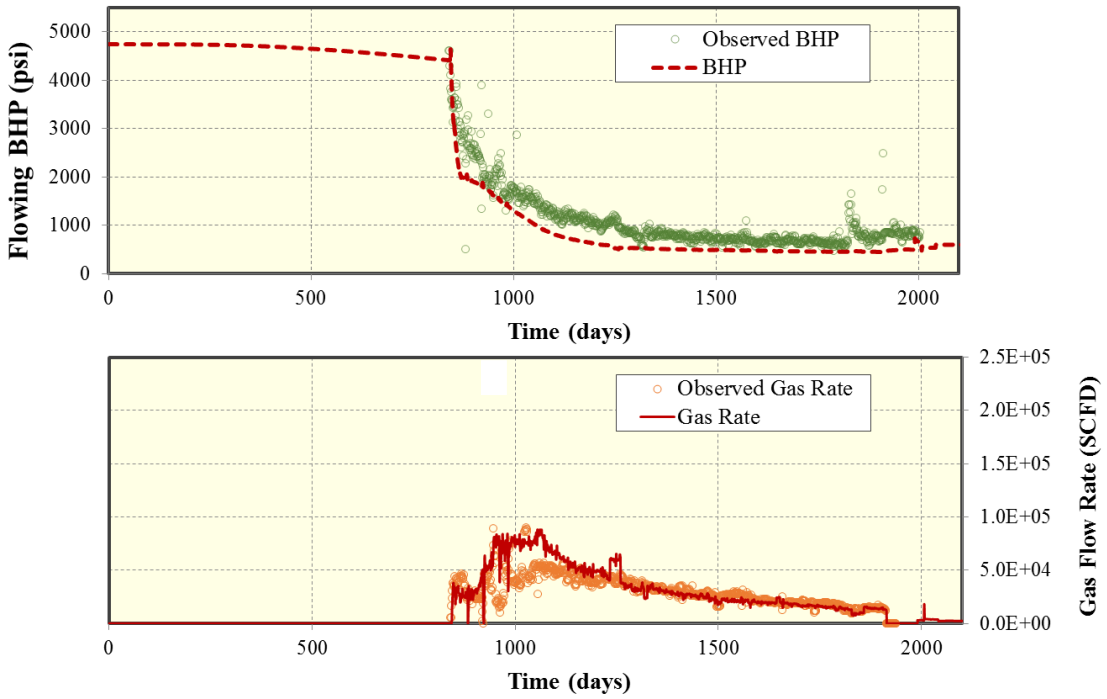

Figure 4.17: (a) BHP match and (b) Gas flow rate match of parent well of W4H in the sector model.

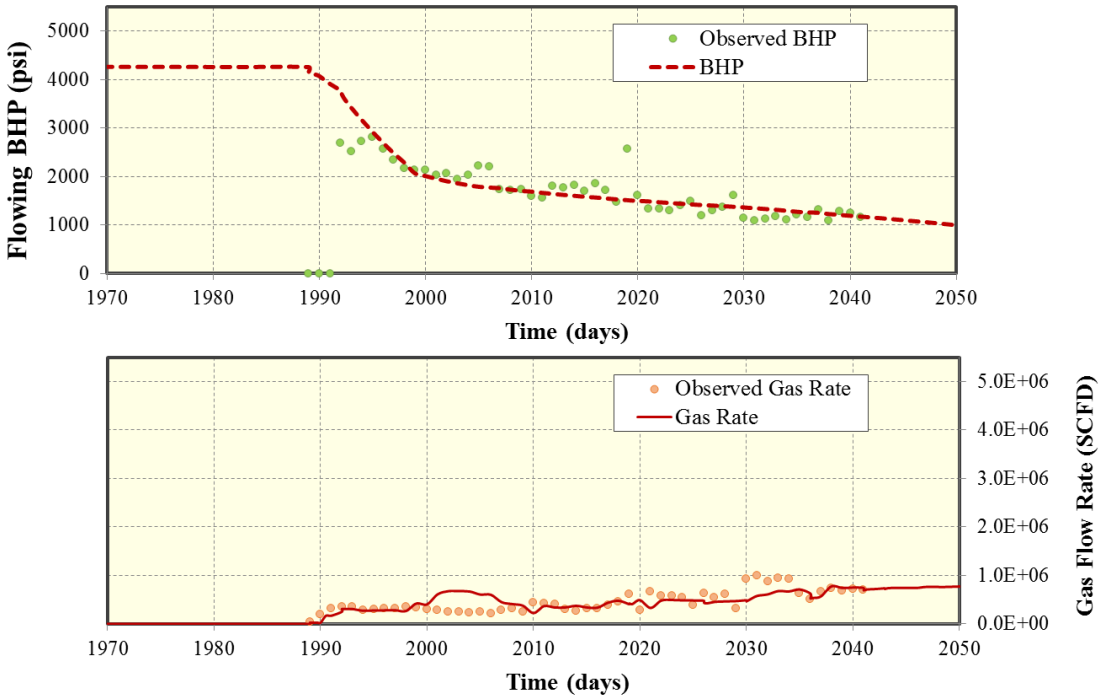

Figure 4.18: (a) BHP match & (b) Gas flow rate match of child well W5H in the sector model.

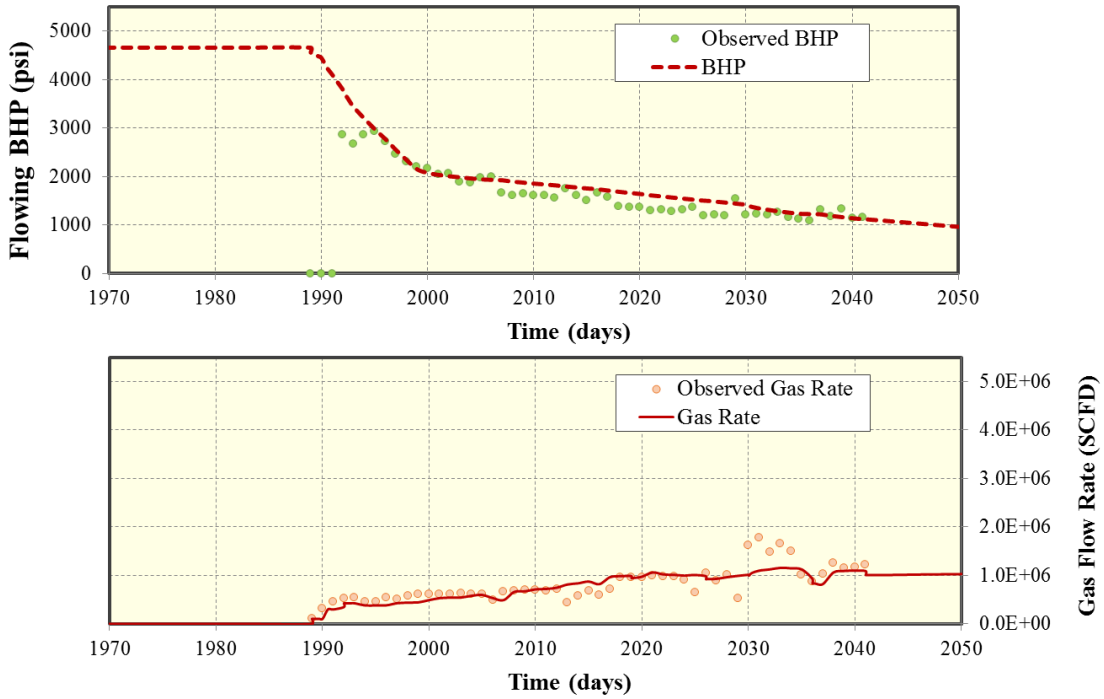

Figure 4.19: (a) BHP match & (b) Gas flow rate match of child well W6H in the sector model.

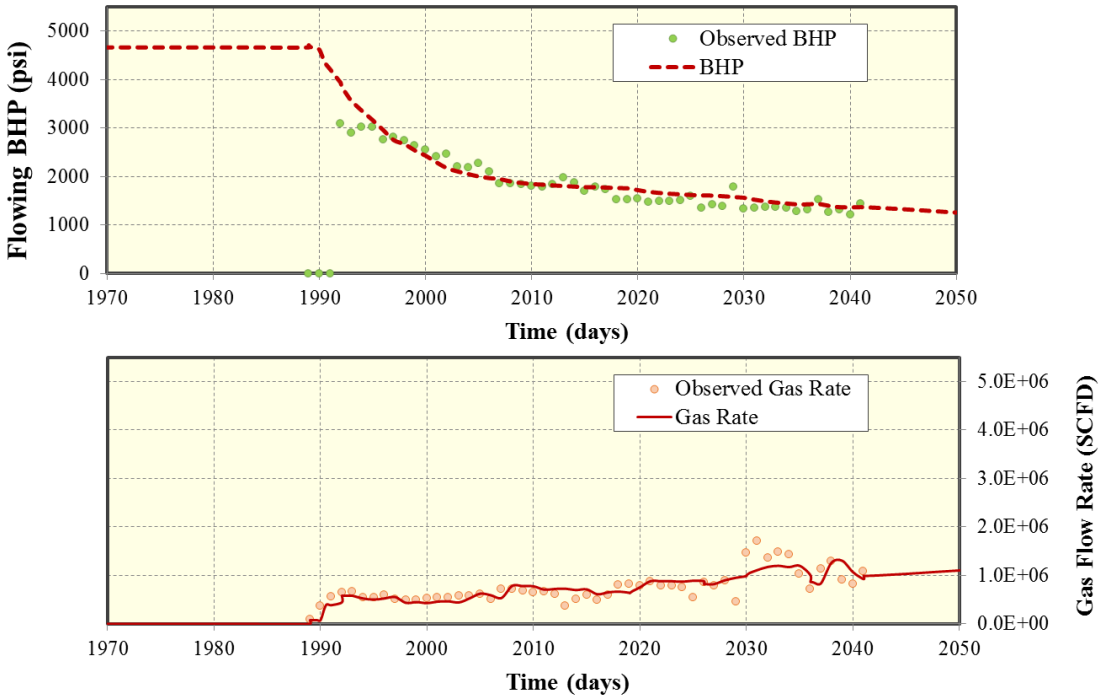

Figure 4.20: (a) BHP match & (b) Gas flow rate match of child well W7H in the sector model.

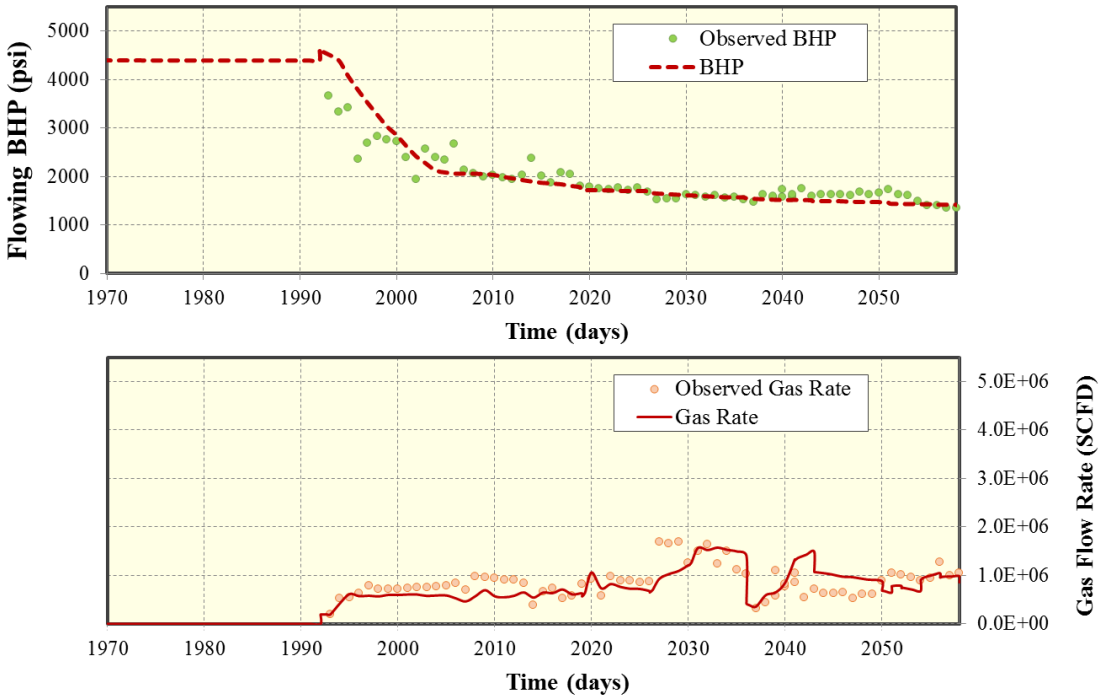

Figure 4.21: (a) BHP match & (b) Gas flow rate match of child well W8H in the sector model.

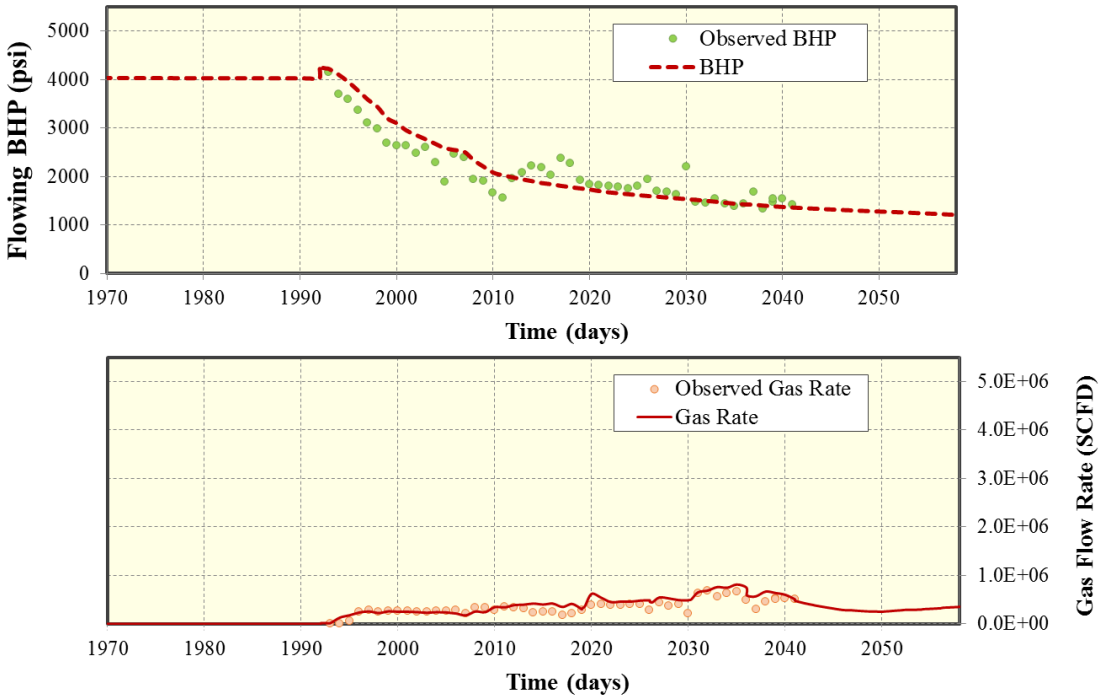

Figure 4.22: (a) BHP match & (b) Gas flow rate match of child well W9H in the sector model.

4.2.3 Huff-n-Puff Forecasts Results

Huff-n-Puff recoveries are downgraded due to interwell communication or interference by long natural fractures with very high conductivity. The additional cumulative oil recovery reaches up to 12% in 8 years of forecast. This simulation outcome is validated by field data, which detects the presence of the injected gas in further zones of the reservoir. As shown below, the average reservoir pressure is initially not increased sufficiently by the Huff-n-Puff injection after the primary depletion stage, indicating reduced reservoir pressure maintenance ability. Consequently, pressure leak occurrence seems inevitable in this part of the field so that it is characterized in this sector model to determine optimal changes.

4.2.4 Pressure Leak Off

For this study, modeling the long interwell fractures is fundamental to show this unfavorable pressure containment phenomenon and its impact on the EOR Huff-n-Puff implementation and to show the favorable outcomes of cycle timing and production efficiency if containment is enhanced. Even though shale formation with a high fracture intensity is, in general, considered to have a great enhancement in oil recovery by using gas injection (Alfarge et al., 2018), it can also be detrimental to the oil recovery economics if the interwell interference is excessive and not well understood or mitigated as presented in this study case in this part of the black oil window of Eagle Ford. Hence, the compositional sector model characterized this pressure leak-off through the long interwell fractures whose extension reached up to 2,000 ft as reported by the operator. For instance, Figure 4.23 compares pressure profiles communication among the seven wells located in the fifth layer of the model at different subsequent times.

The pressure is not properly contained in the sector when simulating one single injector for the EOR huff-n-puff process at low gas injection rates. The results in this case, which are not very satisfactory, demanded attempts with different scenarios of Huff-n-Puff. Likewise, gas saturation changes in the model do not replicate a broader dispersion behavior in the sector model as previously reported by the field operation of a pilot test in a similar area of the reservoir.

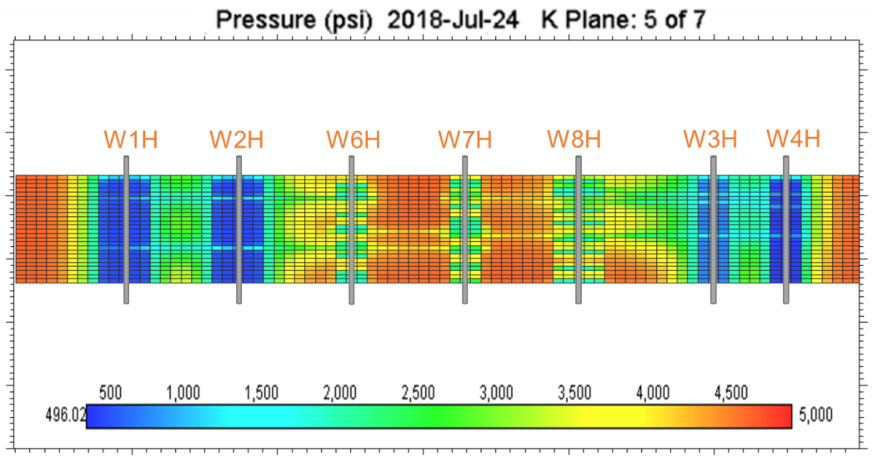

(a)

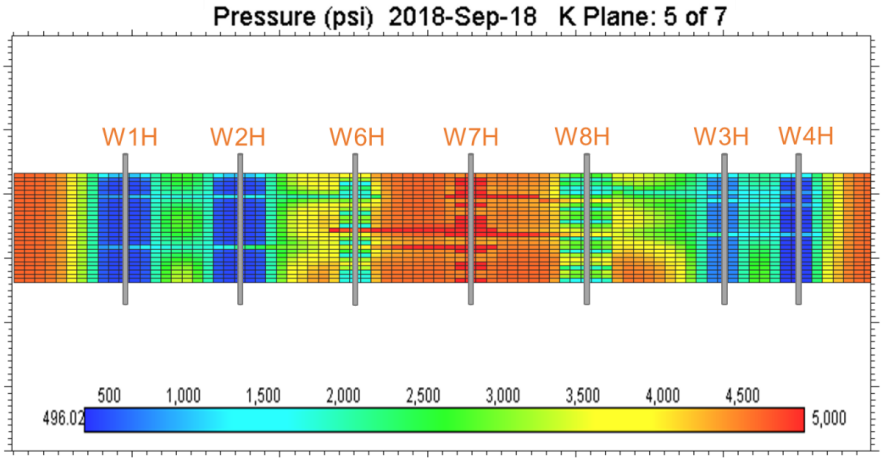

(b)

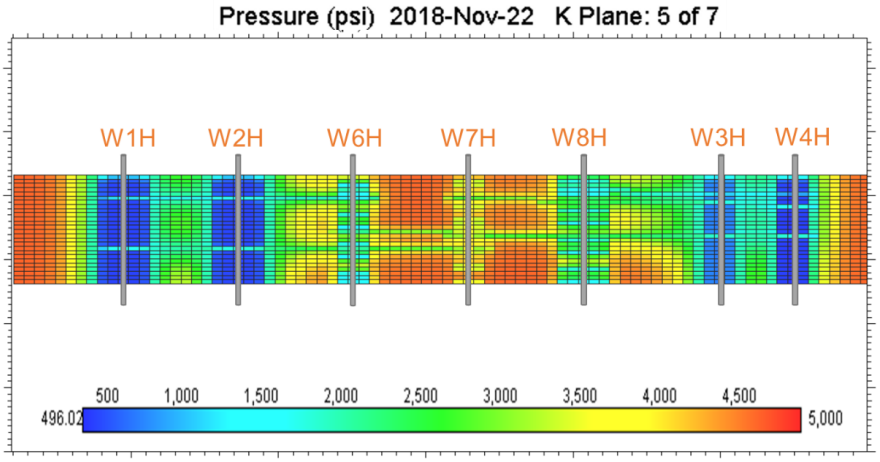

(c)

Figure 4.23: Pressure response through the interwell fractures displayed in a 2D grid (layer 5) of the sector model: (a) before initiating an injection cycle, (b) after 50 days of injection and (c) after another 50 days of production.

4.2.5 Cycle time reduction optimization

One of the most popular and challenging questions in Huff-n-Puff process is to define optimum injection and production periods. Optimized Huff-n-Puff strategies consider that each cycle should increase the production rate compared to the wells initial rate. Once the oil rate starts to drop, another injection cycle should start. The purpose of this scheme is that not only the first cycle, but also subsequent cycles may be able to increase production. This optimization of cycle times applies to gas and water injection in our study. As a result of the sensitivities in this thesis related to this matter, recoveries are maximized. Figure 4.24 exhibits the BHP profile of a forecast case in which the number of cycles is evaluated.

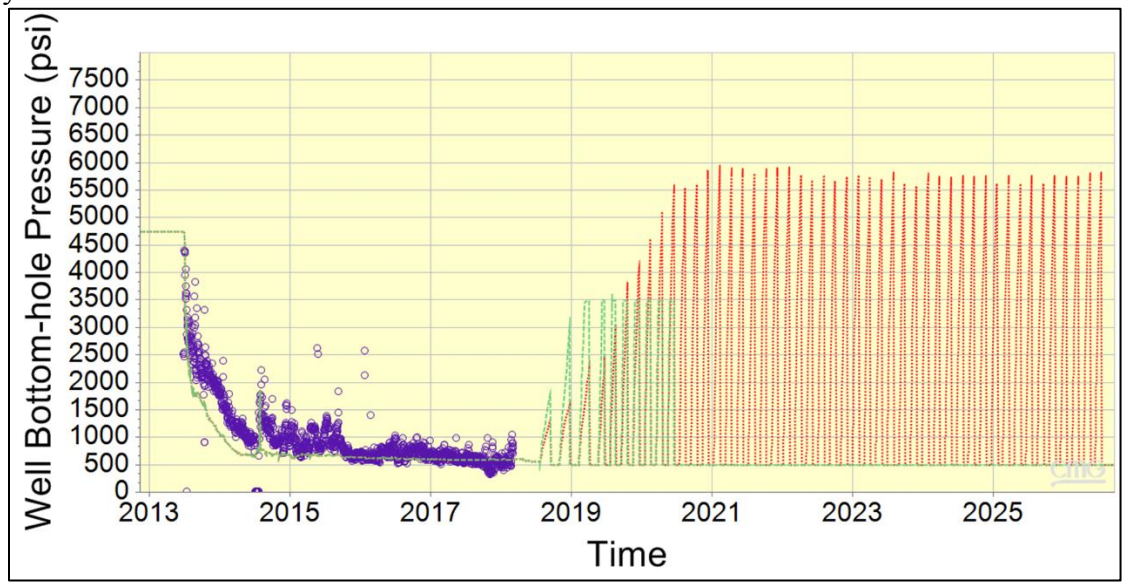

Figure 4.24: BHP profile forecasts for water injector well W2H throughout nine years (red) or three years (green) considering different number of cycles of 30 days.

4.3 Final Estimated Results

The efficiency of applying Huff-n-Puff in combination with adequate pressure maintenance strategies was assessed by comparing the estimated cumulative oil volume with other production mechanisms. Therefore, for the sector model described in this

document, these volumes and their recoveries are exhibited in Figure 4.25 and in Table 4.3. The comparison includes cumulative oil volumes and incremental percentage with respect to Primary production (143 MBBLS). The other production mechanisms considered are Huff-n-Puff, Huff-n-Puff plus pressure containment with water injection for short term, and Huff-n-Puff plus additional pressure containment strategies.

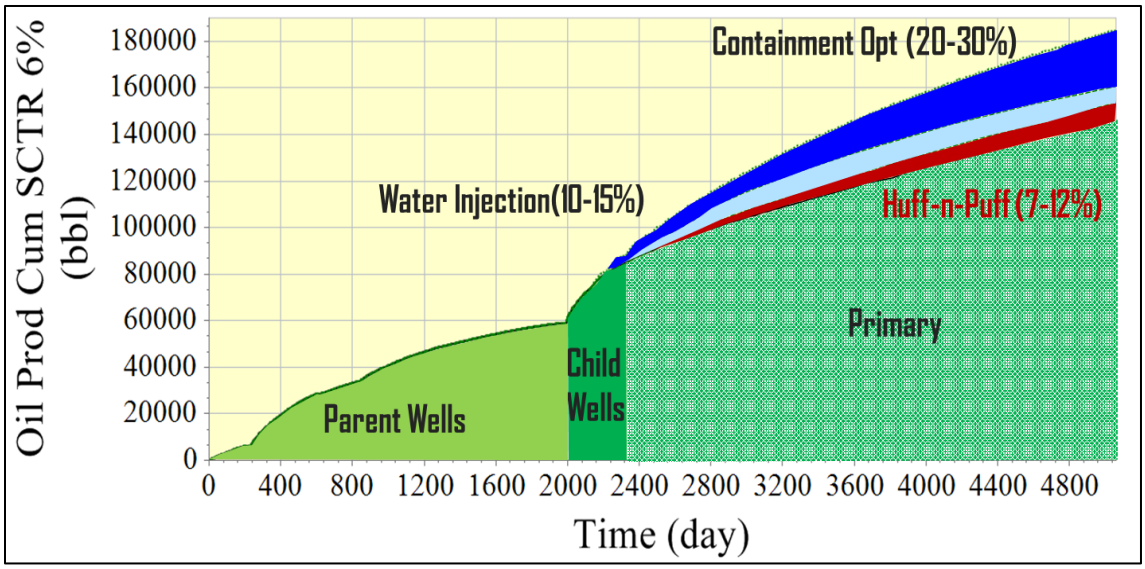

Figure 4.25: Cumulative oil volumes comparison among Primary production, only Huff-n-Puff, Huff-n-Puff and short term water injection, and Huff-n-Puff and additional pressure containment strategies.

Production Strategy	Cumulative Oil Prod (6% Sector model)	Incremental Oil recovery
Primary	143,255 BBLS	-
Huff-n-Puff	153,802 BBLS	7%
Huff-n-Puff+ Water	160,420 BBLS	12%
2 Gas Huff-n-Puff + Pressure containment	184,000 BBLS	29%

Table 4.3: Final results of cumulative oil volume and incremental oil comparison among primary production, only Huff-n-Puff, Huff-n-Puff and short term water injection, and Huff-n-Puff and additional pressure containment strategies.

In particular, the highest cumulative oil recoveries were achieved by contemplating the Huff-n-Puff and pressure containment arrange that is show in Figure 4.26. This optimum case considers: 2 gas injectors wells, with an injection rate of 900,000 MMscf/d for each well in the sector model (equivalent to 6% of the total volume,) or 15 MMscf/d for the full field model, and 50 cycles with duration of 30 days per cycle. Simultaneously, this optimum scenario considers one water injector in the middle of the nine wells with an injection rate of 4,320 bpd for the full field model or 260 bpd (6%) for the sector model, only 10 initial cycles of 30 days each. For both kind of injectors (i.e. gas and water) the considered injection BHP is 3,500 psi.

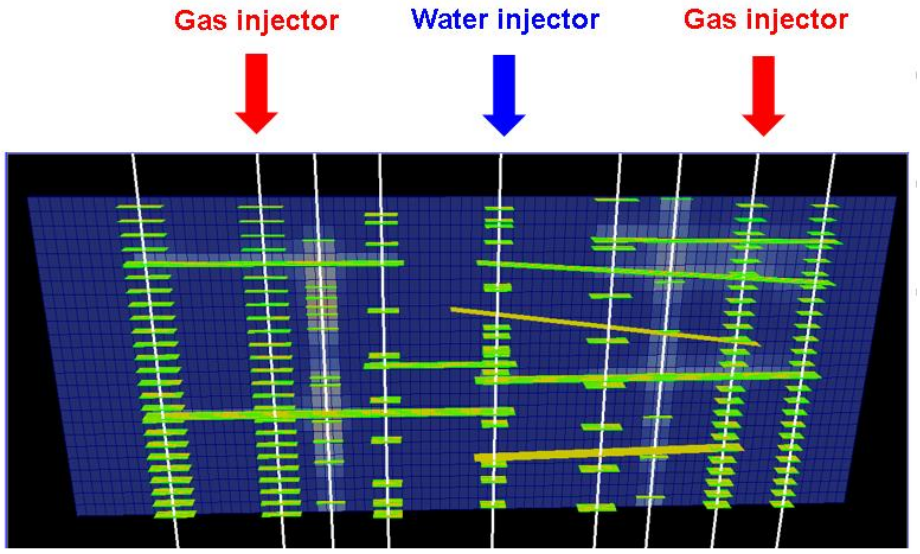

Figure 4.26: Optimal Huff-n-Puff design considering water injection as a pressure maintenance supplementary strategy.

The results presented above aim to forecast optimal designs for implementing Huff-n-Puff in a black oil area of the Eagle Ford reservoir considering multiple well fracture interference modeled with EDFM method. The descriptive outcomes of the simulation taking into account the inferential solutions were presented, as well the respective analysis for reservoir best performance when implementing this EOR technology. Furthermore, graphical representations of different properties such as 3D visuals of fracture

arrangements, pressure dynamics, and gas saturation variations in the model help to develop a holistic idea of the different oil recoveries forecasts studied with respect to the field and surface facilities constrains. Finally, it is clear from the results that the Huff-n-Puff with proper containment pressure strategies is both efficient and simple as an enhanced oil recovery method in unconventional reservoirs. In fact, it relates a real field case production data with interwell fracture interference where the behavior for the reservoir and the fractures is well modeled with EDFM. A more detailed summary and discussion of the findings are presented in the following Chapter 6.

CHAPTER 5

ECONOMIC EVALUATION

The fifth chapter of this thesis briefly performs an economic feasibility evaluation on the Huff-n-Puff implementation which has been modeled in this study by both deterministic and probability Discounted cash flow models. The principal sections of this chapter summarize the economic terms, methodology, and results for coupling their connotation in the research context of this work.

5.1 UNCONVENTIONAL RESERVOIRS ECONOMICS BACKGROUND

The extraction and development of unconventional resources from shale rocks has incited an exponential growth of oil and gas wells drilling and has changed the energy landscape not only in the United States but also worldwide. Nevertheless, as a dynamic as the oil market is, oil and gas companies have experienced a recent setback in 2015 and 2019 because of falling oil prices. The industry has been struggling to optimize their expenses and accommodate capital investments to the current economic conditions.

The economic feasibility of production from shale reservoirs differs from conventional ones in many aspects. First, there exists great uncertainty in characterizing shale and tight sands rocks, and therefore, in forecasting their production. This limited great uncertainty is transmitted when evaluating the economics of drilling new wells in these reservoirs. Second, shale formations are very complex and come along with extra associated costs, such as different well designs, handling flow-black water, implementing fracking among others. Therefore, questions arise when analyzing their cash flow and balance sheets to wonder what economic aspects are considered when improving the economics of new wells and developing these unconventional reservoirs.

5.2 ECONOMICAL PARAMETERS

5.2.1 Costs

The appraisal of the costs (capital as well as operating) is not only important for the required economic analysis, but also for the preparation of the company's budgets. Underestimating costs may lead to project costs overruns that result in disappointing profitability, not to mention the painful justification of budget increases. On the other half, overestimating these costs may result in prematurely killing a project or unnecessary freezing (or spending) funds that could have been usefully employed elsewhere in the company's plan.

5.2.1.1 Capital Costs (CAPEX)

Capital costs or capital expenditures (CAPEX) are funds invested by a company to start a new project or to improve the useful life of an existing capital asset. CAPEX is developed through a cost estimate, very often by a company's internal cost estimation department. The main characteristic of CAPEX is that they are one-off costs, usually incurred at the beginning of a project. These costs are also known as front-end costs (Mian, 2011). Thus, the operating costs during the project implementation phase are also considered as capital cost. However, the capital costs may also occur during the economic life of a project. For example:

- Recompletion of wells into another depth.
- Sidetracking an existing well with a horizontal well.
- Drilling child infill wells
- Major upgrading/replacement of existing facilities
- Installing facilities for gas injection or enhanced oil recovery Huff-n-Puff.

CAPEX normally consists of geological and geophysical (G&G) costs, drilling, facility costs, tankers flow lines, camps and accommodation. Nevertheless, when analyzing the economics of shale plays, CAPEX are usually focused on the economic feasibility of drilling a new well or a group of wells in a certain area where G&G costs can be disregarded as shale reservoirs have little discovery risk and very few wells are dry ones (Lake et al., 2013). Hence, this economic analysis also disregards facilities and pipelines costs on an already productive play due to the fact that they were already considered when evaluating the initial development of the play.

Furthermore, drilling costs estimates may require technical aspects of the well to be drilled such as the type of well (i.e. development or exploratory), the configuration of the well (i.e. producer or injector), the type of drilling contract (i.e. based on the supply and demand of rigs available in that area), the rig type (i.e. rig size), and completion equipment. Also, notwithstanding with conventional wells and regarding completion expenditures, shale wells need additional operations after drilling to be able to produce. From those, hydraulic fracturing is the major element of the completion cost, which considerably adds to the capital cost of putting a well into production. Finally, additional expenditures must be included in the CAPEX when planning to implement Huff-n-Puff due to the need of facilities to treat the produced gas and use it as an injection gas,

Nonetheless, for the purposes of this thesis, CAPEX variables are not exhaustively examined nor analyzed individually. Yet, the capital costs used in this economic evaluation per injector well include the standard costs breakdown for D&C in the Eagle Ford, which is shown in Table 5.1. Plugging and abandonment costs are not included in the drilling costs, but they will be used in the economics feasibility model separately. The rest of these values have been corroborated by the operator of the Omega field. Therefore, CAPEX under this circumstances of this thesis are composed by drilling and completion costs

(D&C), Huff-n-Puff implementation costs, and in a diminished extent by abandonment costs.

DRILLING	**Cost (x10^3)**
Set Up costs	$210.00
35 Rig days @20k/d	$700.00
Fluids, chemicals, transportation & fuel	$270.00
Services & rental equipment	$540.00
Bits, expendable equipment & Misc.	$60.00
Labor, engineering & overhead	$70.00
Casing and other tangibles	$190.00
Contingencies	$240.00
Sub-total for drilling	$2,280.00
COMPLETION	
Set up	$35.00
Rig & daywork	$115.00
Fluid, chemicals, transportation & fuel	$65.00
Services & rental equipment	$200.00
Formation Stimulation	$2,560.00
Expendable equipment & Misc.	$15.00
Casing and other tangibles	$430.00
Contingencies	$300.00
Sub-Total for completion	$3,720.00
HUFF-N-PUFF	
Gas processing and facilities	$1,000.00
Total D&C budget	**$7,000.00**

Table 5.1: Drilling and Completion Standard Capital Costs (Rigzone, 2011)

5.2.1.2 Operation Costs (OPEX)

Operation costs (OPEX), also known as lease operating expenditures (LOE), arise periodically and are necessary for daily operations. These costs are usually expressed in expenditure per year or per unit of production, and typically include: utilities, production costs, maintenance, administrative and general (A&G) overhead, transportation costs, evacuation costs, and insurance costs (Mian, 2011). OPEX are highly variable ranging from 6.00 to 24.50$/BOE influenced by location, well performance, play type, and company

efficiency (U.S. EIA, 2016). The operating costs normally consider the following components: fixed costs, and variable costs per unit of production (i.e. determined as a function of production rate).

For this economic evaluation OPEX is divided in three main categories: OPEX for producing oil which includes all the operational costs associated to have a barrel of oil on surface, OPEX for gas processing which includes rich gas transportation and processing for injection, and OPEX for taxation payments which consider severance and ad-valorem tax percentages. Finally, since OPEX values varies widely, minimum and maximum estimates were provided by the operator for each of these categories. Further analysis of these OPEX parameters will be presented below.

5.2.1.3 Financing Costs

Financing costs include the expenses associated to securing financing for a project. International Accounting Standard 23 defines finance costs as "interest and other costs that an entity incurs in connection with the borrowing of funds" (IFRS, 2009). Since oil and gas projects are capital-intensive, companies finance their operations either from equity financing or through borrowings and loans. As a result, the financing costs include interest payments and other costs paid to the suppliers of the funds. Additionally, other costs can include amortization of discounts or premiums that are connected to the borrowings, finance charges applied to finance leases, and exchange differences from foreign currency borrowings (IFRS, 2012). Consequently, there exists two sources of raising capital, debt and equity. Despite debt is cheaper, it is considered a burden and a risk. Therefore, companies should try to raise equity to maintain an appropriate balance (Inkpen and Mofett, 2011).

Furthermore, opportunity cost needs to be included when discussing financing costs since it is defined as "the potential benefit lost or sacrificed when the choice of one course of action requires giving up an alternative course of action" (Mian, 2011). Normally, companies maintain a portfolio of projects, and they must select the proper one that will generate attractive returns on their investments. Therefore, the opportunity cost must be taken into consideration when performing economic analysis through the discounted cash flow method. This opportunity cost is reflected in the discount rate used for the evaluation. The discount rate is the risk-adjusted cost of capital for the specific project. For instance, this economic evaluation for the application of Huff-n-Puff considers as discount rate of 10%, which is the value provided by the operator the Omega field.

A company generates value for their shareholders when it invests in projects that yield results above their cost of capital (Inkpen and Moffet, 2011). Due to the fact that companies usually employ financing mechanisms to increase capital, they must choose a discount rate that is above their weighted average cost of capital (WACC). This WACC is the corporate hurdle, meaning the proportion of debt and equity, and depends on the capital structure of the company (Inkpen and Moffett, 2011).

5.2.2 Taxes

Despite Texas does not charge a property tax on the value of oil and gas property or a state federal income tax, it collects tax revenues via a severance tax. Additionally, companies also pay federal income tax.

5.2.2.1 Severance Tax:

The baseline for Texas is 4.6% on the market value of produced oil and condensate, and it is 7.5% on the market value of gas produced. For this study, the employed severance tax is 4.6% due to the model is for oil wells.

5.2.2.2 Ad Valorem Tax:

An ad valorem tax is a tax based on the assessed value of an item, such as real estate or personal property. The most common ad valorem taxes are property taxes levied on real estate. However, ad valorem taxes may also extend to a number of tax applications, such as import duty taxes on goods from abroad.

5.2.2.3 Federal income Tax:

The considered federal income tax for this model is 35%. This corporate tax is imposed on the net taxable income (the difference between gross income and allowable tax deductions). Some allowable tax deductions include depletion, depreciation, and amortization (DD&A). This economic model includes a cost depletion calculation.

5.2.3 Production Forecast

Forecasting the production of a well or a group of wells is essential to estimate the feasibility of an oil and gas project investment because this hydrocarbons production forecasts are strongly related to variable OPEX costs. Furthermore, the production pattern of shale oil and gas wells differs widely to conventional ones. For instance, unconventional reservoirs production declines faster than conventional reservoirs due to their low flow capacity characterized by ultra-low permeability. In that sense, a shale well can reach its total production life within the first five years in contrast to the projected thirty-year longevity for most conventional wells. Therefore, economic performances are appraised within the first 5 to 10 years of production

This economic evaluation considers the oil and gas production forecasts that are obtained from the numerical simulations presented in Chapter 4. Specifically, the feasibility analysis contemplates only the Huff-n-Puff optimal design. In that sense, oil and gas production from the 6% compositional sector model, which contains 9 wells, is

cumulated and tabulated per year, and upscaled to a full field scale. Also, the forecasts employed in this economic appraisal considers 9 years, starting from January 1st, 2018 and extending until January 1st, 2026. Moreover, the gas production of Omega field needs to be corrected by volumetric analysis between the produced gas and the injected gas. As a consequence, the input values for production are presented in Table 5.2.

		6% Sector model		Full Field Gross Production	
Time (day)	Date	Oil (bbl)	Gas (MMscf)	Oil (bbl)	Gas (MMscf)
1875	1/1/2018	5,269.67	16.50	87,827.83	275.06
2240	1/1/2019	25,366.80	-	422,780.00	-
2605	1/1/2020	22,278.67	36.83	371,311.22	613.79
2971	1/1/2021	17,181.52	26.48	286,358.68	441.35
3336	1/1/2022	14,232.95	22.21	237,215.78	370.18
3701	1/1/2023	12,315.52	14.72	205,258.67	245.30
4066	1/1/2024	10,785.72	3.40	179,762.07	56.60
4432	1/1/2025	9,717.61	0.58	161,960.10	9.75
4797	1/1/2026	8,849.52	-	147,491.99	-
	Cumulative	176,991.91	120.72	2,949,865.18	2,012.02

Table 5.2: Full field gross production forecast from numerical simulation

5.2.4 Royalty

It is the stipulated fraction of the oil and gas produced that is paid to an owner for the ongoing use of their asset or property (lessor of the land) either in kind or its equivalent in money. Royalties are usually negotiable in Texas, and therefore vary by lease. The base royalty used in the model is 25%, which has been verified by the operator company. Moreover, this percentage is used when evaluating projects in the Eagle Ford (TRRC, 2016) and it is also the common rate from 34,904 leases from 2005 and 2011 in Hanesville field area (Herrnstadt et al., 2019).

5.2.5 Market Pricing

The price approach has a tremendous impact in the feasibility of a project in unconventional reservoirs. These prices imply market-based control and responds to volatile behavior of global supply and demand. Data for West Texas Intermediate (WTI) crude oil prices have been considered for this economic evaluation as well as data for Henry Hub natural gas spot prices. Historical data and forecast prices of both of these resources are collected from EIA. Also, the operator of the field has provided its crude oil base price estimation, which lays within the EIA margin for the upcoming years. Likewise, stochastic forecasts will be employed in oil and gas pricing further in this evaluation to generate different scenarios with Monte Carlo simulation due to the randomness of the market price.

5.2.5.1 Crude Oil Market Price

The operator defined a base price of 55$/bbl. as input for the economic appraisal. Also, EIA's January Short-Term Energy Outlook (2019) forecasts that U.S. benchmark West Texas Intermediate (WTI) crude oil will average $59 per barrel in 2019 and $58/bbl. in 2020, but overall it will remain lower than the 2018 average of $65/bbl. (Figure 5.1).

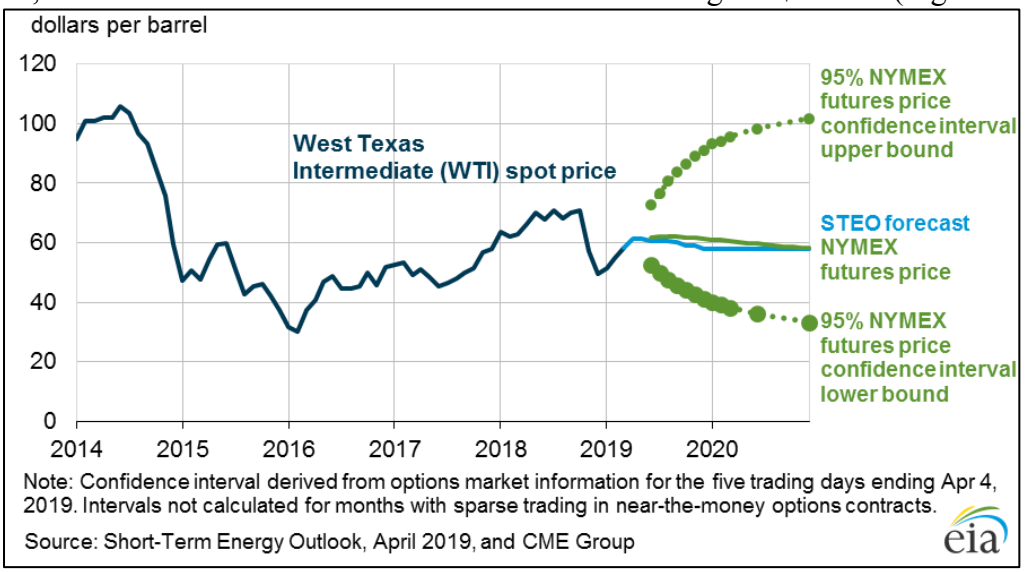

Figure 5.1: West Texas Intermediate (WTI) crude oil price and NYMEX confidence intervals (EIA, 2019).

Additionally, all this historical data from January 2015 is statistically tabulated and processed, including the forecasts from April 2019 until December 2020 in order to find a possible statistical distribution of the WTI spot price. From Figure 5.2 it can be observed a normal distribution of the prices during these years.

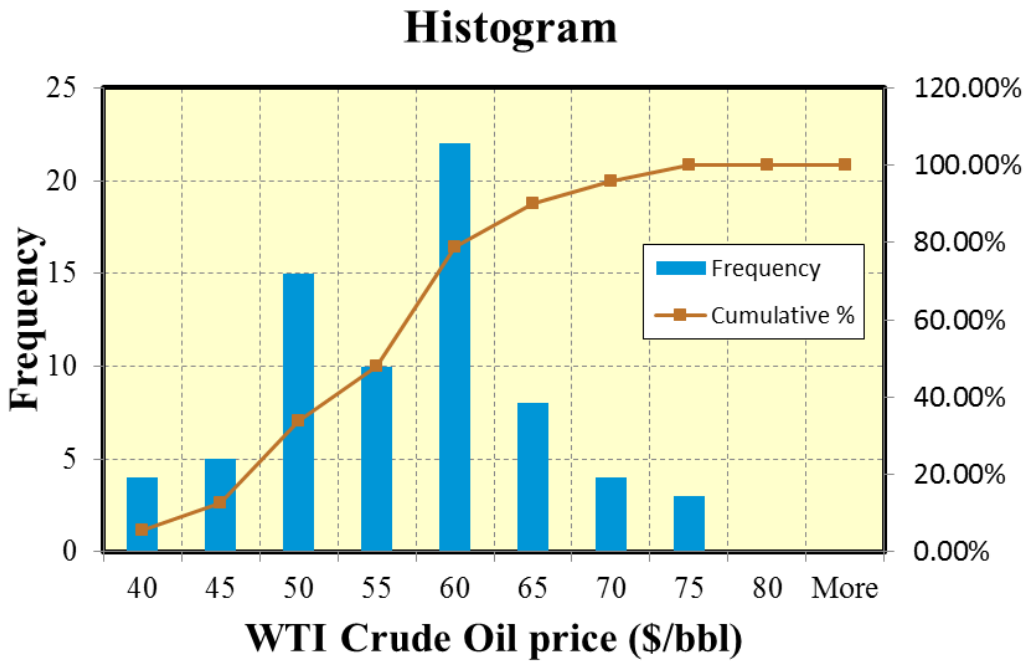

Figure 5.2: Histogram of spot WTI crude oil prices from 2015 to 2020.

5.2.5.2 Gas Market Price

The price of natural gas is also extracted from EIA's January 2019 Short-Term Energy Outlook (STEO), which expects the U.S. benchmark Henry Hub natural gas spot price to average $2.92 per thousand of cubic feet (Mscf) in 2019 and $2.88/Mscf in 2020 (see Figure 5.3).

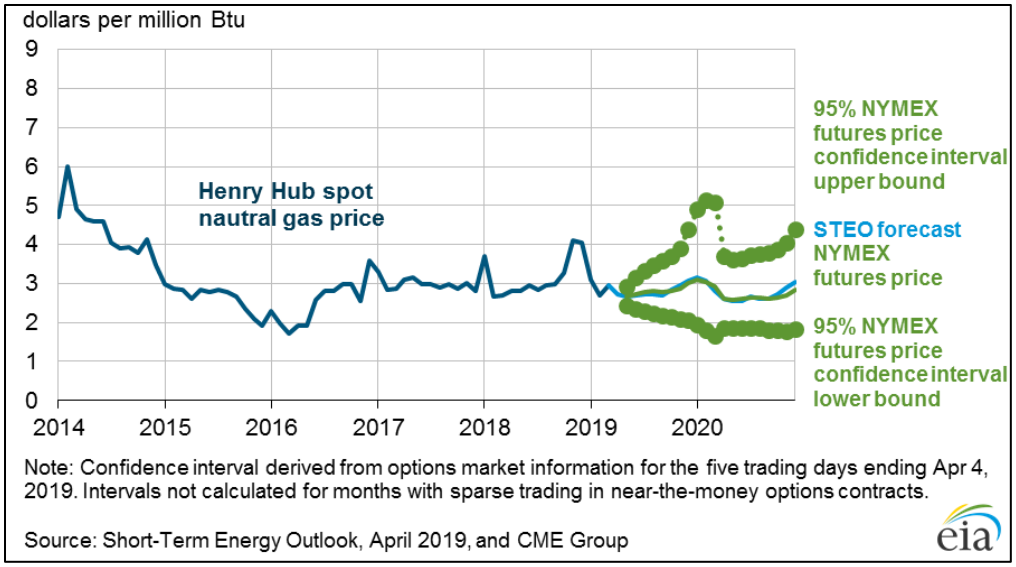

Figure 5.3: Henry Hub natural gas price and NYMEX confidence intervals (EIA, 2019).

Additionally, all the historical data from January 2015 were statistically tabulated and processed including the forecasts from April 2019 in order to find a possible statistical distribution of the spot price. A normal distribution of the gas price is observed during 2015 to 2020 (Figure 5.4).

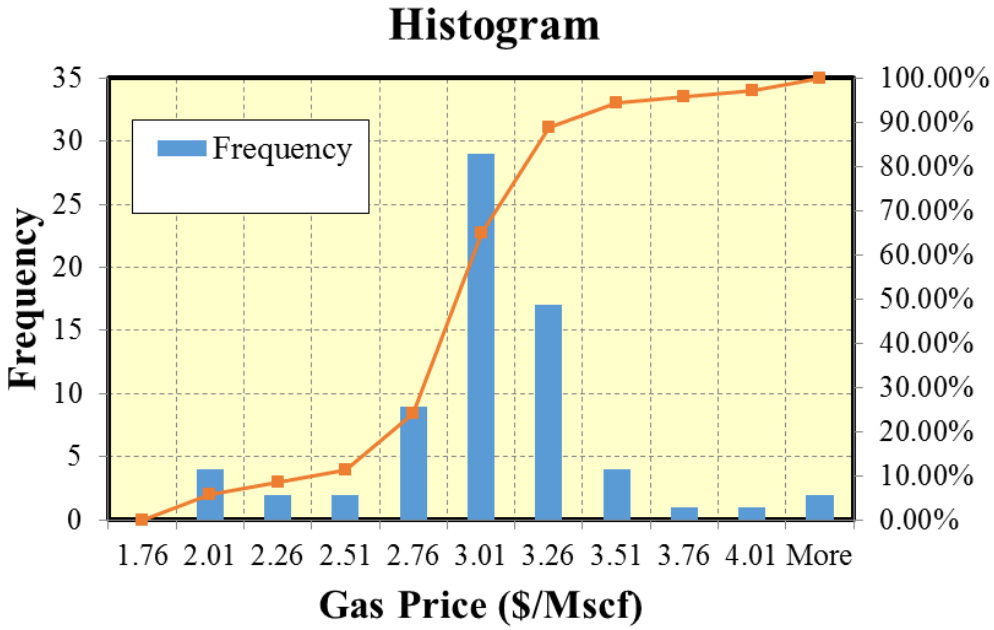

Figure 5.4: Histogram of spot gas prices from 2015 to 2020.

5.2.6 Discounted Cash Flow

The discounted cash flow (DCF) analysis is a collective accepted valuation method to assess the economic feasibility or desirability of an investment opportunity regarding the time value of money (Chavez, 2016). In order to account for the time value of money, all future expenditures and revenues need to be converted to a common denominator. This common point in time is habitually the present or time zero. This is achieved by discounting future cash flow streams. Discounting is the mirror to the compounding interest calculations. Compounding converts a present sum of money into its equivalent future sum. Discounting converts a future sum of money into its equivalent present sum (Mian, 2011).

5.2.6.1 Net Present Value

DCF analysis estimates future cash flows and discounts them to the present. Net present value estimation relies on the premise that a dollar invested today is worth more than a dollar payable in the future because of the risk of not receiving revenue from that investment. (Knull et al., 2007). NPV can be calculated as

$$NPV = \sum_{t=0}^{n} \frac{CF_t}{(1+i)^t} \tag{6}$$

where,

CF = Cash flow at time t ($)

i = Discount rate ($/year)

n = Number of periods (year)

The discount rate *i* is the key component of the equation as the "risk adjusted cost of capital" (Inkpen and Moffett, 2011). This discounted rate depends on the company's capital structure. Also, the NPV is defined by the cash flow for each period during the lifespan of the project.

5.2.6.2 Cash Flow (Before Tax & After Tax)

The cash flow that considers only costs, royalty and severance tax is called cash flow before tax (CFBFIT) and yields the NPVBFIT. On the other hand the cash flow that considers depletion allowance and federal income tax is called cash flow after tax (CFAFIT) and yields the NPVAFIT. The depletion allowance is calculated using the cost depletion method. In that sense the cash flow before federal income tax (BFIT) for each year in the DCF model is computed as shown in the following:

$$Net\ Oil = Gross\ Oil - Royalty \tag{7}$$

$$CF_{BFIT} = [Net\ Oil\ \cdot Price\ Oil + Net\ Gas \cdot Price\ Gas] - CAPEX - OPEX - [Net\ Oil\ \cdot Price\ Oil + Net\ Gas \cdot Price\ Gas] \cdot Sev\ tax \tag{8}$$

where,

Gross Oil = Total oil produced (BBL)

Gross Gas = Total gas produced (Mscf)

Royalty = Fraction of the oil paid to the lessor of the land ($)

Price Oil = Estimated selling price of oil ($/bbl)

Price Gas = Estimated selling price of gas ($/Mscf)

CAPEX = Capital expenditures ($)

OPEX = Operating expenditures ($/boe), where 1 Mscf of gas = 1/5.8 bbl of oil

Sev. tax = Severance tax (fraction)

The cash flow after federal income tax (AFIT) for each year in the DCF model is estimated as

$$CF_{AFIT} = CF_{BFIT} - [(CF_{BFIT} - Depletion\ Allowance) \cdot Federal\ Income\ Tax] \tag{9}$$

where,

Federal Income Tax = Corporate tax imposed on net taxable income (fraction)

Depletion Allowance = Tax reduction for the recovery of capital investments ($)

5.2.6.3 Depletion Allowance

Depletion is the gradual exhaustion of the original amounts of the resources acquired (Mian, 2011). The depletion deduction is available to company operators if they partake a legal economic interest in the oil and gas reserves. Thus, each operator accounts for their portion of the depletion deduction against their share of the costs paid for the acquisition of these reserves and the proportional share of the reserves and production. The depletion allowance used in the model is the Cost Depletion method for each year, and it is calculated by

$$Depletion\ Allowance = \left[\left(\frac{CAPEX}{CumProd}\right) \cdot Net\ Production\right] \quad (10)$$

where:

CumProd = Estimated total production of oil and a gas during the life of the well (boe)

Net Production = Net production of oil and gas produced in the year (boe).

5.3 HUFF-N-PUFF PROJECT ECONOMICS

Multimillion fund decisions are required in EOR Huff-n-Puff implementation. These decisions might involve drilling a new well or a group of wells, or converting one producer well to an injector one, and as such, an appraisal of the investment opportunity is essential. Therefore, a DCF valuation is employed to determine the economic feasibility of implementing the presented Huff-n-Puff project in Chapters 3 and 4, by using production forecasts of the numerical simulation and costs estimates, as well as royalty, taxes and price assumptions, which have been discussed in this chapter and validated by the actual field operator of Omega field in the Eagle Ford shale.

A deterministic and a probabilistic model are developed for estimating DCF. The base model will be considered as deterministic in order to fully define by the initial parameter values. The probabilistic model assumes inherent randomness to account for a possible under-appreciation of the complexity and risks associated to Huff-n-Puff

implementation. In that sense, the probabilistic approach will employ Monte Carlo analysis in order to know the net present value of different economic and financing variables on the profitability of implementing Huff-n-Puff in the 9-well black oil field in Eagle Ford.

5.3.1 Base Input Parameters

A summary of the input variables is exposed in Table 5.3.

Economic Parameters	Unit	Value
Discount Rate	fraction/yr	0.10
Working interest	fraction/yr	1.00
Royalty rate	fraction/yr	0.25
Net revenue interest	fraction/yr	0.75
Severance tax	fraction	0.046
Federal income tax	fraction	0.35
Ad valorem tax	fraction	0.03
Drilling cost (CAPEX)	$	2,280,000
Completion cost (CAPEX)	$	3,720,000
Huff-n-Puff (CAPEX)	$	1,000,000
OPEX	$/boe	6.00-10.00
Gas Processing	$/MSCF	0.15-0.40
Gas Transportation	$/MSCF	0.10-0.20
Oil Marketing Cost	$/bbl	3.91
Oil Price	$/bbl	55
Abandonment cost	$	75,000
Economic Limit	bbl/d	10

Table 5.3: Summary of economic input vaiables for the Determnistic and Probabilistic cash flow and NPV calculations.

5.3.2 Deterministic Economic NPV Model

The deterministic NPV model aids to define boundaries and expected NPV values before and after tax. This initial model starts calculating the Net Operational Revenues from 2018 until 2026 by considering a constant crude oil price of 55 $/bbl (given by operator), and a gas price of 2.92 $/Mscf (see Table 5.4). Also, gross gas production that

is negative is neglected since it means that the field is injecting more water than what it produces.

	END DATE	GROSS PRODUCTION		NET PRODUCTION		NET OPER REVENUES
Year	DD/MM/YYYY	Oil (bbl)	Gas (MMscf)	Oil (bbl)	Gas (MMscf)	$
1	1/1/2018	87,828	275.06	65,871	206.29	4,225,272
2	1/1/2019	422,780	(195.51)	317,085	-	17,439,675
3	1/1/2020	371,311	613.79	278,483	460.34	16,660,779
4	1/1/2021	286,359	441.35	214,769	331.01	12,778,853
5	1/1/2022	237,216	370.18	177,912	277.64	10,595,852
6	1/1/2023	205,259	245.30	153,944	183.98	9,004,138
7	1/1/2024	179,762	56.60	134,822	42.45	7,539,131
8	1/1/2025	161,960	9.75	121,470	7.31	6,702,196
9	1/1/2026	147,492	(5.19)	110,619	-	6,084,045

Table 5.4: Net operational revenues in the Deterministic model.

The next step is to estimate OPEX as function of the production and the cash flow before federal income tax (BFIT) (see Table 5.5).

	OPERATIONS					
	NET OPER REVENUES	TAXES SEV +ADV	OPEX OIL	OPEX GAS PROCESSING	CAPEX	CASH FLOW BFIT
Year	$	$	6-10 $/boe	$	$	$
1	4,225,272	321,121	1,411,010	123,776	14,150,000	(11,780,634)
2	17,439,675	1,325,415	4,410,652	-	-	11,703,608
3	16,660,779	1,266,219	4,977,725	276,204	-	10,140,631
4	12,778,853	971,193	3,781,297	198,608	-	7,827,756
5	10,595,852	805,285	3,140,604	166,582	-	6,483,380
6	9,004,138	684,315	2,582,592	110,387	-	5,626,844
7	7,539,131	572,974	1,977,167	25,468	-	4,963,521
8	6,702,196	509,367	1,707,177	4,385	-	4,481,266
9	6,084,045	462,387	1,538,710	-	-	4,082,947

Table 5.5: Cash Flow before Federal Incoe Tax calculation.

Even though OPEX oil is estimated to include any value from 6–10 $/boe for producing oil, it encompasses the highest expected value of 10 $/boe and an additional 3.91

$/boe for the marketing oil cost. Also, cumulative oil production of 937,727 bbls of the reservoir is employed in the first year of implementing Huff-n-Puff for the Depletion Allowance calculation. Finally, NPV values are estimated before and after tax as shown in Table 5.6 and in Figure 5.5 and Figure 5.6.

	CASH FLOW BFIT	NPVbfit	Depletion Allowance	CF AFIT	NPVafit
Year	$	$	$	$	$
1	(11,780,634)	(10,709,668)	4,784,713	(5,982,763)	(5,438,875)
2	11,703,607	(1,037,265)	3,308,204	8,765,216	1,805,105
3	10,140,631	6,581,541	3,139,904	7,690,376	7,582,999
4	7,827,756	11,928,004	2,454,059	5,946,962	11,644,854
5	6,483,380	15,953,673	2,225,797	4,993,226	14,745,254
6	5,626,844	19,129,879	1,947,234	4,338,980	17,194,495
7	4,963,521	21,676,951	1,589,278	3,782,536	19,135,535
8	4,481,266	23,767,495	1,444,069	3,418,247	20,730,172
9	4,082,947	25,499,063	1,336,599	3,121,725	22,054,088

Table 5.6: NPV values for the deterministic model.

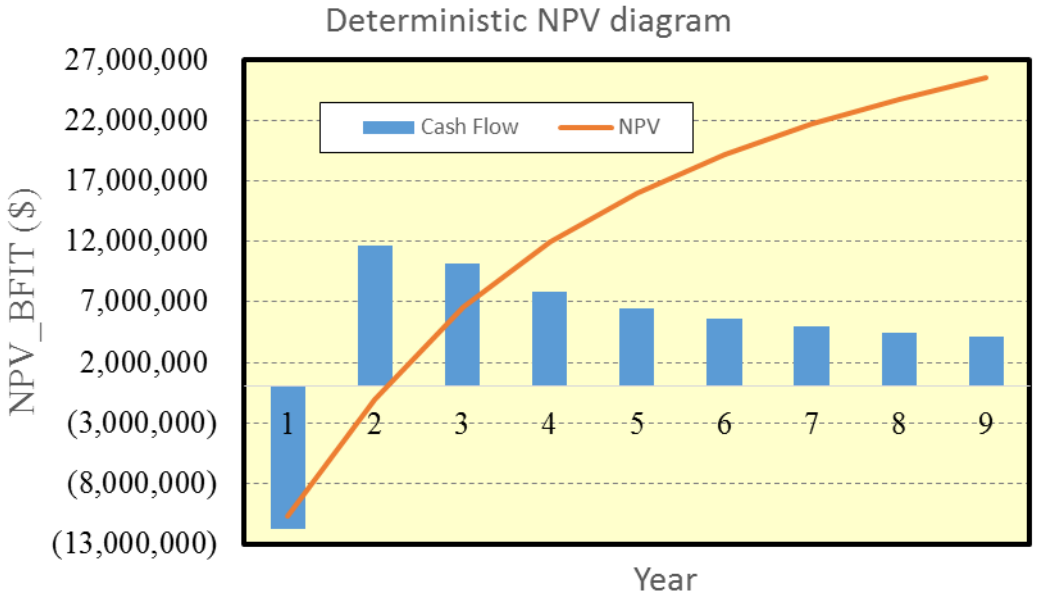

Figure 5.5: NPV before federal income tax diagram (Deterministic model).

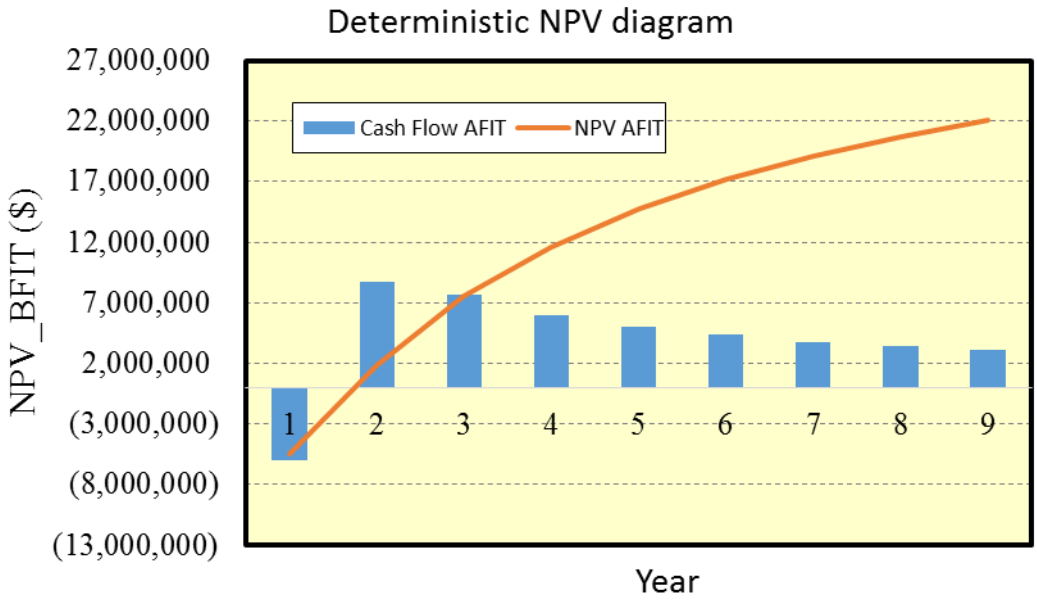

Figure 5.6: NPV after federal income tax diagram (Deterministic model).

5.3.3 Probabilistic Monte Carlo NPV Model

The final part of the economic evaluation uses stochastic approaches to generate myriad input data and explore broader scenarios with Monte-Carlo simulation and multiple different realizations. Furthermore, as the uncertainties surround each physical and economic parameter involved in the financial model, the need to perform a probabilistic model was prioritized. For instance, the probabilistic model calculates yearly expenses by sourcing assumptions, data from literature and company operator planning for financial input parameters, all of which have been mentioned previously in this chapter. As a consequence, this probabilistic model computes NPV based on Cash flows before and after federal income tax is applied.

The conducted Monte-Carlo simulation considers 100 iterations in 10 sets by year which results in a total of 1,000 realizations per year. The input parameters are statistically generated individually, following their statistical distributions, whose parameters are

presented in Table 5.7. Furthermore, each considered variable distribution has been plotted and contrasted to the deterministic input parameters in order to set initial maximum and minimum values (Figure 5.7).

Variable	units	Distribution	μ	δ	σ	median	λ	ζ
Oil price	$/bbl	Normal	55	0.18	10	50		
Gas Price	$/Mscf	Normal	2.917	0.1457	0.4249	2.917		
Royalty	%	Lognormal	25	0.08	2	24.9204	3.2157	0.0799
OPEX oil	$/bbl	Lognormal	8	0.1611	1.2885	7.8982	2.0666	0.1600
OPEX gas	¢/Mscf	Lognormal	42.5	0.1560	6.6284	41.9923	3.7375	0.1550
CAPEX	MM$	Deterministic	14.150					

Table 5.7: Input parameters that describe statistical distribution of the Monte-Carlo variables.

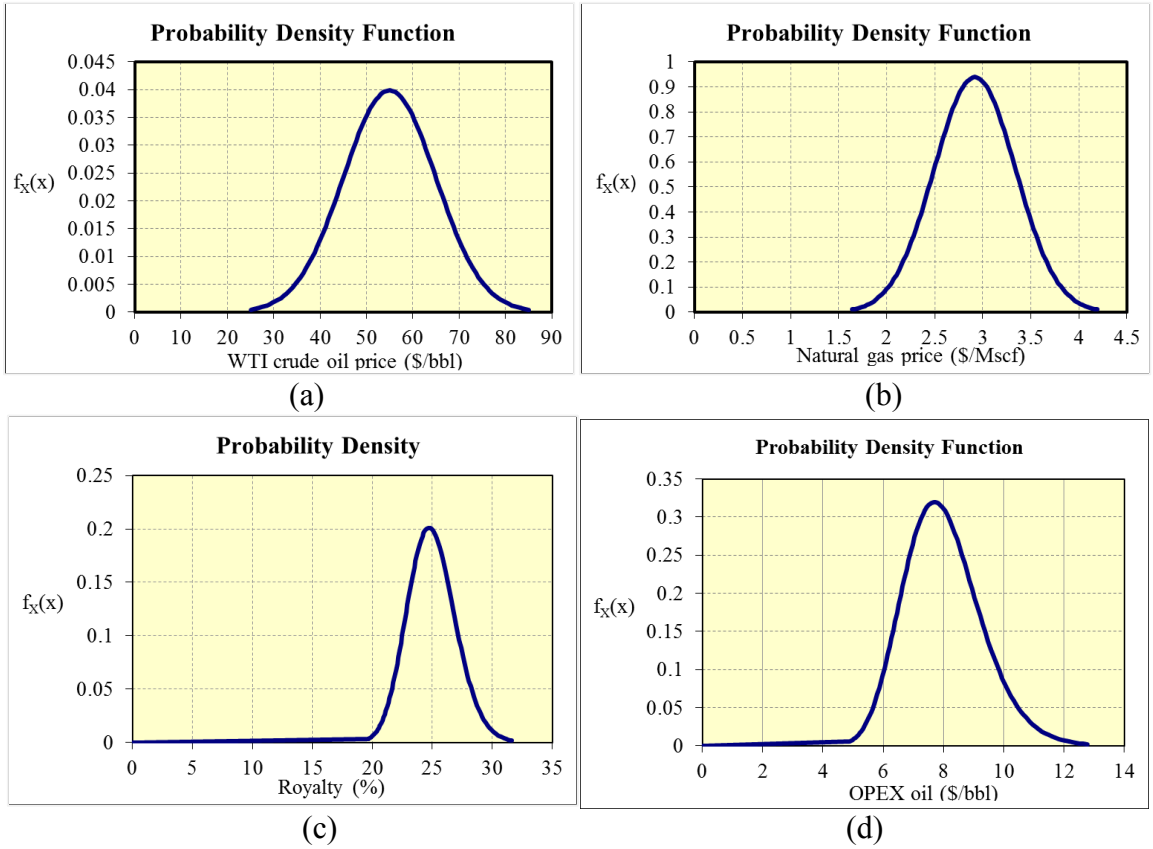

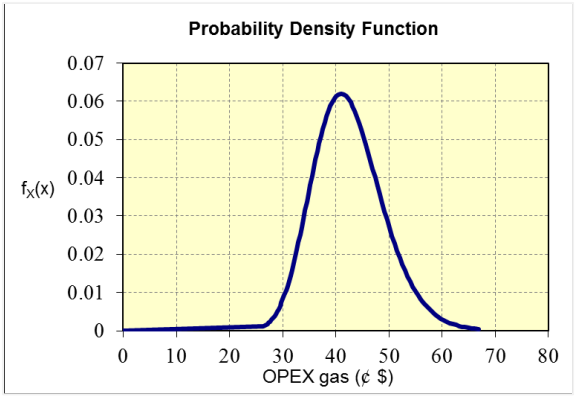

(e)

Figure 5.7: Normal and lognormal statistical distributions for Monte-Carlo input parameters. (a) WTI crude oil price, (B) Natural gas price, (c) Royalty, (d) OPEX oil, and (e) OPEX gas.

The final results of the probabilistic NPV model are exhibited in Table 3.1. More detailed results are presented the Appendix A-3 with expected values, standard deviations, P10, P90, and Standard errors from the Monte-Carlo Simulation.

Year	Date	E(CF_bfit) ($)	E(NPVbfit) ($)	E(CF_afit) ($)	E(NPVafit) ($)
1	1/1/2018	-11,475,769	-10,432,517	-5,784,600	-5,258,728
2	1/1/2019	12,597,645	-21,240	9,346,341	2,465,521
3	1/1/2020	11,185,392	8,382,511	8,129,426	8,573,279
4	1/1/2021	8,616,207	14,267,496	6,459,455	12,985,174
5	1/1/2022	7,141,788	18,701,984	5,421,192	16,351,307
6	1/1/2023	6,159,054	22,178,610	4,684,917	18,995,820
7	1/1/2024	5,358,069	24,928,146	4,038,992	21,068,462
8	1/1/2025	4,825,724	27,179,382	3,642,145	22,767,549
9	1/1/2026	4,393,032	29,042,457	3,323,281	24,176,945

Table 5.8: Sumary of results of the probabilistic NPV model.

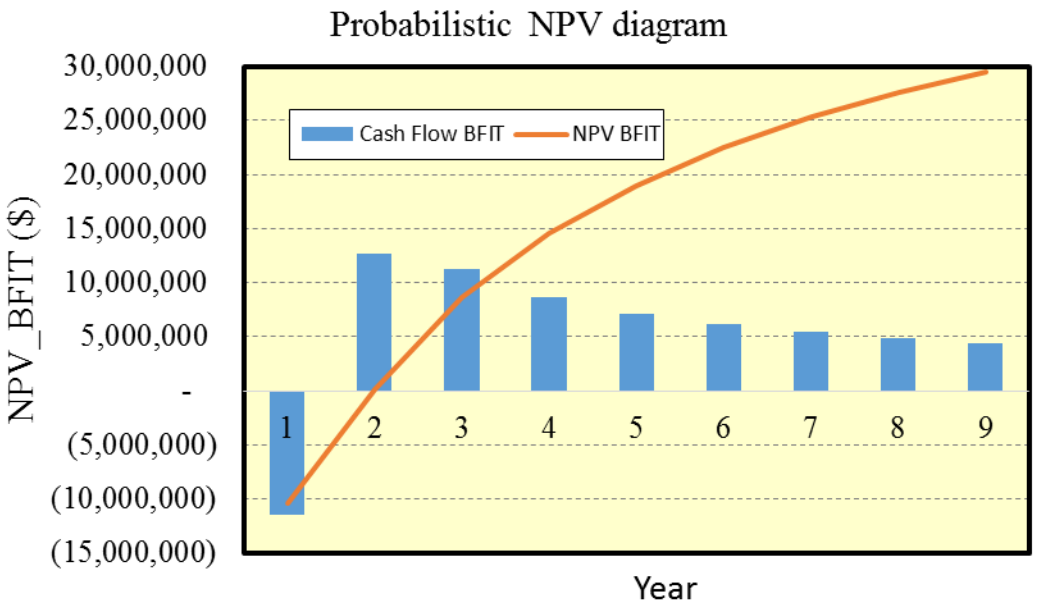

Figure 5.8: Cash flow diagram of NPV before tax probabilistic model.

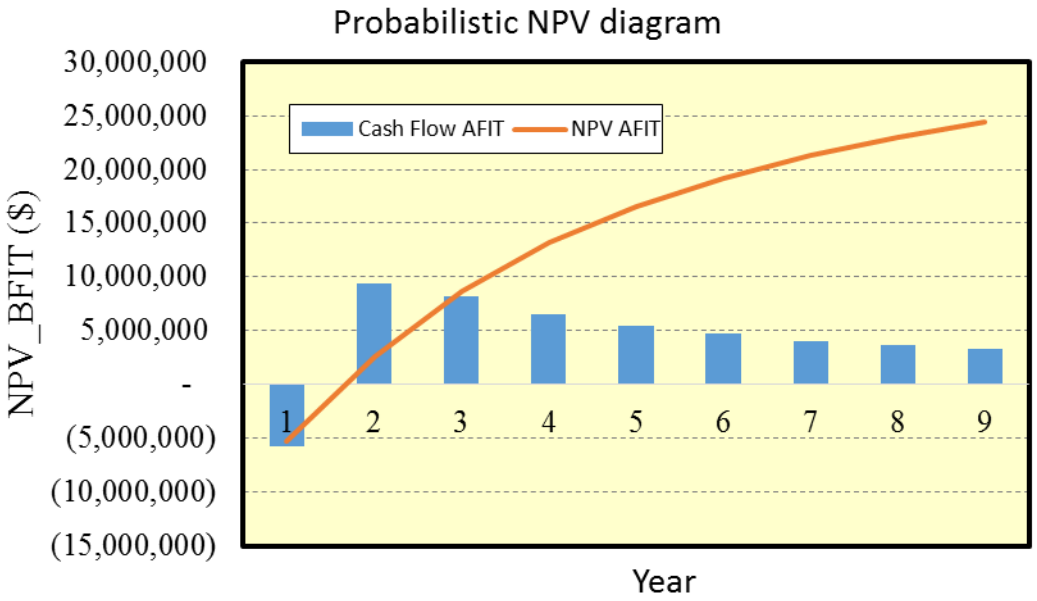

Figure 5.9: Cash flow diagram of NPV after tax probabilistic model.

CHAPTER 6

SUMMARY, DISCUSSION, and CONCLUSIONS

The final chapter of this thesis briefly restates the problem statement and the main methods used in this study. The principal sections of this chapter summarize the results and discuss their connotation in the research context of this work.

6.1 REVIEW OF THE PROBLEM AND METHODS

This work had the objective to model Huff-n-Puff considering multiple well fracture interference in a black oil area of Eagle Ford shale using the non-intrusive EDFM method and numerical reservoir simulation, focusing in two main challenges. The first challenge was directed to narrow down uncertainties associated with multiple well induced fractures characterization. Afterward, the second main challenge appraised modeling optimal pressure containment strategies for efficient Huff-n-Puff designs in a multiwell black oil field.

Because of the approaches mentioned in the previous paragraph, this research employed a novel iterative workflow for modeling unconventional reservoirs to an actual field case. This extensive workflow includes WBI logs interpretation of child wells, fractures preprocessing, numerical simulation, sensitivity analysis, history matching, and EOR implementation forecasts. In particular, multiwell fracture interference was addressed after inferential depth correlation among the wells which lead to identify these interwell induced fractures. Equally important is to expose that all the fracture modeling was conducted by EDFM methodology in the simulation models. The results allowed us to recommend optimal cluster spacing execution in future fracturing designs for the operator. Furthermore, the reservoir dynamic characterization has been validated by the current

performance of the field, so that the forecast scenarios might exhibit higher reliability. EOR Huff-n-Puff implementation was also assessed in the field with different designs. The cumulative oil recovery of the different forecasts was plotted to summarize and compare Huff-n-Puff scenarios. Likewise, the analysis of the pressure leak off in the field and its adequate containment strategies yield to optimize field cumulative oil recovery. Finally, an economic feasibility evaluation was performed through a cash flow and NPV estimation to reinforce the value of this work.

6.2 SUMMARY OF THE RESULTS

The summary of the results of this study will be displayed in the same order of the sections discussed in Chapter 4.

6.2.1 Interwell Fracture Interference Results

This innovator study applies numerical simulation to multiwell fracture designs and identifies long interwell fractures by coupling iterative procedures of sensitivity analysis with WBI interpretation. More than 2,000 hydraulic fractures and 28 long interwell fractures were computed for 9 wells of the Omega field in the Eagle Ford shale. Moreover, different complex fracture geometries and fracture conductivities estimates were modeled. Two simulation models were constructed using non-intrusive EDFM and commercial simulators. One corresponded to a full field black oil model to history match field production data. The second one was a sector compositional model to ease the interpretation of results for fast evaluation of Huff-n-Puff implementation. The results of this latter model will be discussed in detail further in this chapter. Nevertheless, the multiple well fracture interference was studied for both models. The main findings of this sections are listed next.

- The length of the induced interwell fractures include ranges from 750 ft up to 3,400 ft (see Figure 4.1), and this is directly in track with offset pressure/water communication, and gross fracture lengths.
- Some of these cases show very close fracture offset distances (less than 100 ft) among the interwell fractures as seen in the Figure 4.2, which is likely related to cluster spacing and rock heterogeneities along the wellbore that impact production performance.
- The recommended child inner wells fracture designs consider cluster spacing of 70 ft as a result of sensitivities in the model in order to maximize recovery by mitigating well interference and locating the clusters at a distance far enough from long induced interwell fractures but without losing oil.
- Although history matching results are not unique, the presented ones are satisfactory to demonstrate that great agreements between simulation results and field data are obtained.

6.2.2 Modeling Huff-n-Puff Eagle Ford Results

The second problem statement of this thesis had the purpose to not only analyze the EOR Huff-n-Puff application in Eagle Ford, but also to use the adequate pressure containment strategies to evaluate the performance of this EOR process, but in particular, the gas injection effectiveness in terms of pressure build up. Therefore, a comparison of cumulative oil volumes from different mechanisms was used to appraise the recovery results (see Figure 4.25). The findings obtained are described up next.

- More than 150 hydraulic fractures and 11 interwell induced fractures were modeled with EDFM method in a 6% sector model to reach history match solutions that lead to forecasts with higher pressure depletion (main reason to implement Huff-n-Puff).

- The forecast of cumulative oil volume from primary production reaches 143 Mbbls in the 6% sector model, which is equivalent to 2.387 MMbls in 8 years.
- Different Huff-n-Puff designs achieve additional cumulative oil recovery from 7% up to 12% in 8 years of forecast contemplating only one single gas injector well.
- Pressure leak occurrence seems inevitable in this part of the Omega field so that it is characterized in this sector model through higher fracture intensity modeling.
- Water blockage was the pressure containment strategy employed when coupling with rich gas Huff-n-Puff in one single injector well. These designs achieved from 10% to 15% of additional cumulative oil.
- The highest incremental oil recovery is the result of using two gas injectors, with an injection rate of 900,000 MMscf/d for each well in the sector model and 50 cycles with duration of 30 days per cycle. Concurrently, one water injector is blocking gas flow in the middle of the nine wells with an injection rate of 3 bpm in only 10 initial cycles of 30 days each. For both kind of injectors (i.e. gas and water) the considered injection BHP was 3,500 psi (Figure 4.26). The cumulative oil production reaches around 184 Mbbls in the sector model, which is equivalent to an additional 29% (see Table 4.3).

6.2.3 Economical Feasibility Results

The simulation results provide positive benefit to the operator in terms of Expected recoveries, reduced EOR costs, and improved capital efficiencies. Two discounted cash flow models (DCF), a deterministic and a probabilistic one, were calculated for implementing the previously simulated Huff-n-Puff design in the Omega Field. Both of the DCF models consider NPV estimation before and after federal taxation. Before the procedure took place a screening of the input economic variables was performed with

information from available literature and the operator company (Table 5.3). Three main factors employed in this economic analysis were a mean of the WTI crude oil price of 55 usd/bbl, a mean Henry Hub natural gas spot price of 2.92 usd/Mscf, and a discount rate of 10%. From the previous process, the following findings are observed.

- Despite CAPEX variables were acknowledged in this economic evaluation, it was considered as a fixed initial value of $ 14.15 million of dollars for implementing two gas injection wells and transforming one producer to water injector.
- Royalty was set as the standard 25% of the gross production used in Eagle Ford.
- The deterministic model shows a return of capital investment in 4.5 years, so that after 9 years the NPV before tax reaches around 27 million of dollars, almost doubling the capital expenditure.
- For the stochastic DCF model, the mean and standard deviation of five main input economic parameters were obtained from statistical distribution in similar studies in the Eagle Ford or from fitting EIA forecasts (See Figure 5.7).
- A total of 1,000 realizations per year of Monte-Carlo Simulations were used to evaluate the stochastic DCF model before and after federal tax; in the appendix of this thesis an extended summary of all the simulation realizations is presented with their expected NPVs, standard deviations, P10 and P90.
- The stochastic model shows a slightly more optimistic return of capital investment in less than 4 years, so that after 9 years the NPV before tax reaches around 29 million of dollars, doubling the capital expenditure.
- In terms of applying federal income tax to both DCF models, there exists a reduction of $3 - $5 million dollars to the NPV before the tax at the end of the 9 years of forecast.

6.3 Discussion of Results and Conclusions

A final discussion of the results of this work will be presented next to formally conclude with some brief recommendations.

6.3.1 Multiple Well Fracture Interference

The Omega field, located in the black oil window of the Eagle Ford reservoir, exhibits intermediate presence of induced interwell fractures based on the estimated correlations from the available WBI logs (Figure 4.3). Since this interwell fractures generate interference inevitably and starting from the assumption that production declination is impacted by interwell fracture interference, history matching infill wells was definitely altered by pre-existing hydraulic fractures from existing wells. Therefore, quantifying the existence/effect of these fractures is critical to understanding infill well behavior.

The non-intrusive EDFM methodology has added great value to this work and to the novel proposed workflow. The reason behind this, is that EDFM can handle complex fractures more easily and efficiently by creating additional virtual fracture grids, assigning NNC among the matrix of these cells and the fractures, and calculating accurate standard transmissibility factors. For instance, EDFM resolved well the challenge of modeling two or more induced fractures in one single grid block with different inclination in these fractures characterization due to contrast of grid size and high fracture intensity. Consequently, EDFM application in this study corroborates its capabilities that surpass other traditional fracture simulation methods in terms of accuracy, flexibility, gridding, and computational efficiency.

Even though there is not an absolute consensus about how to prevent fracture hits, interwell interference could be foreseen with the presented very detailed workflow that includes multiwell fracture hits characterization, based on data diagnostics, production

analysis, pressure response analysis, and numerical simulation. It might be obvious that interwell interference provokes BHP equalization among the wells connected by these long induced fractures in unconventional reservoirs. However the long distances up to which these induced fractures can extend are not expected, communicating pressure changes through more than 3,000 ft. Consequently, the development of estimating fracture interwell interference due to fracture hits through recent years has exhorted the academia and the industry to validate processes and generate meaningful representations that should be considered in the completion optimization process of child wells further field development plans.

This thesis has proven that uncertainties regarding interwell long fracture locations can be mitigated strongly by introducing iterative procedures of sensitivity analysis and WBI interpretation as displayed in the very particular solutions to this field. Initially, this study used black oil simulation in order to capture multiple well fracture interference faster than if using a compositional model. Also, despite there may be other multiple history match solutions, the one presented shows great BHP and gas rate fit so that it has been verified and validated by actual field data. Thus, another value of this work has been assessing cluster spacing, contemplating staying away from the identified induced interwell fractures. In fact, the operator of the field adopted the suggestion from this work to design fracture schemes considering cluster spacing of at least 70 ft. As a result, the operator improves their capital efficiencies in terms of investing less and not losing much. These capital efficiencies are out of the scope of this work and cannot be published due to confidentiality agreements. Therefore, interwell interference modeling using the non-intrusive EDFM method altogether with commercial reservoir simulators can lead to robust history matching for unconventional reservoirs.

6.3.2 Modeling Huff-n-Puff in Eagle Ford

Huff-n-Puff in Eagle Ford can be successful using produced gas according to this work, but the design (i.e. injection timing, length, injector location and, injection pressure) must be optimized for economic success. In this part of the reservoir, this thesis proposes that the Huff-n-Puff recoveries are downgraded due to interwell communication or interference by long natural fractures reactivation. Thus, there exists reduced pressure maintenance ability in the reservoir in spite of EOR Huff-n-Puff injection.

Furthermore, it can be concluded that small gas injections will do little in producing wells. Hence, definitively, large volumes of gas need to be injected in order to obtain feasible recoveries and mitigate pressure leak off. Moreover, the results could be enhanced if higher injection pressure is employed. However, as mentioned previously, due to facilities capabilities of the operator on surface, 3500 psi was defined as injection pressure. Also, the effectiveness of huff and puff gas injection with constant duration cycles decreases as the cycles continue. Late cycles require more gas to restore the reservoir pressure as more fluids have been withdraw. Therefore, further analysis might be needed when designing the length of the cycles.

One of the reasons why determining adequate periods of time for injecting and producing cycles aids recovery optimization is the increase of the contact area exposure as much as possible. Thus, exposing the injected gas to the reservoir for the proper time will allow to augment the contact area exposure and penetrating deeper into the shale matrix reservoir, interact/swell with more oil, and make it less viscous. In that sense, if the gas is injected and the matrix is exceeded to take up all of the gas, the gas will continue to migrate through the fracture network with the potential to re-inflate closed fractures, generating dilation of the induced fractures). This dilation/compaction might be the phenomena

behind gas migrating to further zones of the reservoirs when injecting the produced gas as modeled in this study.

Again, the Huff-n-Puff needs additional pressure containment strategies if implemented in this area of the Eagle Ford because it considers interwell fracture interference. Water injection, as a technique to generate blockage the flow of gas through the induced fractures, has been proposed in this thesis. The idea of using a water injection is based on generating physical barriers to the flow of the gas and to reduce the influence area where the pressure can be contained and then it can build up. For Huff-n-Puff gas injection to be effective, and affordable, the formation must allow the operator to pressure up the reservoir, keep the gas in the reservoir long enough to have an effect, and produce it back for reuse, reinjection or sale. For instance, the results of the forecasts are very satisfactory as long as pressure can build up more than 20 psi/day. In conclusion, Huff-n-Puff might be successful in Eagle Ford if two gas injectors are inserted in the field plus one water injector as suggested by this thesis.

6.3.3 Economical Feasibility tests

One of the greatest challenges of big capital projects such EOR Huff-n-Puff is to justify and forecast economically positive scenarios. The inferential statistics of the input economic parameters used in this thesis play a huge impact on the two DCF models presented in the previous chapter. Results suggest that the Huff-n-Puff is economically feasible with great rewards in long term scenarios. The economics are based on a deterministic approach initially, and later, on stochastic realizations within the ranges of different researched input parameters. Furthermore, in deterministic models, the output of the model is fully determined by the parameter values and the initial conditions. All the initial assumptions of the deterministic DCF model were corroborated by the operator.

However, stochastic models possess some inherent randomness, which allow us to explore broader scenarios. The same set of parameter values and initial conditions will lead to an ensemble of different sensitivities.

When decomposing CAPEX variables, we can infer that although drilling and completion costs vary depending on the well design and its complexity (i.e. fracture stages, lateral length), from Table 5.1, the highest costs corresponds to the formation stimulation which refers to hydraulic fracturing; a process that uses large amounts of water. Another relevant component of hydraulic fracturing is the proppant used in the fracking fluid which keeps fractures opened in order to allow the flow of hydrocarbons. As a result, the CAPEX employed in the proposed DCF models added up to be around 14 million of dollars, which was recoverable in 2 to 2.5 years.

On the other hand, when decomposing OPEX costs, it was necessary to defined fixed costs and variables costs according to production. OPEX oil referred to the costs of producing one barrel of oil. OPEX gas include gas processing fees and gas transportation. OPEX also considered taxation costs related to severance tax and ad-valorem tax. Furthermore, defining the correct spot prices is fundamental since they are every time more unpredictable. Therefore, the probabilistic approach comes to mitigate the uncertainties by modeling normal distributions for these market prices based on historical price values since 2015. When comparing the distribution of other parameters such as Royalty, OPEX oil and OPEX gas, they are modeled with lognormal distribution due to their relationship with production rate.

As a fact, in the yearly 1,000 realizations, the stochastic model seems to generate better economic returns in 9 years of implementing the Huff-n-Puff in the field (see Appendix B). Thus, it can be concluded that in the case of the Omega field in Eagle Ford it is more likely that Huff-n-Puff will be successful as studied in this thesis.

6.4 RECOMMENDATIONS FOR FURTHER RESEARCH

Additional research might be needed to evaluate the efficacy of implementing EOR Huff-n-Puff with the pressure containment strategies suggested. Although this thesis acknowledges gas diffusion, it did not include it in the modeling process. Some researchers consider that physics of fluid flow in shale reservoirs cannot be predicted from standard flow or mass transfer models because of the nanopore-low permeabilities. Others do not think minimize the impact of diffusion since it there are a lot of uncertainties when estimating (not measuring) the diffusivity factor or the area of contact for general modeling. Therefore, diffusion phenomena could be included in the Huff-n-Puff modeling process as further research of this thesis.

Also, another recommendation to address would be to how to define the correct simulation grid size in order to capture the actual gas flow. In that sense, simulation gridding must be sufficiently small to avoid artificially optimistic Huff-n-Puff recovery.

Another recommendation might be to implement sensitivities about the use of cycles with variable increasing-time spans, so that they can improve the performance of the Huff-n- Puff injection in the long term.

Finally, in this research, only the probability of different values was considered for the OPEX parameters but not the probability of parameters associated to CAPEX since the operator plans might differ in every scenario. In addition, most the economic parameters might need to be updated for further research.

Appendices

APPENDIX A

A summary table of different properties for lumped components of the crude oil PVT studied from the Omega field in Eagle Ford is presented. The table details the fundamental PVT properties that are the basis of the Huff-n-Puff modeling. Moreover, the Peng Robinson equation of state was employed in the phase behavior of the fluid model. Thus its binary interaction coefficients are also specified.

Comp.	P_c, atm	T_c, K	Acentric Factor	Molecular Weight	Specific Gravity	Volume Shift	V_c for Viscosity	Parachor	Composition, Mole Frac.
C1+N2	45.3731	190.838	0.00808	16.029	0.26426	-0.19396	0.09977	77.213	0.32550
C2+C3+CO2	46.1742	331.954	0.12209	35.858	0.47918	-0.1285	0.16637	124.744	0.14906
C4-C6	33.5282	461.193	0.23442	70.443	0.62051	-0.04667	0.30629	224.9726	0.10303
C7-C10	25.2	538	0.418	114	0.676	0.0346	0.447	330	0.14634
C11-C20	17.8	722	0.76	199	0.839	0.119	0.753	544	0.19183
C21-C45	13.7	843	1.24	383	0.92	-0.0693	0.938	999	0.07997
C46-C80	12	1120	1.15	745	1.2	-0.29	1.48	1840	0.00427

Table A1—Peng-Robinson EOS parameters and composition for reservoir fluid model.

Comp.	C1+N2	C2+C3+CO2	C4-C6	C7-C10	C11-C20	C21-C45	C46-C80
C1+N2	0	0.00331	0.00021	0.00019	0.00019	0.00019	0.00019
C2+C3+CO2	0.00331	0	0.00314	0.00253	0.00253	0.00253	0.00253
C4-C6	0.00021	0.00314	0	0	0	0	0
C7-C10	0.00019	0.00253	0	0	0	0	0
C11-C20	0.00019	0.00253	0	0	0	0	0
C21-C45	0.00019	0.00253	0	0	0	0	0
C46-C80	0.00019	0.00253	0	0	0	0	0

Table A2—Peng-Robinson binary interaction coefficients for the Eagle Ford oil.

APPENDIX B

The results of the Monte-Carlo simulation for estimating deterministic and stochastic discounted cash flow models are presented in this appendix.

	Year= 1			
Set	E(CF_bfit) ($)	E(NPVbfit) ($)	E(CF_afit) ($)	E(NPVafit) ($)
1	(11,472,506)	(10,429,551)	(5,782,479)	(5,256,799)
2	(11,370,340)	(10,336,673)	(5,716,072)	(5,196,429)
3	(11,351,862)	(10,319,875)	(5,704,061)	(5,185,510)
4	(11,404,351)	(10,367,591)	(5,738,178)	(5,216,526)
5	(11,447,483)	(10,406,803)	(5,766,215)	(5,242,013)
6	(11,513,869)	(10,467,154)	(5,809,365)	(5,281,241)
7	(11,471,552)	(10,428,683)	(5,781,859)	(5,256,236)
8	(11,432,149)	(10,392,863)	(5,756,247)	(5,232,952)
9	(11,473,855)	(10,430,777)	(5,783,356)	(5,257,596)
10	(11,431,913)	(10,392,648)	(5,756,094)	(5,232,813)
Sample Mean	(11,436,988)	(10,397,262)	(5,759,393)	(5,235,812)
Sample Std. Dev.	50,154	45,595	32,600	29,636
n	10	10	10	10
Standard Error	15,860	14,418	10,309	9,372
10 percentile	(11,457,314)	(10,415,740)	(5,772,604)	(5,247,822)
90 percentile	(11,416,662)	(10,378,784)	(5,746,181)	(5,223,801)

	Year= 2			
Set	E(CF_bfit) ($)	E(NPVbfit) ($)	E(CF_afit) ($)	E(NPVafit) ($)
1	12,591,550	(23,311)	9,342,379	2,464,175
2	13,121,269	507,351	9,686,696	2,809,105
3	13,159,889	556,066	9,711,799	2,840,770
4	12,984,362	363,287	9,597,707	2,715,464
5	12,613,768	17,799	9,356,821	2,490,897
6	12,434,868	(190,403)	9,240,536	2,355,565
7	12,693,193	61,559	9,408,447	2,519,340
8	12,892,862	262,395	9,538,232	2,649,884
9	12,574,813	(38,370)	9,331,500	2,454,387
10	12,780,128	169,441	9,464,955	2,589,464
Sample Mean	12,784,670	168,581	9,467,907	2,588,905
Sample Std. Dev.	246,523	248,178	160,240	161,316
n	10	10	10	10
Standard Error	77,957	78,481	50,672	51,013
10 percentile	12,684,764	68,004	9,402,968	2,523,530
90 percentile	12,884,577	269,158	9,532,846	2,654,280

Set	Year= 3 E(CF_bfit) ($)	E(NPVbfit) ($)	E(CF_afit) ($)	E(NPVafit) ($)
1	11,146,313	8,351,079	8,104,024	8,552,848
2	11,711,973	9,306,730	8,471,703	9,174,021
3	11,748,121	9,382,604	8,495,199	9,223,339
4	11,679,770	9,138,471	8,450,771	9,064,653
5	11,381,111	8,568,596	8,256,643	8,694,235
6	10,957,439	8,042,082	7,981,256	8,352,001
7	11,186,805	8,466,371	8,130,344	8,627,788
8	11,433,947	8,852,888	8,290,986	8,879,024
9	11,214,924	8,387,568	8,148,621	8,576,566
10	11,251,864	8,623,132	8,172,632	8,729,683
Sample Mean	11,371,227	8,711,952	8,250,218	8,787,416
Sample Std. Dev.	269,131	444,503	174,935	288,927
n	10	10	10	10
Standard Error	85,107	140,564	55,319	91,367
10 percentile	11,262,158	8,531,812	8,179,323	8,670,325
90 percentile	11,480,295	8,892,092	8,321,113	8,904,507

Set	Year= 4 E(CF_bfit) ($)	E(NPVbfit) ($)	E(CF_afit) ($)	E(NPVafit) ($)
1	8,706,342	14,297,628	6,518,043	13,004,759
2	9,054,057	15,490,773	6,744,058	13,780,304
3	8,997,533	15,528,040	6,707,317	13,804,527
4	8,871,795	15,198,026	6,625,587	13,590,018
5	8,697,154	14,508,869	6,512,071	13,142,066
6	8,508,770	13,853,687	6,389,621	12,716,198
7	8,589,871	14,333,368	6,442,337	13,027,991
8	8,799,914	14,863,348	6,578,865	13,372,477
9	8,650,261	14,295,813	6,481,590	13,003,580
10	8,932,577	14,724,203	6,665,096	13,282,033
Sample Mean	8,780,827	14,709,375	6,566,458	13,272,395
Sample Std. Dev.	180,542	557,560	117,353	362,414
n	10	10	10	10
Standard Error	57,093	176,316	37,110	114,605
10 percentile	8,707,660	14,483,417	6,518,900	13,125,523
90 percentile	8,853,994	14,935,333	6,614,017	13,419,268

Set	Year= 5			
	E(CF_bfit) ($)	E(NPVbfit) ($)	E(CF_afit) ($)	E(NPVafit) ($)
1	7,164,249	18,746,063	5,435,791	16,379,958
2	7,569,463	20,190,814	5,699,180	17,319,046
3	7,383,757	20,112,772	5,578,471	17,268,319
4	7,378,182	19,779,297	5,574,847	17,051,560
5	7,196,054	18,977,053	5,456,464	16,530,102
6	7,065,601	18,240,869	5,371,670	16,051,582
7	7,201,154	18,804,719	5,459,779	16,418,084
8	7,320,230	19,408,635	5,537,179	16,810,630
9	7,185,146	18,757,223	5,449,374	16,387,212
10	7,219,705	19,207,071	5,471,837	16,679,613
Sample Mean	7,268,354	19,222,452	5,503,459	16,689,611
Sample Std. Dev.	145,189	642,649	94,373	417,722
n	10	10	10	10
Standard Error	45,913	203,224	29,843	132,095
10 percentile	7,209,515	18,962,010	5,465,214	16,520,324
90 percentile	7,327,194	19,482,893	5,541,705	16,858,897

Set	Year= 6			
	E(CF_bfit) ($)	E(NPVbfit) ($)	E(CF_afit) ($)	E(NPVafit) ($)
1	6,118,534	22,199,816	4,658,579	19,009,604
2	6,410,507	23,809,378	4,848,361	20,055,819
3	6,457,843	23,758,056	4,879,129	20,022,460
4	6,354,505	23,366,249	4,811,960	19,767,786
5	6,258,398	22,509,755	4,749,490	19,211,065
6	6,021,232	21,639,698	4,595,333	18,645,527
7	6,146,895	22,274,481	4,677,013	19,058,136
8	6,287,266	22,957,632	4,768,255	19,502,185
9	6,168,685	22,239,285	4,691,177	19,035,259
10	6,232,172	22,724,970	4,732,444	19,350,955
Sample Mean	6,245,604	22,747,932	4,741,174	19,365,880
Sample Std. Dev.	136,759	718,181	88,893	466,818
n	10	10	10	10
Standard Error	43,247	227,109	28,111	147,621
10 percentile	6,190,180	22,456,880	4,705,149	19,176,696
90 percentile	6,301,027	23,038,984	4,777,199	19,555,063

Set	Year= 7			
	E(CF_bfit) ($)	E(NPVbfit) ($)	E(CF_afit) ($)	E(NPVafit) ($)
1	5,383,464	24,962,384	4,055,499	21,090,717
2	5,592,269	26,679,096	4,191,222	22,206,579
3	5,581,396	26,622,194	4,184,155	22,169,593
4	5,564,407	26,221,670	4,173,112	21,909,252
5	5,355,149	25,257,794	4,037,094	21,282,733
6	5,253,563	24,335,606	3,971,063	20,683,311
7	5,341,700	25,015,617	4,028,352	21,125,318
8	5,466,319	25,762,718	4,109,354	21,610,934
9	5,365,706	24,992,741	4,043,956	21,110,448
10	5,460,634	25,527,139	4,105,659	21,457,807
Sample Mean	5,436,461	25,537,696	4,089,947	21,464,669
Sample Std. Dev.	115,463	776,129	75,051	504,484
n	10	10	10	10
Standard Error	36,513	245,434	23,733	159,532
10 percentile	5,389,668	25,223,160	4,059,531	21,260,221
90 percentile	5,483,254	25,852,232	4,120,362	21,669,117

Set	Year= 8			
	E(CF_bfit) ($)	E(NPVbfit) ($)	E(CF_afit) ($)	E(NPVafit) ($)
1	4,812,550	27,207,474	3,633,582	22,785,809
2	5,068,313	29,043,501	3,799,827	23,979,226
3	5,021,303	28,964,669	3,769,271	23,927,986
4	5,013,740	28,560,617	3,764,355	23,665,352
5	4,892,522	27,540,191	3,685,563	23,002,075
6	4,733,894	26,544,003	3,582,455	22,354,553
7	4,794,120	27,252,110	3,621,602	22,814,822
8	4,952,254	28,072,981	3,724,389	23,348,388
9	4,807,493	27,235,472	3,630,294	22,804,007
10	4,860,303	27,794,506	3,664,621	23,167,380
Sample Mean	4,895,649	27,821,552	3,687,596	23,184,960
Sample Std. Dev.	113,117	827,727	73,526	538,022
n	10	10	10	10
Standard Error	35,771	261,750	23,251	170,138
10 percentile	4,849,807	27,486,106	3,657,799	22,966,920
90 percentile	4,941,491	28,156,999	3,717,393	23,403,000

Set	Year= 9			
	E(CF_bfit) ($)	E(NPVbfit) ($)	E(CF_afit) ($)	E(NPVafit) ($)
1	4,402,846	29,074,711	3,329,659	24,197,910
2	4,571,389	30,982,216	3,439,212	25,437,788
3	4,614,812	30,921,800	3,467,438	25,398,518
4	4,515,105	30,475,462	3,402,628	25,108,398
5	4,448,351	29,426,726	3,359,238	24,426,720
6	4,317,535	28,375,059	3,274,208	23,743,136
7	4,396,417	29,116,620	3,325,481	24,225,151
8	4,484,891	29,975,012	3,382,988	24,783,106
9	4,374,749	29,090,792	3,311,396	24,208,363
10	4,458,398	29,685,302	3,365,768	24,594,794
Sample Mean	4,458,449	29,712,370	3,365,802	24,612,388
Sample Std. Dev.	91,298	865,713	59,344	562,713
n	10	10	10	10
Standard Error	28,871	273,763	18,766	177,946
10 percentile	4,421,450	29,361,529	3,341,752	24,384,342
90 percentile	4,495,449	30,063,211	3,389,851	24,840,435

Glossary

NOMENCLATURE

A&G	=	Administrative and General costs
BHP	=	Bottom-hole pressure
BOE	=	Barrels of oil equivalent
CAPEX	=	Capital expenditures
DCF	=	Discounted cash flow
DPDK	=	Double Porosity Double Permeability
DTS	=	Distributed temperature sensor
D&C	=	Drilling and completions
EIA	=	Energy Information Administration
EDFM	=	Embedded Discrete Fracture Model
EDWM	=	Embedded Discrete Wellbore Model
EOR	=	Enhanced oil recovery
F&D	=	Funding and development
GOR	=	Gas Oil Ratio
G&G	=	Geological and geophysical
IFT	=	Interfacial tension
LGR	=	Local grid refinement
LOE		lease operating expenditures
LWD	=	Logging while drilling
MMP	=	Minimum miscibility pressure
NNCs	=	Non-neighbor connections
OPEX	=	Operative expenditures
PSS	=	Pseudo steady state
PVT	=	Pressure, volume and temperature
ROP	=	Rate of penetration
THP	=	Tubing head pressure
TOC	=	Total organic carbon content
TRRC	=	Railroad Commission of Texas
WBI	=	Wellbore image
WI	=	Well Index

SI METRIC CONVERSION FACTORS

ft	×	3.048	e-01	=	m
ft^3	×	2.832	e-02	=	m^3
cp	×	1.0	e-03	=	Pa·s
psi	×	6.895	e+00	=	kPa
md	×	1e-15	e+00	=	m^2
BBL	×	1.6	e-01	=	m^3

References

Ahmed, M., and Rezaei-Gomari, S. 2018. Economic Feasibility Analysis of Shale Gas Extraction from UK's Carboniferous Bowland-Hodder Shale Unit. MDPI Resources Publication, Basel Switzerland.

Ahmed, T. R. 2010. Reservoir Engineering Handbook, fourth ed. Amsterdam; Boston. Gulf Professional Pub.

Ajani, A.A., and Kelkar, M.G. 2012. Interference Study in Shale Plays. The Woodlands, Texas, USA, Society of Petroleum Engineers. Paper SPE 151045, presented at the SPE Hydraulic Fracturing Technology Conference, The Woodlands, Texas, 6-8 February.

Alharthy, N., Teklu, T.W., Kazemi, H., Graves, R.M., Hawthorne, S.B., Braunberger, J., Kurtoglu, B., 2018. Enhanced Oil Recovery in Liquid-Rich Shale Reservoirs: Laboratory to Field. SPE Reserv. Eval. Eng. 21, 137–159.

Amaefule, J., and Handy, L. 1982. The effect of Interfacial Tensions on Relative Oil/Water Permeabilities of Consolidated Porous Media. SPE Journal 22 (3): 371-381.

Ambrose, R. J., Clarkson, C.R., Youngblood, J. et al. 2011. Life-Cycle Decline Curve Estimation for Tight/Shale Gas Reservoirs. Paper SPE 140519 presented at the SPE Hydraulic Fracturing Technology Conference and Exhibition, The Woodlands, Texas, 24-26 January.

Ambrose, R. J. 2011. Micro-structure of Gas Shales and its Effect on Gas Storage and Production Performance. PhD dissertation, University of Oklahoma, Norman, OK (August 2011).

Awada, A., Santo, M., Lougheed, D., Xu, D., and Virues, C. 2016. Is That Interference? A Work Flow for Identifying and Analyzing Communication through Hydraulic Fractures in a Multiwell Pad. SPE Journal 21 (5): 1554-1566.

Alfarge, D., Wei, M., & Bai, B. 2018. A Parametric Study on the Applicability of Miscible Gases Based EOR Techniques in Unconventional Liquids Rich Reservoirs. Paper SPE 189785 presented at the SPE Canada Unconventional Resources Conference, Calgary, Alberta, Canada 13-14 March.

Blum, J. 2015. Fees for Oil Field Drillers Plummeted Amid the Crude Crash, Federal Data Shows. Fuelfix. Retrieved April 10, 2019 from http://fuelfix.com/blog/2015/06/18/fees-for-oil-field-drillers-plummeted-amid-the-crude-crash-federal-data-shows/#30727101=0

Cardneaux, A.P. 2012, Mapping of the Oil Window in the Eagle Ford Shale Play of Southwest Texas Using Thermal Modeling and Log Overlay Analysis, M.S. Thesis, Louisiana State University, 74 p.

Chavez, G. 2016. Eagle Ford Shale: Evaluation of Companies and Well Productivity. The University of Texas at Austin. MS Thesis from Energy and Earth Resources department. Austin, Texas.

Cipolla, C.L., Warpinski, N.R., Mayerhofer, M.J., Lolon, E., Vincent, M.C. 2010. The Relationship Between Fracture Complexity, Reservoir Properties, and Fracture Treatment Design. Paper SPE 115769, presented at the SPE Annual Technical Conference and Exhibition, Denver, Colorado, 21-24 September. 90

Dachanuwattana, S., Jin, J., Zuloaga-Molero, P., Li, X., Xu, Y., Sepehrnoori, K., Yu, W., and Miao, J. 2018a. Application of Proxy-based MCMC and EDFM to History Match a Vaca Muerta Shale Oil Well. Fuel 220: 490-502.

Dachanuwattana, S., Xia, Z., Yu, W., Qu, L., Wang, P., Liu, W., Miao, J., and Sepehrnoori, K. 2018b. Application of Proxy-based MCMC and EDFM to History Match a Shale Gas Condensate Well. Journal of Petroleum Science and Engineering 167: 486-497.

Eltahan, E., Yu, W., Sepehrnoori, K., Kerr, E., Miao, J., and Ambrose, R. 2019. Modeling Naturally and Hydraulically Fractured Reservoirs with Artificial Intelligence and Assisted History Matching Methods Using Physics-Based Simulators. Paper SPE 195269, presented at SPE Western Regional Meeting, San Jose, California, 23-26 April.

Fragoso, A., Selvan, K., and Aguilera, R. 2018. An Investigation on the Feasibility of Combined Refracturing of Horizontal Wells and Huff and Puff Gas Injection for Improving Oil Recovery from Shale Petroleum Reservoirs. Paper SPE 190284 presented at the SPE Improved Oil Recovery Conference, Tulsa Oklahoma, 14-18 April.

Fiallos Torres, M.X., Yu, W., Ganjdanesh, R., Kerr, E., Sepehrnoori, K., Miao, J., Ambrose, R. 2019a. Modeling Interwell Fracture Interference and Huff-N-Puff Pressure Containment in Eagle Ford Using EDFM. Paper SPE 195240, presented at SPE Oklahoma City Oil and Gas Symposium, Oklahoma City, Oklahoma, 9-10 April.

Fiallos Torres, M.X., Yu, W., Ganjdanesh, R., Kerr, E., Sepehrnoori, K., Miao, J., Ambrose, R. 2019b. Modeling Interwell Interference Due to Complex Fracture Hits in Eagle Ford Using EDFM. Paper IPTC 19468, presented at International Petroleum Technology Conference, Beijing, China, 26-28 March.

Gamadi, T., Elldakli, F., Sheng, J. 2014. Compositional Simulation Evaluation of EOR Potential in Shale Oil Reservoirs by Cyclic Natural Gas Injection. Paper URTEC

1922690 presented at Unconventional Resources Technology Conference, Denver, Colorado, 25-27 August.

Gharbi, R., and Peters, E. 1993. Scaling coreflood experiments to heterogeneous reservoirs. Journal of Petroleum Science and Engineering 10 (2): 83-95.

Gunter, B., and Longworth, H. 2013. Overcoming the Barriers to Commercial CO2-EOR in Alberta, Canada: Final Report. Alberta Innovates - Energy and Environment Solutions.90

Hentz, T.F., Ambrose, W.A., and Smith, D.C. 2014. Eaglebine play of the southwestern East Texas Basin: Stratigraphic and depositional framework of the Upper Cretaceous (Cenomanian-Turonian) Woodbine and Eagle Ford Groups. AAPG Bulletin.

Hentz, T.F., and Ruppel. 2011, Regional Stratigraphic and Rock Characteristics of Eagle Ford Shale in Its Play Area: Maverick Basin to East Texas Basin, Search and Discovery Article #10325, based on oral presentation at AAPG Annual Convention and Exhibition, Houston, Texas, April 10-13, 2011

Herrnstadt, E., Kellogg, R., Lewis E. 2019. Royalties and Deadlines in Oil and Gas Leasing: Theory and Evidence. Compass Lexecon. Washington, District of Columbia.

Hoffman, B. T., and Evans, G., 2016. Improved Oil Recovery IOR Pilot Projects in the Bakken Formation. Paper SPE 195223 presented at the SPE Oklahoma City and Gas Symposium, Oklahoma City, Oklahoma, 9-10 April.

Hoffman, B. T., and Rutledge, J., 2019. Mechanisms for Huff-n-Puff Cyclic Gas Injection into Unconventional Reservoirs. Paper SPE 180270 presented at the SPE Low Perm Symposium, Denver Colorado, 5-6 May.

Hughes, D. 2013. Drill, Baby, Drill: Can Unconventional Fuels Usher in a New Era of Energy Abundance?. Santa Rosa, CA: Post Carbon Institute.

IFRS. 2009. IAS 23 Borrowing Costs. International Financial Reporting Tool. Retrieved March 24, 2019 from https://www.ifrs.org/issued-standards/list-of-standards/ias-23-borrowing-costs/#about

Inkpen, A., and Moffett, M. 2011. The Global Oil & Gas Industry: Management, Strategy & Finance. Tulsa, Oklahoma: PennWell.

Jacobs, T. 2016. EOR-For-Shale Ideas to Boost Output Gain Traction. Journal of Petroleum Technology SPE-0616-0028-JPT. 68 (6): 28-31.

Jacobs, T. 2017. Oil and Gas Producers Find Frac Hits in Shale Wells a Major Challenge. Journal of Petroleum Technology 69 (4): 29-34.

Jin, L., Hawthorne, S., Sorensen, J., Pekot, L., Bosshart, N., Gorecki, C., Steadman, E., and Harju, J. 2017.Utilization of Produced Gas for Improved Oil Recovery an Reduced

Emissions form the Bakken Formation. Paper SPE 184414, presented at the SPE Health, Safety, Security, Environment and Social Responsibility Conference – North America, New Orleans, Louisiana, 18-20 April.

Jin, L., Sorensen, J., Hawthorne, S., Smith, S., Bosshart, N., Burton-Kelly, M., Miller, D., Grabanski, C., and Harju, J. 2016. Improving Oil Transportability Using CO2 n the Bakken System – A Laboratory Investigation. Paper SPE 178948, presented at the SPE International Conference and Exhibition of Formation Damage Control, Lafayette, Louisiana, 24-26 February.

Kanfar, M. S., Ghaderi, S. M., Clarkson, C. R., Reynolds M. M., and Hetherington, C. 2017. A Modeling Study of EOR Potential for CO_2 Huff-n- Puff in Tight Oil Reservoirs – Example form the Bakken Formation. Paper SPE 185026 presented at SPE Unconventional Resources Conference, Calgary, Alberta, Canada, 15-16 February.

Kalla, S., Leonardi, S., Berry, D., Poore, L., Sahoo, H., Kudva, R., and Braun, E. 2015. Factors that affect Gas-Condensate Relative Permeability. Paper SPE 173177. SPE Reservoir Evaluation & Engineering 18 (1): 5-10.

Khan, M. 2017. Falling oil prices: Causes consequences and policy implications. Journal of Petroleum Science and Engineering. 149:409-427.

Klenner, R., Liu, G., Stephenson, H., Murrell, G., Lyer, N., Virani, N., and Charuvaka, A. 2018. Characterization of Fracture-Driven Interference and the Application of Machine Learning to Improve Operational Efficiency. Paper SPE 191789, presented at the SPE Liquids-Rich Basins Conference - North America, Midland, Texas, 5-6 September.

Knull, W. III, Jones, S., Tyler, T., and Deutsch, R. 2007. Accounting For Uncertainty In Discounted Cash Flow Valuation Of Upstream Oil And Gas Investments. Journal of Energy & Natural Resources Law 25(3): 268-302.

Kovscek, A., Tang, G.Q., and Vega, B. 2008. Experimental Investigation of Oil Recovery from Siliceous Shale by CO2 Injection. Paper SPE 115679 presented at SPE Annual Technical Conference and Exhibition, Denver, Colorado, 21-24 September.

Kurtoglu, B., and Salman, A. 2015. How to Utilize Hydraulic Fracture Interference to Improve Unconventional Development. Paper SPE 177953, presented at the Abu Dhabi International Petroleum Exhibition and Conference, Abu Dhabi, UAE, 9-12 November.

Lake, L., Martin, J., Douglas, Ramsey, J.D., and Titman, S. 2013. A Primer on the Economics of Shale Gas Production Just How Cheap is Shale Gas?. Journal of Applied Corporate Finance 25(4): 87-96.

Lee, J. 1982. Well Testing, Society of Petroleum Engineers Textbook Series, 159 p.

Melodie, M., Crenes, M., Hafner, M., Aoun, M. 2017. Shale gas production costs: historical developments and outlook. Insight Energy Inc. Energy Brief

Mian, M. A. 2011. Project Economics and Decision Analysis Volume I: Deterministic Models. 2nd Edition. Tulsa, Oklahoma. PennWell.

Mittal, R., Oruganti, Y., McBurney, C. 2015. Re-Fracturing Simulations: Pressure-Dependent SRV and Shear Dilation of Natural Fractures. SPE 178631 and URTEC 2154943 paper presented at the Unconventional Resources Technology Conference, San Antonio, Texas, 20-22 July

Manchanda, R., Sharma, M.M., and Holzhauser, S. 2013. Time Dependent Fracture Interference Effects in Pad Wells. Paper SPE 164534, presented at the SPE Unconventional Resources Conference-USA, The Woodlands, Texas, 10-12 April.

Moinfar, A., Varavei, A., Sepehrnoori, K., and Johns, R.T. 2012. Development of a Novel and Computationally-Efficient Discrete-Fracture Model to Study IOR Processes in Naturally Fractured Reservoirs. Paper SPE 154246, presented at the SPE Improved Oil Recovery Symposium, Tulsa, Oklahoma, 14-18 April.

Mohtar, R., Shafiezadeh, H., Blake, J., Bassel, D. 2018. Economic, social and environmental evaluation of energy development in the Eagle Ford shale play. Journal of Science of the Total Environment. 646: 1601-1614

Morales, A., Zhang, K., Gakhar, K., Porcu, M.M., Lee, D., Shan, D., Malpani, R., Pope, T., Sobernheim, D., and Acock, A. 2016. Advanced Modeling of Interwell Fracturing Interference: An Eagle Ford Shale Oil Study - Refracturing. Paper SPE 179177, presented at the SPE Hydraulic Fracturing Technology Conference, The Woodlands, Texas, 9-11 February.

Parra, P.A., Rubio, N., Ramírez, C., Guerra, V.A., Campos, I.R., Trejo, M.D., Olguín, J. Vargas, C.H., Valbuena, R., Soler, D.F., Weimann, M.I., Lujan, V., Bonningue, P., Reyes, P.G., Martínez, R., Muñoz, R., Rodríguez, E., and García, M. 2013. Unconventional Reservoir Development in Mexico: Lessons Learned From the First Exploratory Wells, Paper SPE 164545 presented at Unconventional Resources Conference, The Woodlands, Texas, 10-12 April 2013,

Peters, E.J. 2012. Advanced Petrophysics, first ed., vol. 1. Austin, TX. Live Oak Book Company.

Portis, D.H., Bello, H., Murray, M., Barzola, G., Clarke, P., and Canan, K. 2013. Searching for the Optimal Well Spacing in the Eagle Ford Shale: A Practical Tool-Kit. Paper URTeC 1581750, presented at the SPE/AAPG/SEG Unconventional Resources Technology Conference, Denver, Colorado, 12-14 August.

Rassenfoss, S. Shale EOR Works, But Will It Make a Difference?. Journal of Petroleum Technology SPE-1017-0034-JPT. 69(10):34-40

Rezaree, R. 2015. Fundamentals of Gas Shale Reservoirs. John Wiley & Sons Inc. Hoboken New Jersey. ISBN 978-1-118-64579-6

Rigzone. 2011. Costs for Drilling The Eagle Ford. Rigzone. June 20. Retrieved March 24, 2019.http://www.rigzone.com/news/oil_gas/a/108179/Costs_for_Drilling_The_Eagle_Ford.

Sani, A.M., Podhoretz, S.B., and Chambers, B.D. 2015. The Use of Completion Diagnostics in Haynesville Shale Horizontal Wells to Monitor Fracture Propagation, Well Communication, and Production Impact. Paper SPE 175917, presented at the SPE/CSUR Unconventional Resources Conference, Calgary, Alberta, Canada, 20-22 October.

Sardinha, C.M., Petr, C., Lehmann, J., Pyecroft, J.F., and Merkle, S. 2014. Determining Interwell Connectivity and Reservoir Complexity through Frac Pressure Hits and Production Interference Analysis. Paper SPE 171628, presented at the SPE/CSUR Unconventional Resources Conference–Canada, Calgary, Alberta, Canada, 30 September-2 October.

Schlumberger. 2019. Huff and puff. Oilfield Glossary. Retrieved February 12, 2019 from https://www.glossary.oilfield.slb.com/en/Terms/h/huff_and_puff.aspx

Seth, P., Manchanda, R., Kumar, A., and Sharma, M. 2018. Estimating Hydraulic Fracture Geometry by Analyzing the Pressure Interference between Fractured Horizontal Wells. Paper SPE 191492, presented at the SPE Annual Technical Conference and Exhibition, Dallas, Texas, 24-26 September.

Shakiba, M., and Sepehrnoori, K. 2015. Using Embedded Discrete Fracture Model (EDFM) and Microseismic Monitoring Data to Characterize the Complex Hydraulic Fracture Networks. Paper SPE 175142, presented at the SPE Annual Technical Conference and Exhibition, Houston, Texas, 28-30 September.

Sheng, J. 2017. Critical review of field EOR projects in shale and tight reservoirs. Journal of Petroleum Science and Engineering. 159:654-665

Shi, J., Zhang, L., Li, Y., Yu, W., He, X., Liu, N., Li, X., and Wang, T. 2013. Diffusion and Flow Mechanisms of Shale Gas through Matrix Pores and Gas Production Forecasting. Paper SPE 167226, presented at SPE Unconventional Resources Conference Canada, Calgary, Alberta, Canada, 5-7 November.

Shojaei, H., and Jessen, K. 2014. Diffusion and Matrix-Fracture Interactions during Gas Injection in Fractured Reservoirs. Paper SPE 169152, presented at the SPE Improved Oil Recovery Symposium, Tulsa Oklahoma, 12-16 April.

Song, C., and Yang, D. 2013. Performance Evaluation of CO_2 Huff-n-Puff Processes in Tight Oil Formations. Paper SPE 167217 presented at the SPE Unconventional Resources Conference, Calgary, Alberta, Canada, 5-7 November.

Taron, J., Hickman, S., Ingebritsen, S.E, and Williams, C. 2014. ARMA Paper presented at the 48th US Rock Mechanics / Geomechanics Symposium, Minneapolis, MN, 1-4 June.

Tripoppoom, S., Yu, W., Huang, H., Sepehrnoori, K., Song, W., and Dachanuwattana, S. 2018. A Practical and Efficient Iterative History Matching Workflow for Shale Gas Well coupling Multiple Objective Functions, Multiple Proxy-based MCMC and EDFM. Journal of Petroleum Science and Engineering 176: 594-611.

Texas Railroad Commission. 2019. Texas Eagle Ford Shale Oil Production 2008 through November 2018. Retrieved March 14, 2019 from https://www.rrc.texas.gov/media/41519/eaglefordproduction_oil_perday.pdf.

Tovar, F. D., Eide, O., Graue, A., & Schechter, D. S. 2014. Experimental Investigation of Enhanced Recovery in Unconventional Liquid Reservoirs using CO2: A Look Ahead to the Future of Unconventional EOR. Paper SPE 169022 presented at the SPE Unconventional Resources Conference, Woodlands, Texas, 1-3 April.

U.S. EIA. 2014, Updates to the EIA Eagle Ford Play Maps. U.S. Energy Information Administration. U.S. Department of Energy. Washington, District of Columbia, December. Retrieved March 22, 2019 from https://www.eia.gov/maps/pdf/eagleford122914.pdf

U.S. EIA. 2016. Drilling Productivity Report. U.S. Energy Information Administration. Washington, District of Columbia. Retrieved April 18, 2019 from https://www.eia.gov/petroleum/drilling/#tabs-summary-2

U.S. EIA. 2016b. Trends in U.S. Oil and Natural Gas Upstream Costs. Report. U.S. Energy Information Administration. Washington, District of Columbia. Retrieved April 16, 2019 from https://www.eia.gov/analysis/studies/drilling/pdf/upstream.pdf

U.S. EIA. 2019a. Annual Energy Outlook 2019. U.S. Energy Information Administration. U.S. Department of Energy. Washington, District of Columbia. Retrieved March 15, 2019 from http://www.eia.gov/

U.S. EIA. 2019b. EIA forecasts world crude oil prices to rise gradually, averaging $65 per barrel in 2020. U.S. Energy Information Administration. Retrieved April 18, 2019 from https://www.eia.gov/todayinenergy/detail.php?id=38032

U.S. EIA. 2019c. Short-Term Energy Outlook. U.S. Energy Information Administration. U.S. Department of Energy. Washington, District of Columbia, March. Retrieved March 15, 2019 from https://www.eia.gov/outlooks/steo/report/natgas.php

U.S. EIA. 2019d. Weekly Production. U.S. Energy Information Administration. U.S. Department of Energy. Washington, District of Columbia, March. Retrieved March 15, 2019 from https://www.eia.gov/outlooks/steo/.

Veeken, C., Wahleitner, L. and Keedy, C. 1994. Experimental modelling of casing deformation in a compacting reservoir. Paper SPE 28090 presented in the Rock Mechanics in Petroleum Engineering, Delft, Netherlands, 29-31 August.

Vega, B., O'Brien, W. J., and Kovscek, A. R. 2010. Experimental Investigation of Oil Recovery from Siliceous Shale by Miscible CO2 Injection. Paper SPE 135627 presented at the SPE Annual Technical Conference and Exhibition, Florence, Italy, 19-22 September.

Wang, Q., Chen, X., Jha, A., and Rogers, H. 2014. Natural Gas From Shale Formation – The Evolution, Evidences And Challenges Of Shale Gas Revolution In The United States. Renewable And Sustainable Energy Reviews 30: 1-28.

Wan, T., Mu, Z., 2018. The use of numerical simulation to investigate the enhanced Eagle Ford shale gas condensate well recovery using cyclic CO2 injection method with nano-pore effect. Fuel 233, 123–132.

Xian, H., Tueckmantel, C., Giorgioni, M., Wei, L., Lai, C. 2018. Fracture Characterization through Image Log Conductive Feature Extraction. Paper OTC 28462, presented at the Offshore Technology Conference Asia, Kuala Lumpur, Malaysia, 20-23 March.

Xu, Y., Cavalcante Filho, J.S.A., Yu, W., and Sepehrnoori, K. 2017a. Discrete-Fracture Modeling of Complex Hydraulic-Fracture Geometries in Reservoir Simulators. SPE Reservoir Evaluation & Engineering 20 (2): 403-422.

Xu, Y., Yu, W., and Sepehrnoori, K. 2017b. Modeling Dynamic Behaviors of Complex Fractures in Conventional Reservoir Simulators. Paper URTeC 2670513, presented at the SPE/AAPG/SEG Unconventional Resources Technology Conference, Austin, Texas, 24-26 July.

Xu, Y., Yu, W., Li, N., Lolon, E., and Sepehrnoori, K. 2018. Modeling Well Performance in Piceance Basin Niobrara Formation Using Embedded Discrete Fracture Model. Paper URTeC 2901327, presented at the SPE/AAPG/SEG Unconventional Resources Technology Conference, Houston, Texas, 23-25 July.

Yu, W., Sepehrnoori, K. 2018. Shale Gas and Tight Oil Reservoir Simulation, 1st Ed.; Publisher: Elsevier, Cambridge, USA. ISBN: 978-0-12-813868-7.

Yu, W., Tripoppoom, S., Sepehrnoori, K., and Miao, J. 2018b. An Automatic History-Matching Workflow for Unconventional Reservoirs Coupling MCMC and Non-Intrusive EDFM Methods. Paper SPE 191473, presented at the SPE Annual Technical Conference and Exhibition, Dallas, Texas, 24-26 September.

Yu, W., Wu, K., Liu, M., Sepehrnoori, K., Miao, J. 2018c. Production Forecasting for Shale Gas Reservoirs with Nanopores and Complex Fracture Geometries Using an Innovative Non-Intrusive EDFM Method. Paper SPE 191666, presented at the SPE Annual Technical Conference and Exhibition, Dallas, Texas, 24-26 September.

Yu, W., Wu, K., Zuo, L., Tan, X., and Weijermars, R. 2016. Physical Models for Inter-Well Interference in Shale Reservoirs: Relative Impacts of Fracture Hits and Matrix Permeability. Paper URTeC 2457663, presented at the SPE/AAPG/SEG Unconventional Resources Technology Conference, San Antonio, Texas, 1-3 August.

Yu, W., Xu, Y., Liu, M., Wu, K., and Sepehrnoori, K. 2018b. Simulation of Shale Gas Transport and Production with Complex Fractures using Embedded Discrete Fracture Model. AIChE Journal 64(6): 2251-2264.

Yu, W., Xu, Y., Weijermars, R., Wu, K., and Sepehrnoori, K. 2018a. A Numerical Model for Simulating Pressure Response of Well Interference and Well Performance in Tight Oil Reservoirs with Complex-Fracture Geometries Using the Fast Embedded-Discrete-Fracture-Model Method. SPE Reservoir Evaluation & Engineering 21 (2): 489-502.

Yu, W., Zhang, Y., Varavei, A., Sepehrnoori, K., Zhang, T., Wu, K., and Miao, J. 2019. Compositional Simulation of CO2 Huff-n-Puff in Eagle Ford Tight Oil Reservoirs with CO2 Molecular Diffusion, Nanopore Confinement and Complex Natural Fractures. SPE Reservoir Evaluation & Engineering, in preprint.

Zaza Energy Company Corporation. 2013. Investor Presentation December 2014, p. 14. Retrieved from https://www.slideshare.net/BRSResources/december-2013-za-za-investor-presentation, March 12, 2019

Zuloaga-Molero, P., Yu, W., Xu, Y., Sepehrnoori, K., and Li, B. 2016. Simulation Study of CO2-EOR in Tight Oil Reservoirs with Complex Fracture Geometries. Scientific Reports 6:33445.

Vita

Mauricio Xavier Fiallos Torres was born in Quito, Ecuador. After completing his high school education at COTAC High School, Quito, Ecuador, in 2007, he joined North Miami High School in Indiana, USA. In 2008, he started his undergrad studies in Electrical/Electronic Engineering at Universidad San Francisco in Cumbaya, Ecuador. Later, he decided to change his university and major and he was admitted by Universidad Central del Ecuador in Quito, majoring Petroleum Engineering. He graduated in 2015 as Bachelor of Science in Petroleum Engineering. Mauricio worked in field internships for Andes Petroleum Company LTD. And REPSOL. Later, he worked for Schlumberger in Quito as part of the PTS-GPE consulting team.

In 2016, he worked for the consulting field of engineering as Reservoir Engineering for Reservoir Dynamics LLC providing services to Schlumberger and Petroamazonas EP. After being awarded a scholarship from the Department of State of the United States by Fulbright, he entered the Graduate School at the University of Texas at Austin in Fall 2017.

Permanent email address: maxafito@gmail.com

This thesis was typed by the author.